INSTITUTO IMDEA NANOCIENCIA
UNIVERSIDAD AUTÓNOMA DE MADRID
FACULTAD DE CIENCIAS

TESIS DOCTORAL – PhD THESIS:

Mechano-chemistry and dynamics of biological and synthetic systems

Kateryna Lemishko

Memoria presentada para optar al título de Doctor en Física de la Materia Condensada, Nanociencia y Biofísica

Junio 2020

Directores:
Dr. Borja Ibarra Urruela
Dr. José López Carrascosa

Resumen

La tesis está enfocada en caracterizar las bases moleculares y mecano-químicas del funcionamiento de motores moleculares biológicos y artificiales. Por una parte, de las proteínas implicadas en la replicación del genoma mitocondrial humano, y por otra, de un interruptor molecular artificial (rotaxano[2]).

Motores moleculares biológicos: replisoma mitocondrial humano.

Las mitocondrias humanas contienen varias copias de un ADN circular de doble cadena (mtADN) que codifica, entre otras, 13 subunidades esenciales para el correcto funcionamiento del sistema de fosforilación oxidativa (OXPHOS). La regulación de la expresión de mtADN implica diferentes niveles de control esenciales para la función mitocondrial y supervivencia celular. Uno de estos niveles de control es la replicación de mtADN. Dicha replicación se lleva a cabo mediante una maquinaria de replicación dedicada. En humanos, el replisoma de mtADN mínimo puede ser reconstituido *in vitro* con la polimerasa Pol γ, la proteína de unión al ADN de cadena sencilla mitocondrial (mtSSB) y la helicasa de ADN mitocondrial (también conocida como TWINKLE).

Según el modelo de desplazamiento de banda para la replicación de mtADN, la replicación de mtADN de mamíferos es unidireccional y asimétrica: Pol γ y mtSSB interactúan funcionalmente en la realización de la síntesis de la cadena L desplazada, mientras que Pol γ, TWINKLE y mtSSB coordinan sus actividades para una síntesis eficiente de la cadena principal o cadena H.

Según lo propuesto para los sistemas de replicación de ADN, durante la síntesis de la cadena principal (cadena pesada o cadena H en las mitocondrias), se cree que estas tres proteínas coordinan sus actividades en la horquilla de replicación mediante interacciones dinámicas funcionales, que son absolutamente necesarias para una síntesis de ADN eficiente y precisa. Hasta la fecha, se sabe poco acerca de cómo los tres componentes principales de la maquinaria de replicación de mtADN organizan sus actividades en la horquilla de replicación. Con el fin de comprender la base molecular de la sinergia y la coordinación entre la polimerasa mitocondrial, la helicasa y el SSB durante la síntesis de la cadena principal, en el segundo capítulo de esta tesis proponemos abordar las siguientes preguntas: ¿Cómo la helicasa acopla sus actividades de unión a ADN de cadena sencilla y de cadena doble con translocación y desenrrollamiento del ADN? ¿Cuál es el efecto de Pol γ en la cinética en tiempo real de la helicasa? ¿Cuál es el mecanismo utilizado por Pol γ para desestabilizar la horquilla? ¿Qué proteína desestabiliza la horquilla en mayor medida? ¿Cómo se ayudan entre sí las dos enzimas individuales? ¿Cómo modula el mtSSB la cinética en tiempo real de Pol γ y TWINKLE en la horquilla de replicación? ¿Cuál es el papel específico del mtSSB en la reacción?

Interruptores moleculares sintéticos: rotaxano[2].

En las últimas décadas, los investigadores que trabajan en el campo de la química supramolecular han demostrado que los sistemas supramoleculares, debido a su organización estructural e integración funcional de sus componentes, pueden realizar tareas útiles. Ello demuestra que el concepto de un dispositivo puede transferirse a nivel molecular. En estos dispositivos moleculares, diferentes componentes de la molécula pueden cambiar sus posiciones relativas en respuesta a estímulos externos. Uno de los ejemplos más destacados de estos sistemas supramoleculares sintéticos son los interruptores moleculares basados en rotaxano. Estos dispositivos están compuestos por una cadena molecular rodeada por un macrociclo que puede moverse entre dos o más sitios de reconocimiento en la cadena, en respuesta a algún estímulo externo. Los interruptores moleculares son actualmente de gran interés para la investigación debido a sus posibles aplicaciones en diferentes campos, desde la biomedicina hasta la maquinaria molecular. El paso de las moléculas a la maquinaria molecular, que incorpora diferentes componentes moleculares para generar trabajo, requerirá un control exquisito de la dinámica y los procesos mecano-químicos que gobiernan el funcionamiento de estos sistemas a nanoescala.

Aunque se conoce mucho sobre la termodinámica y la cinética de los rotaxanos en solución, todavía es necesaria una mejor comprensión de su dinámica operativa y propiedades mecano-químicas a nivel de moléculas individuales y aún quedan por responder preguntas muy básicas sobre el funcionamiento de los motores moleculares a nanoescala: ¿Cómo es la cinética (dinámica) en tiempo real del funcionamiento de un motor sintético? ¿Cómo responde la dinámica de los motores a estímulos externos como el estrés mecánico, las variaciones químicas, las fluctuaciones térmicas, la luz, etc.? ¿Cuánta fuerza puede ejercer un motor en particular? ¿Cuáles son los mecanismos mecano-químicos que gobiernan la operación del motor? ¿Cuáles son las eficiencias termodinámicas de los motores moleculares sintéticos? Responder a estas preguntas es de fundamental importancia para el diseño, uso y control de dispositivos eficientes basados en maquinaria molecular sintética capaces de llevar a cabo innumerables operaciones de forma continua. Sin embargo, hasta la fecha no existe una cuantificación experimental de la dinámica en tiempo real de los motores moleculares sintéticos, y se sabe muy poco acerca de sus propiedades mecano-químicas. Además, para aplicaciones nano-biotecnológicas, los motores moleculares sintéticos deberían funcionar en condiciones casi fisiológicas. Sus mecanismos operativos deben ser probados en condiciones acuosas y biocompatibles. En esta tesis, utilizamos pinzas ópticas para probar las propiedades mecánicas y estudiar la dinámica operativa de los interruptores moleculares individuales en dichas condiciones casi fisiológicas.

Abstract

This thesis is focused on characterization of molecular and mechano-chemical basis of the operation of biological and synthetic molecular motors: on the one hand, of the proteins involved in replication of the human mitochondrial genome, and on the other hand, of a synthetic molecular switch (rotaxane[2]).

Biological molecular motors: human mitochondrial replisome.

Human mitochondria contain several copies of a circular double-stranded DNA (mtDNA) that encodes, among others, 13 essential subunits for the proper operation of the oxidative phosphorylation (OXPHOS) system. The regulation of mtDNA expression involves different levels of control, which are all essential for mitochondrial function and cell survival. One of these control levels is mtDNA replication. Replication of mtDNA is carried out by dedicated replication machinery. In humans, the minimal mtDNA replisome can be reconstituted *in vitro* by the DNA polymerase holoenzyme Pol γ, the mitochondrial single-stranded DNA binding protein (mtSSB) and the mitochondrial DNA helicase (also known TWINKLE).

According to the strand-displacement model for mtDNA replication, mammalian mtDNA replication is unidirectional and asymmetric: Pol γ and mtSSB interact functionally in carrying out synthesis of the displaced L-strand, whereas Pol γ, TWINKLE and mtSSB coordinate their activities for efficient synthesis of the leading or H-strand.

As proposed for DNA replication systems, during synthesis of the leading strand (heavy or H-strand in mitochondria), these three proteins are thought to coordinate their activities at the replication fork through functional dynamic interactions, which are absolutely required for efficient and accurate DNA synthesis. To date, little is known about how the three main constituents of the mtDNA replication machinery orchestrate their activities at the replication fork. In order to understand the molecular basis of the synergy and coordination between the mitochondrial polymerase, helicase and SSB during leading strand synthesis, in the second chapter of this thesis, we propose to address the following questions: How does the helicase couple its single- and double- stranded DNA binding activities with translocation and unwinding of the DNA? What is the effect of Pol γ on the real-time kinetics of the helicase? What is the mechanism used by Pol γ to destabilize the fork junction? Which protein destabilizes the fork junction to a greater extent? How do the two individual enzymes assist each other? How does the mtSSB modulate the real-time kinetics of Pol γ and TWINKLE at the replication fork? What is the specific role of the mtSSB on the reaction?

Synthetic molecular switches: rotaxane[2].

Over the last few decades, researchers working in the field of supramolecular chemistry have shown that supramolecular systems, due to their structural organization and functional integration of their components, can perform useful tasks thus demonstrating that the concept of a device can be transferred to the molecular level. In such molecular devices, different components of the molecule can change their relative positions in response to external stimuli. One of the most prominent examples of such synthetic supramolecular systems are rotaxane-based molecular shuttles. These devices are constructed of a molecular chain encircled by a macrocycle that can move between two or more recognition sites on the thread as a response to some external stimulus. Molecular shuttles are currently of great research interest due to their potential applications in different fields, from biomedicine to molecular machinery. Making the step from molecules to molecular machinery, which incorporates different molecular components to generate work, will require an exquisite control of the dynamics and mechano-chemical processes governing the operation of these systems at the nanoscale.

Although the thermodynamics and kinetics of rotaxanes in bulk are well-understood, a good understanding of their operational dynamics and mechano-chemical properties at the single-molecule level is still missing and very basic questions about the operation of molecular motors at the nanoscale have still to be answered: What are the real-time kinetics (dynamics) of the operation of a synthetic motor? How do the motors dynamics respond to external stimuli like mechanical stress, chemical variations, thermal fluctuations, light, etc.? How much force is a particular motor able to exert? What are the mechano-chemical mechanisms governing the motor operation? What are thermodynamic efficiencies of synthetic molecular motors? Answering these questions is of fundamental importance for the design, use and control of efficient devices based on synthetic molecular machinery able to carry our countless operations continuously. However, to date there is none experimental quantification of the real-time dynamics of synthetic molecular motors, and very little is known about their mechano-chemical properties. In addition, for nano-biotechnological applications synthetic molecular motors should operate in near-physiological conditions. Then, their operational mechanisms should be tested under aqueous, bio-compatible conditions. In this thesis, we used optical tweezers to probe the mechanical properties and study the operational dynamics of individual molecular shuttles under near-physiological conditions.

Contents

Chapter 1

INTRODUCTION

1.1 Biological molecular motors and synthetic molecular devices.

Biological motors, in the form of motor proteins, participate in almost every significant cellular process, such as ATP synthesis [1], DNA replication [2], DNA repair [3], RNA transcription [4], viral genome packaging [5], muscle contraction [6], protein folding [7] and many others [8]. A common feature of biological motors is that they use chemical energy, generally derived from the hydrolysis of triphosphate nucleotides (NTPs) to perform mechanical work and promote a thermodynamically unfavorable processes in the cell. Some remarkable examples (Figure 1) include kinesin, that steps unidirectionally along microtubules to transport cargo [9], the F1F0-ATPase that rotates during ATP production/degradation [10] or the DNA packaging machinery of some bacteriophages, or [5].

Biological molecular motors are highly efficient and robust in performing their biological tasks. For example, it has been shown that a single conventional kinesin (Figure 1A) moves stepwise along a microtubule in approximately 8 nm increments and throughout its single encounter with a microtubule kinesin can make hundreds of steps and exert the force of about 5-7 pN with an energy conversion efficiency of over 40% ([11] - [16]).

As it was mentioned above, the F1F0-ATPase rotary motor is bifunctional: it uses the energy of electrochemical gradient, created by differences in proton concentration across the inner mitochondrial membrane, to produce ATP molecules out of ADP and inorganic phosphate (P_i), and it can also operate in the reverse direction, hydrolyzing ATP and pumping protons across membranes under some specific conditions [17]. F1F0-ATPase consists of a membrane-embedded F0 subunit (see Figure 1B), which transports protons across the membrane and a soluble F1 unit, which catalyzes the synthesis or the hydrolysis of ATP. F1F0-ATPase works with extremely high efficiency: the thermodynamic efficiency of ATP synthesis during oxidative phosphorylation is about 40% and the energy conversion efficiency of the F1 subunit during ATP hydrolysis is near 100% [18].

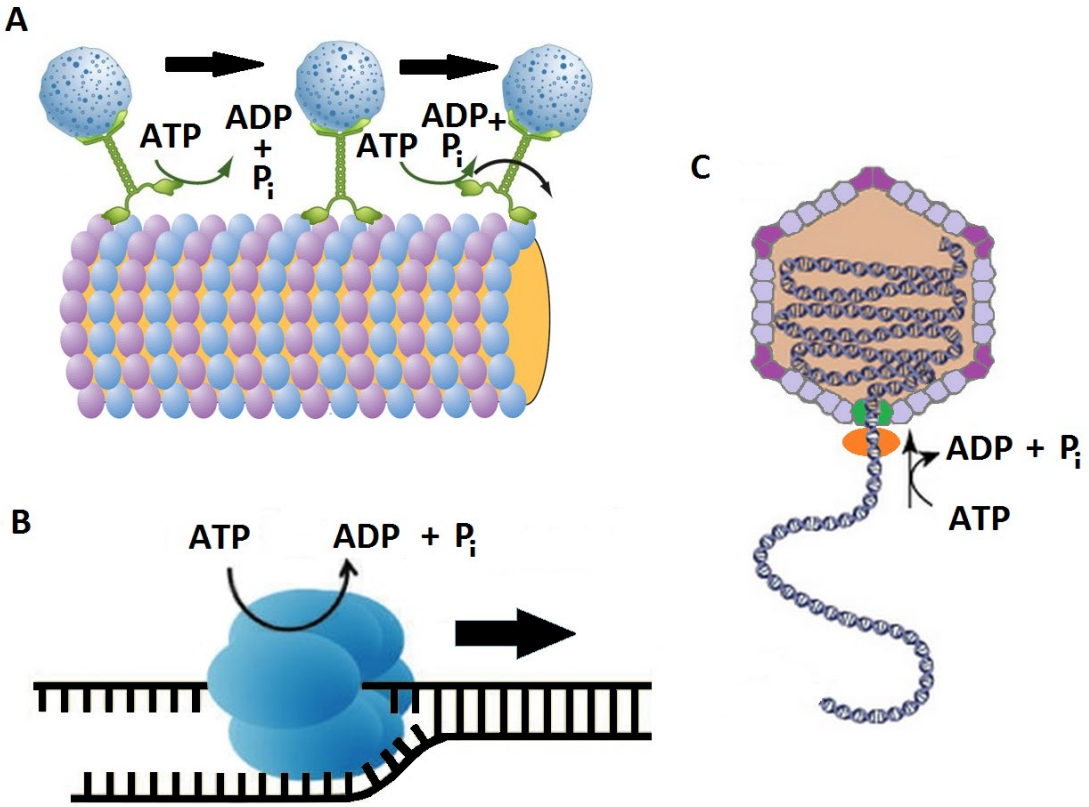

Figure 1. A A schematic representation of the unidirectional movement of a kinesin motor over a microtubule filament. **B** A schematic representation of ATP synthesis/hydrolysis by F1F0-ATPase. **C** A schematic representation of the genome packaging in dsDNA viruses. ATPase activity of a packaging motor (orange) drives DNA translocation, which results in the genome packaging into a capsid.

Double-stranded DNA viruses, like tailed bacteriophages, herpesviruses and dsRNA viruses, like ϕ6 and ϕ12 bacteriophages, use genome packaging motors to pump the genome into a pre-formed protein capsid during viral self-assembly ([19], [20], [5]). During the packaging process, highly negatively charged dsDNA is compacted to near-crystalline densities inside the capsid and, in order to do that, a packaging motor needs to perform a remarkable mechanical work. Phage genome packaging motors are quite efficient: typically, they can convert about 30% of the free energy of ATP hydrolysis into mechanical motion ([21], [22]). For example, the packaging motor of the *Bacillus subtilis* bacteriophage ϕ29 packages a genome of a size of 19,300 base pairs into a capsid of 40 nm in diameter and 50 nm in height, exerting forces as high as ~60 pN [22]. The pressure of the packaged DNA within the capsid, and thus the force opposed in translocating the last segment of DNA, is on the order of 6 MPa**.** A schematic representation of the packaging process is shown in Figure 1C.

The ability of biological molecular motors to transform chemical energy into mechanical work and unidirectional movement has inspired synthetic chemists to try to create

artificial molecular devices, capable of controlled motion. Over the past few decades, researchers working in the field of supramolecular chemistry have demonstrated that supramolecular systems, as a result of their structural organization and functional integration of their components, can perform useful tasks thus showing that the concept of the device can be transferred to the molecular level. [23]. In such molecular devices, different components of the molecule can move relatively to each other a response to some external stimuli ([24], [25]).

The field of synthetic molecular machines began with the creation of rotaxane molecular shuttles. The name 'rotaxane' is derived from the Latin 'rota' (wheel) and 'axis' (axle). Rotaxanes consist of a dumbbell-shaped molecule encircled by a macrocyclic component (Figure 2A). In these compounds, bulky groups (stoppers) on the ends of the dumbbell component prevent the disassembly of the macrocycle from the molecular thread. The macrocycle can move between two or more binding (recognition) sites on the encircled molecular thread. If the binding sites show different affinities for the macrocycle, the molecular shuttle becomes a switch. By modifying the affinities of the binding sites by some external stimuli (e.g. by applying an electrical current, ultraviolet light or changing pH), it is possible to make the macrocycle move between the recognition sites.

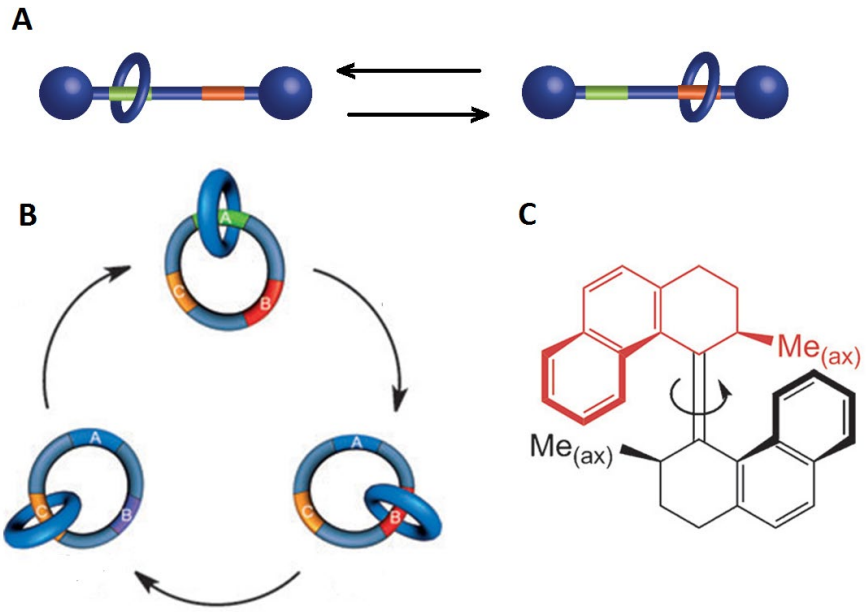

Figure 2. A A schematic representation of a [2]rotaxane molecular switch. The macrocycle can travel from one recognition site on the axle to the other as a response to some external stimuli. **B** A schematic representation of a [2]catenane, in which as a response to an external stimulus, one of the macrocycles switches between three binding sites on the other macrocycle (adapted from [26]). **C** The structure of the first light-powered rotary molecular motor (adapted from [27])

Another example of a mechanically interlocked molecular system, whose different components can move relatively to each other, are catenanes (Figure 2B**)**. The architecture of catenanes consists of two interlocked macrocycles, one of which has binding sites for the other macrocycle. One macrocycle without the binding sites can rotate over the other macrocycle when the affinities of the binding sites are changed as a response to some external stimulus (ultraviolet light, an electrical current etc.) ([28], [29]).

In 1999, the group of Ben Feringa described an overcrowded alkene molecule, in which the components can rotate around the alkene axis during *cis–trans* isomerization upon irradiation with light [27]. This molecule was the first example of a synthetic rotary motor and the first example of an artificial molecular motor of any kind. It can perform a continuous directional movement as long as it is irradiated with ultraviolet light and stays above critical temperature. (Figure 2B)**.**

So far, several research groups managed to use the controlled motion of these molecular devices to generate force in the macroscopic world. In 2005, the group of David Leigh implemented the shuttling of a surface-bound rotaxane triggered by ultraviolet light to mask a polarophobic fluorocarbon unit [30]. Thus, by modifying surface properties it was possible to propel a microliter droplet of diiodomethane along a surface up a twelve-degree slope (Figure 3A). The same year, the group of J. Fraser Stoddart used the contraction of surface mounted [3]rotaxanes as an actuator to bend a gold microcantilever beam [31] (Figure 3B).

In 2006, the group of Prof. Ben L. Feringa designed a synthetic, light-driven molecular motor based on an overcrowded alkyne molecules added to a liquid-crystal film [32]. This motor can rotate objects placed on the film that exceed the size of the motor molecule by a factor of 10,000 (Figure 3C). In 2015, Nicholas Giuseppone and colleagues showed that, by integrating light-driven unidirectional molecular rotors as reticulating units in a polymer gel, it is possible to provoke a macroscopic contraction of the material (Figure 3D) [33]**.**

Overall, in the last 20 years, synthetic chemist have created an impressive array of synthetic molecular devices that can operate at the nanoscale. However, these devices are far from reaching the efficiencies presented by their biological counterparts and cannot operate under physiological conditions, they are not soluble in water, which limits their putative nano-biological applications.

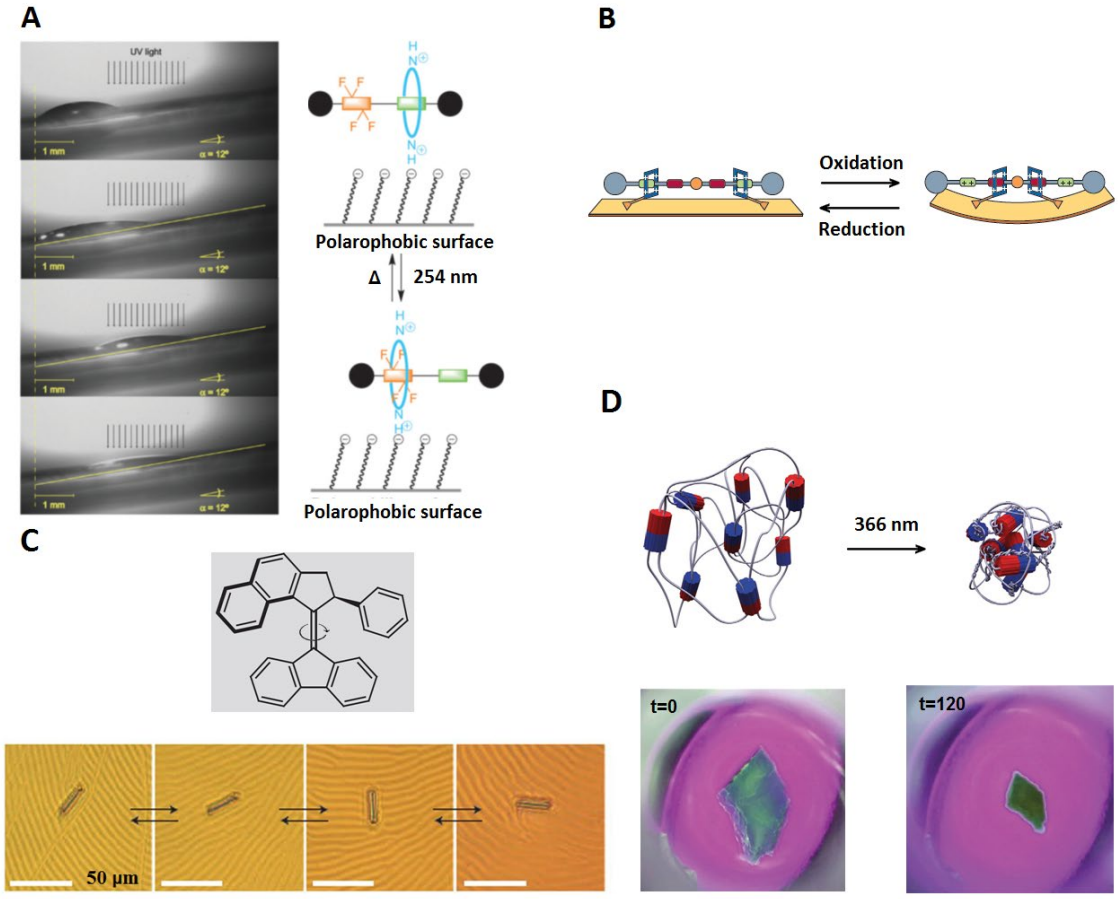

Figure 3. A A [2]rotaxane-based molecular machine that does mechanical work by moving a diodomethane droplet against the force of gravity (image adapted from [30] **B** A schematic representation of a [3]rotaxane-based molecular machine that bends a microcantilever (adapted from [31] **C** The motion of a glass rod on a liquid crystal with embedded molecular motor and the chemical structure of the motor (image adapted from [32])**. D** A Schematic representation of contraction of a crosslinked polymer motor conjugate that leads to macroscopic contraction of a gel (adapted from [33]).

1.2 Ensemble vs. single-molecule experiments

In classical experiments in solution, one measures the average of the properties of an ensemble of molecules present in that solution. For example, if we measure absorbance or fluorescence of a solution, we obtain an average over the total population of the dissolved molecules. Even a volume as small as one microliter of one micromolar solution of a substance contains $6.02 \cdot 10^{11}$ molecules of that substance. The information obtained from classical ensemble-averaged experiments in this solution will only represent the states of the highest probability within the whole population of molecules. Hence, in these experiments, we miss the information about the properties of the molecules of poorly represented states and we cannot follow the trajectories of these molecules during chemical reactions. Identification of these low represented states is very important for understanding the mechanisms/dynamics driving the operation of biological processes at the molecular level ([34], [35]). By studying the properties of one molecule at a time it is possible to identify different free energy states within a population of molecules. In addition, by following a trajectory of a single-molecule we can determine instantaneous reaction rates and recognize events or metastable intermediates along the reaction pathway, both being crucial to unravel the dynamics of the reaction.

The operation of molecular motors is defined by the process of conversion of consumed energy into mechanical work. The energy conversion occurs through conformational changes in the molecular motor, which result in generation of force. The chemical process by which motors transform the energy stored in triphosphate nucleotides into mechanical work has been classically explained in terms of 'Power Stroke' and 'Brownian ratchet' mechanisms. In the first mechanism, either the production of nucleotide diphosphate or the release of the inorganic phosphate during the NTP hydrolysis cycle causes a conformational change that is tightly coupled to the displacement of the motor and force generation [36]. In the second mechanism, the displacement of the motor is produced by rectification of thermal fluctuations caused by the conformational change in the motor induced by NTP hydrolysis [37]. To date, all biological molecular motors are thought to operate as Brownian ratchets. Synthetic motors instead have been designed to operate following either of the two mechanisms.

The development of single-molecule manipulation techniques has permitted to measure forces and displacements generated by a single molecular motor as well as modify the activity of the molecular motor by applying forces to it. The properties, such as the capacity to generate force, step size, transition among different conformational states, that can be characterized with single-molecule manipulation methods are crucial for understanding the operational dynamics of molecular motors and provide unprecedented access to the mechano-chemical coordinate of the process.

1.3 Single-molecule manipulation techniques: Optical tweezers

The so-called single-molecule methods that allow researchers to probe one molecule at a time can be divided into two groups: techniques that allow observation of single-molecules and the methods that permit manipulation of single-molecules by means of applied mechanical force and/or torsion. There is a great variety of single-molecule manipulation techniques available today, however the most commonly used ones are the following three techniques: Atomic Force Microscopy (AFM) [38], magnetic tweezers [39], and optical tweezers [40]. Each of these techniques has its advantages and drawbacks depending mainly on force and displacement ranges and spatial and temporal resolution. The most important features of optical tweezers, AFM and magnetic tweezers can be found in the Table 1. In this thesis, we used optical tweezers to study a biological and a synthetic supramolecular system.Ta

	Optical tweezers	**AFM**	**Magnetic tweezers**
Force range (pN)	0.1-100	$10\text{-}10^5$	0.01-10
Displacement range (nm)	$0.1\text{-}10^5$	$0.5\text{-}10^4$	$5\text{-}10^4$
Spatial resolution (nm)	0.1-2	0.5-1	5-10
Temporal resolution (s)	10^{-4}	10^{-3}	$10^{-1}\text{-}10^{-2}$
Practical advantages	Specific manipulation High force resolution	High spatial resolution	Specificity to magnets Ability to induce torque

Table 1. Comparison of the three most commonly used single-molecule manipulation techniques (Based on [41], [42]).

1.3.1 The physical basis of optical trapping

The physical basis of optical trapping was discovered by Arthur Ashkin in 1970 [43]. The inspiration came to Ashkin form a realization of the large magnitude of the pushing force that arises when light reflects off an object. In his experiment, Ashkin saw that transparent micron-sized latex spheres were pushed along the direction of a tightly focused laser beam, moving with a velocity in agreement with his calculations. He also observed something interesting and unexpected: the spheres, while being pushed forward, were also pushed towards the central axis of the beam. Ashkin found that this additional transverse force comes from the gradient in optical intensity of the Gaussian-profiled laser. When a ray of light hits an object with a higher index of refraction than the

surrounding medium (like transparent latex spheres placed in water), it refracts two times (as it enters the sphere and as it exits the sphere and passes back into the medium). The resulting ray is deflected from its original path, and therefore, its momentum changes. In a non-uniform optical field (such as of a laser beam with the Gaussian-profiled intensity), the forces are stronger where the light is more intense, so the resulting net force points to the direction of higher light intensity. In that work, Ashkin also designed and implemented the first optical trap created with two counter propagating laser beams.

During the subsequent years, Ashkin developed a single beam gradient force radiation pressure trap with the original purpose to trap atoms. It was decided to test the trap on dielectric particles in the size range from 10 μm down to ~0.1 μm. [40]. It was described that a stable optical trap, capable of holding dielectric particles, can be created by a tightly focused laser beam with a Gaussian intensity profile (Figure 4A). A dielectric particle placed near the focus of the beam will experience two kinds of forces: the scattering force, arising when protons are scattered by the surface of the particle, and the gradient force, produced by the gradient of the intensity profile of the laser beam. The scattering force pushes the particle towards the direction of light propagation and the gradient force pushes the dielectric particle towards the region of the greatest light intensity (Figure 4A).

The scattering component dominates, so the laser should be focused sharply enough to create a gradient component that exceeds the scattering force. Besides, the refraction index of the trapped particle should be greater than that of the surrounding media. Near the focus of light, the optical trap behaves as a linear Hookean spring with a fixed stiffness (Figure 4B): the displacement of the trapped bead, $\boldsymbol{\Delta x}$, is proportional to the applied force ($\boldsymbol{F} = -\boldsymbol{k} \cdot \boldsymbol{\Delta x}$ $(eq. 1)$, where $\boldsymbol{k}$ is the stiffness of the trap).

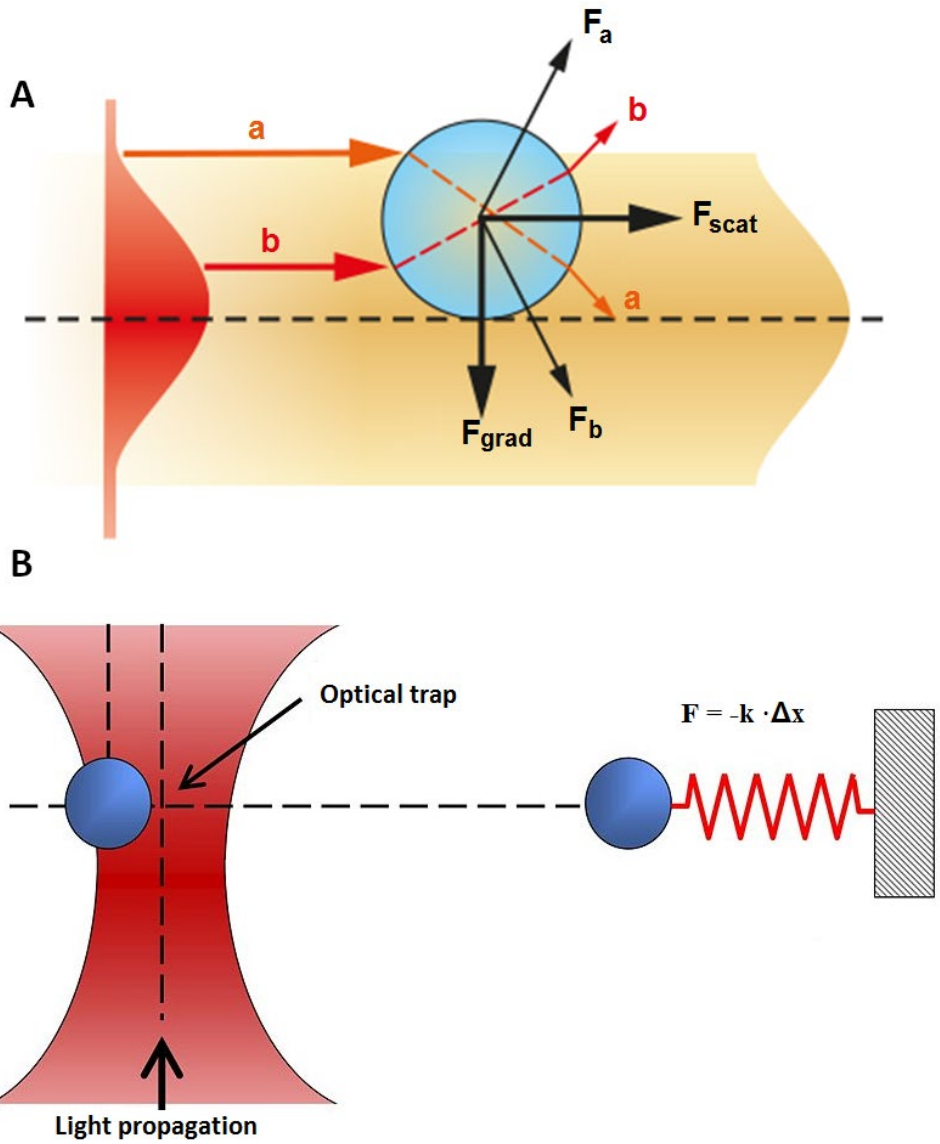

Figure 4. A A dielectric bead is hit by a laser beam of a Gaussian profile, which results in a scattering force in the direction of beam propagation, and a gradient force in the direction of the optical axis. **B** Displacement of the bead from the center of the optical trap due to the external tension is proportional to the applied force. The coefficient of proportionality, k, characterizes the stiffness of the optical trap.

Shortly after the optical trapping or optical tweezers were discovered, they were implemented to physically trap and manipulate single viruses, bacteria and even organelles inside living cells ([44], [45]). Since then, optical tweezers have been transformed into an advanced experimental technique through a number of innovations in optical trapping instrumentation. In 1993, Svoboda *et al*. developed a method to detect displacements of an optically trapped bead by interferometry, [46]. This approach allowed them to study the processive motion of kinesin at the molecular scale. In 1994, Feiner *et al*., using a feedback-stabilized dual optical trap, measured piconewton forces

and nanometer displacements resulted from the interaction of a single myosin molecule with an actin filament [47]. Later, in 1998, Ishijima et al. combined total internal reflection fluorescence microscopy with dual optical trapping to study how mechanical cycles in myosin are coupled to ATP hydrolysis [48].

As an outcome of the improvements in optical trapping instrumentation, optical tweezers have been widely used to study a wide range of different aspects of biological processes. In the last 20 years, this technique has been applied to study the elastic properties of single DNA and RNA molecules ([49], [50]), protein-DNA interactions ([51] - [53]), folding of proteins and nucleic acids ([54] - [56]) and molecular operation of many diverse types of biological molecular motors ([57] - [61]) .

1.3.2 Counter propagating optical tweezers setup

All the measurements of this thesis have been performed using a highly stable miniaturized dual-beam optical tweezers (MiniTweezers), see Figure 5 [62]. One of the main advantages of this instrument consists in the use of two counter propagating laser beams to create an optical trap, in which scattering forces from the two beams are cancelled out. This setup permits to use lasers with lower numerical aperture, which, in combination with objectives with high numerical aperture, allows the collection of all the deflected light from the trap. Thus, in contrast to the case of single beam setups, the setup of MiniTweezers permits the usage of the method of the linear momentum conservation for force calibration. Another important advantage of MiniTweezers results from the miniaturized size of the instrument. The reduced size of MiniTweezers minimizes the effect of temperature change, floor vibrations and acoustic noise.

The MiniTweezers instrument can exert and measure forces from 1 to 200 pN and has resolutions of 0.1 pN in force and ~1nm in distance with a data acquisition frequency of 500-1000 Hz.

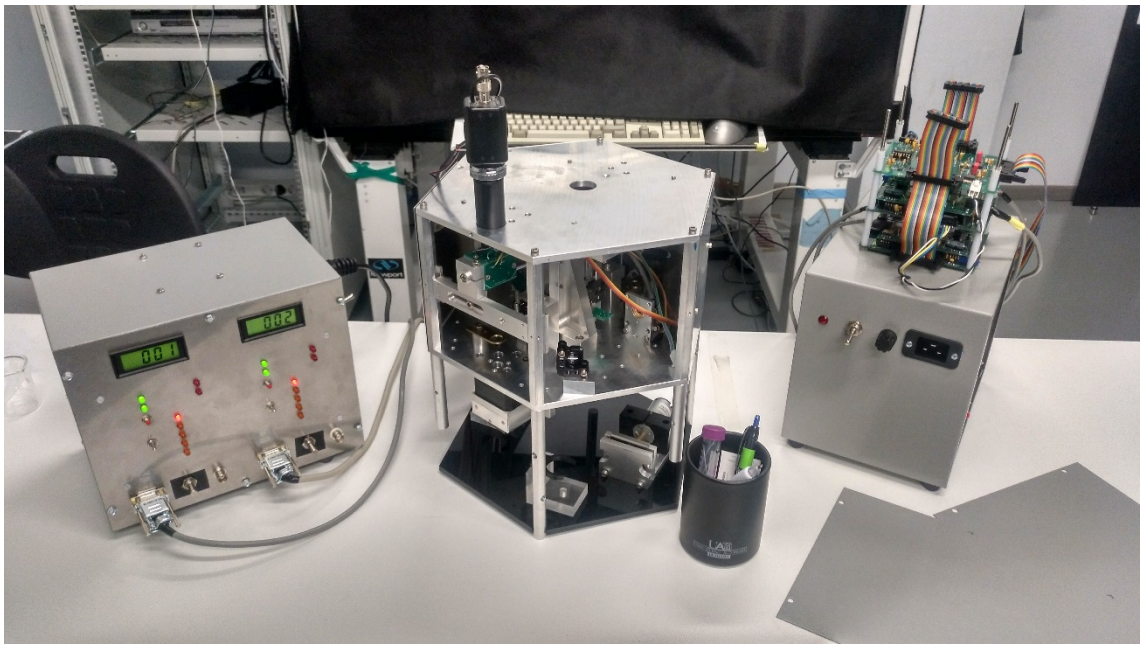

Figure 5. The central piece is the head of the mini-tweezers, where the components of the setup described below are placed.

The main components of the MiniTweezers setup include lasers with Gaussian profile intensity, focusing objective lenses, a flow chamber and photodetectors (Figure 6):

Lasers:
Typically, lasers that are used in optical trapping emit near infrared light (800-1100 nm), thus, avoiding a possible photodamage of biological samples. The laser power should be in the range of a few hundreds of milliwatts, which is high enough to produce forces up to a few hundreds of piconewtons and low enough to prevent photodamage of the sample ([63], [64]). A dual-beam system, in which two counter-propagating laser beams are focused in the same spot, has been also suggested as a way to reduce photodamage [62]. In the instrument used for the measurements (MiniTweezers), two diode lasers (*Lumics, LU0808 M250-FBG*) with the maximum power of 250 mW and 808 nm wavelength, are brought to the same focus with orthogonal polarizations.

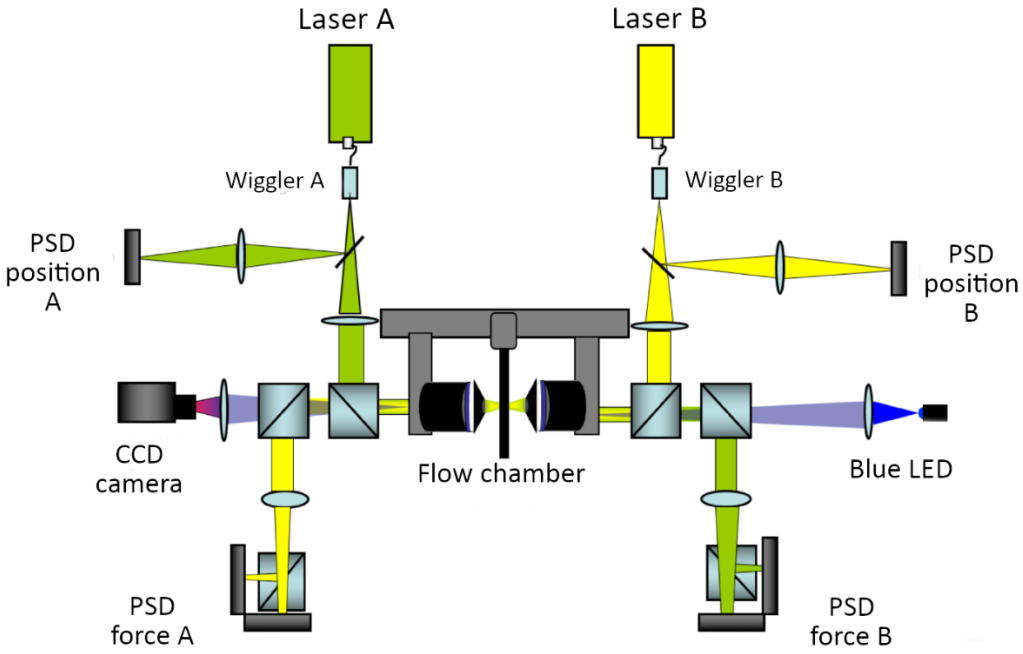

Figure 6. The laser beam is divided in two parts with a beam splitter. One part is directed to a position sensitive detector (PSD) and the other is focused in the center of the flow chamber through an objective lens to create an optical trap together with the counter-propagating beam. The light from these beams is collected by the opposite objective lenses and directed to force PSDs [65].

Objectives:

To create a sharply focused beam, the objective should have high numerical aperture (NA). Water immersion objectives is the most common type of objectives used for optical trapping, because this type of objectives does not create spherical aberrations that affect the stiffness of the trap in aqueous solution ([66], [63]). In MiniTweezers, the counter-propagating beams are focused through opposing water immersion objectives with NA = 1.20 (*Olympus*, UPLSAPO 60XW) to form an optical tram in a flow chamber.

Flow chamber:

The flow chamber is the place where mechano-chemical experimental assays are carried out. A flow chamber for MiniTweezers is made out of two glass cover slips bound together by parafilm layers and contains several channels. (Figure 7). Buffer solutions can be easily introduced to the chamber and can be flowed at a controlled rate. A flow chamber design usually includes a glass micropipette that can immobilize a plastic bead by suction and additional glass tubes used to connect different channels or to dispense reagents. Functionalized plastic beads can be introduced through any of the channels and flowed to the focal region through the connecting glass tubes.

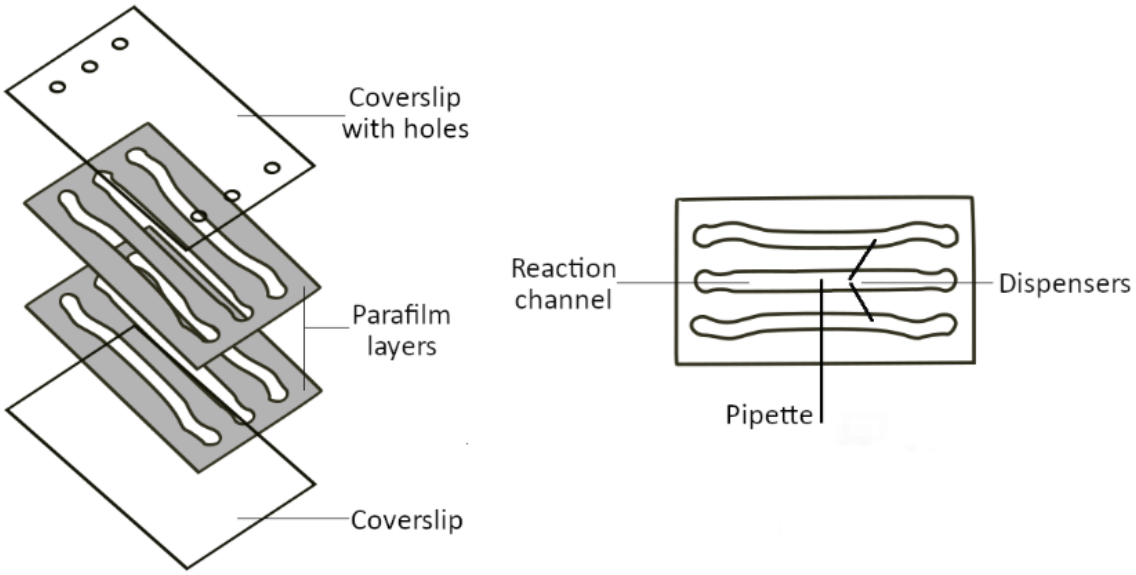

Figure 7. Flow chambers for MiniTweezers are made of two glass coverslips glued together with parafilm layers (on the left). A typical chamber design includes a glass micropipette and glass dispensers, which are used to connect different channels or introduce reagents into the reaction channel from outside (on the right).

Photodetectors:

In the MiniTweezers setup**,** the transverse and axial forces acting on the particle in the trap are measured via position sensitive detectors (PSDs). They are optoelectronic devices that provide an analog output current proportional to the position of the beam. Each laser needs two detectors: a position-sensitive PSD and a force-sensitive PSD (Figure 6). To measure distance, MiniTweezers use additional two PSDS, so-called light-levers.

The optical paths of lasers A and B (see Figure 6) are equal but opposite. The light from each laser is divided into two beams by a pellicle beam splitter. One of the two resulting beams is sent to the position sensitive detector (PSD-position, Figure 6) that is used to measure the changes in the position of the optical trap. And the other beam is focused through a water immersion objective to form an optical trap together with the counter-propagating beam from the other diode laser. The light from this beam is collected by the opposite objective lens and directed to the position sensitive detector (PSD-force, Figure 6) that detects light deflections when an external force is applied to a plastic bead held in the optical trap.

For MiniTweezers (and for short displacements of the bead), the optical trap behaves as a linear spring, so the displacement of the bead from the optical trap, as a response to applied tension, can be obtained from the Hooke's law as $\boldsymbol{F/k}$, where $\boldsymbol{F}$ is applied

tension and $\boldsymbol{k}$ is the stiffness of the trap. In the conditions used in the experiments of this thesis, $\boldsymbol{k} = 0.135 \pm 0.0043$ pN/nm.

Force calibration

The calibration of force in MiniTweezers can be done via three different methods: the conservation of linear momentum method, the method based on the Stokes' law and calibration by Brownian motion [67]. The advantage of the conservation of linear momentum method lies in the fact that this method works independently of the size of the bead, the viscosity and index of refraction of the surrounding medium. This method uses the following equations for force calibration:

$$\boldsymbol{F_x} = \frac{\boldsymbol{D_x} \cdot \boldsymbol{R_D}}{\boldsymbol{c} \cdot \boldsymbol{R_L} \cdot \boldsymbol{\Psi}} \qquad (eq.2),$$

and

$$\boldsymbol{F_y} = \frac{\boldsymbol{D_y} \cdot \boldsymbol{R_D}}{\boldsymbol{c} \cdot \boldsymbol{R_L} \cdot \boldsymbol{\Psi}} \qquad (eq.3).$$

Where $\boldsymbol{D_x}$ and $\boldsymbol{D_y}$ are the signals of the deflection of the light that arrive to the PSDs; $\boldsymbol{R_D}$ is the effective detector radius; $\boldsymbol{c}$ is the speed of light ($\boldsymbol{c} = 2.997 \cdot 10^8$ m/s); $\boldsymbol{R_L}$ is the focal length of the objective lenses and $\boldsymbol{\Psi}$ is the power sensitivity of the PSDs. The values of $\boldsymbol{R_D}$, $\boldsymbol{R_L}$ and $\boldsymbol{\Psi}$ can be obtained from the manufacturer, but they can be also measured.

1.3.3 How do we isolate and manipulate individual molecules with optical tweezers? How do we measure activity?

In optical tweezers assays, a single molecule is tethered between two functionalized polystyrene beads, one of which is held in the optical trap (~3 μm in diameter) and the other (~2 μm in diameter) is placed on the top of a glass micropipette by suction. These beads serve as handles to manipulate individual molecules inside the flow chamber.

In our assays, a molecule of study, e.g. double-stranded DNA, single-stranded DNA, a DNA hairpin or a DNA-functionalized synthetic molecule, contains digoxigenin groups at one end to form an attachment with the anti-digoxigenin coated bead held in the optical trap and, at its other end, the molecule contains a biotin group, so it can be attached to the bead on top of the micropipette through biotin-streptavidin interaction. To isolate

individual molecules with optical tweezers, we follow the procedure shown in Figure 8: first, we flow streptavidin-coated beads (blue beads) into the flow chamber through one of the channels connected with the central (reaction) channel via a dispenser tube (Figure 8(1)). One of these beads is then trapped with optical tweezers and moved to be placed on top of the micropipette and fixed by suction (Figure 8 (2-3)). After that, we flow the beads functionalized with anti-digoxigenin (αDig), previously incubated with the molecules of study (yellow beads) and capture one of them with the optical trap (Figure 8 (4)). Then, the trapped bead covered with molecules of study that contain biotin groups is positioned over the bead on top of the pipette (Figure 8 (4)). Finally, we move the trapped bead in the Y direction to make an attachment with the bead on top of the micropipette via biotin-streptavidin interaction (Figure 8 (5-6)).

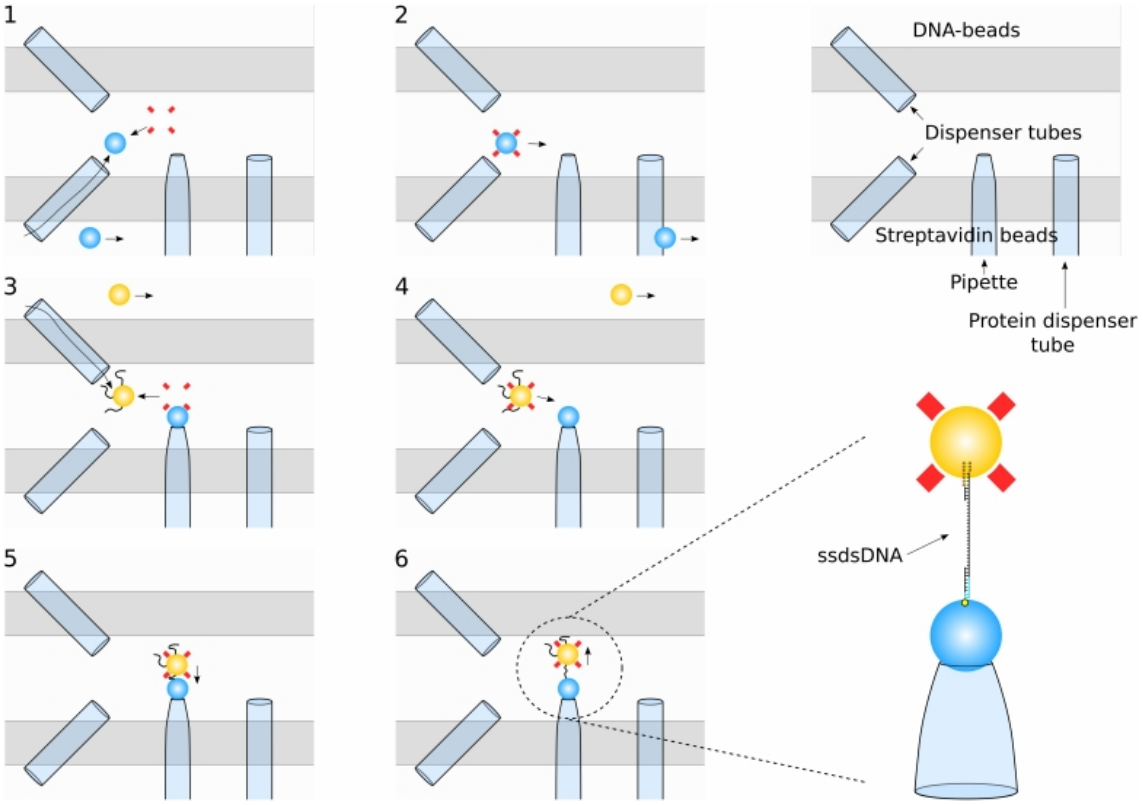

Figure 8. Isolation and manipulation of individual molecules with optical tweezers: **1** The polystyrene beads functionalized with streptavidin are introduced to the flow chamber through the lower channel (see Figure 7) after which they reach the reaction channel (the central channel in Figure 7) through a glass dispenser. **2** Once the beads arrive to the reaction channel, we capture one of them with the optical trap, place it on top of the micropipette and immobilize the bead via suction. **3** Polystyrene beads functionalized with anti-digoxigenin (αDig), previously incubated with the molecules of study (here, hybrid molecules containing ~1000 nt ssDNA segment, see section 2.3.4), are introduced to the flow chamber through the upper channel (Figure 7) connected to the reaction channel by a glass dispenser. **4** When the beads reach the central channel, we capture one of them with the optical trap and position it over the bead held by the micropipette. **5-6** We move the trapped bead with the optical trap in the Y direction, bringing it close to the bead on top of the micropipette to make an attachment.

In the MiniTweezers assays, a molecule tethered between the two beads (one held in the optical trap and the other on top of the micropipette) can be stretched by moving the optical trap away from the micropipette in the Y-axis (Figure 8 (6)). In this way, a force-extension curve characterizing the mechanical properties of the molecule can be recorded. The molecular extension at each force is calculated as the difference between the initial and the current positions of the optical trap, $\boldsymbol{\Delta x_{trap}}$, (it is obtained from the measured deflection of light) minus the force-induced displacement of the bead from the center of the optical trap $\boldsymbol{F/k}$. However, it is important to note that, in our experimental setup, the end-to-end distance of the tethered molecule cannot be measured precisely, because the bead on top of the micropipette is fixed and it cannot rotate, whereas the bead in the optical trap can do it.

Typically, in our experiments, activities were measured in the force-feedback mode of operation. In this mode, , the molecule attached between the two beads is held under constant tension via feedback-stabilized protocol, which is capable of maintaining a preset force within ~0.05 pN by moving the beads closer or further apart. In the force-feedback mode, the bead displacement within the trap is fixed, and it is the displacement of the trap relative to the bead on top of the micropipette that directly measures the change in extension of the molecule as a result of an activity.

Chapter 2

TOWARDS MECHANO-CHEMICAL CHARACTERIZATION OF THE HUMAN MITOCHONDRIAL REPLISOME

2.1 Introduction

2.1.1 Mitochondria

Mitochondria are eukaryotic organelles, responsible for the generation of ATP molecules inside the cell. Mitochondria also have many other important functions: including calcium signaling ([68], [69]) and cell death or apoptosis ([70], [71]).

Mitochondria are surrounded by two membranes, which divide the organelle into four different compartments with their own functions: the smooth outer membrane, the greatly folded inner membrane, the intermembrane space and the matrix (Figure 9). The outer membrane includes porins that form pores and make the mitochondrial membrane permeable for substances with the molecular mass up to 5 kD [68]. The inner membrane of mitochondria, in contrast, is highly impenetrable, so most molecules require transporters to cross it. The inner membrane is characterized by high protein content, most of which are transporters, carrying proteins into the matrix, and proteins involved in the electron transport and ATP synthesis. The mitochondrial matrix contains most of the enzymes responsible for the citric acid cycle reactions.

In the electron transport chain, electrons are passed from protein complex to protein complex until they are passed to oxygen to form water. As electrons are passed along the chain, protons are pushed out of the mitochondrial matrix into the intermembrane space. This creates an electrochemical gradient across the inner membrane. The energy of this gradient is used by the ATP synthase to catalyze the conversion of ADP into ATP molecules [72], see Figure 9.

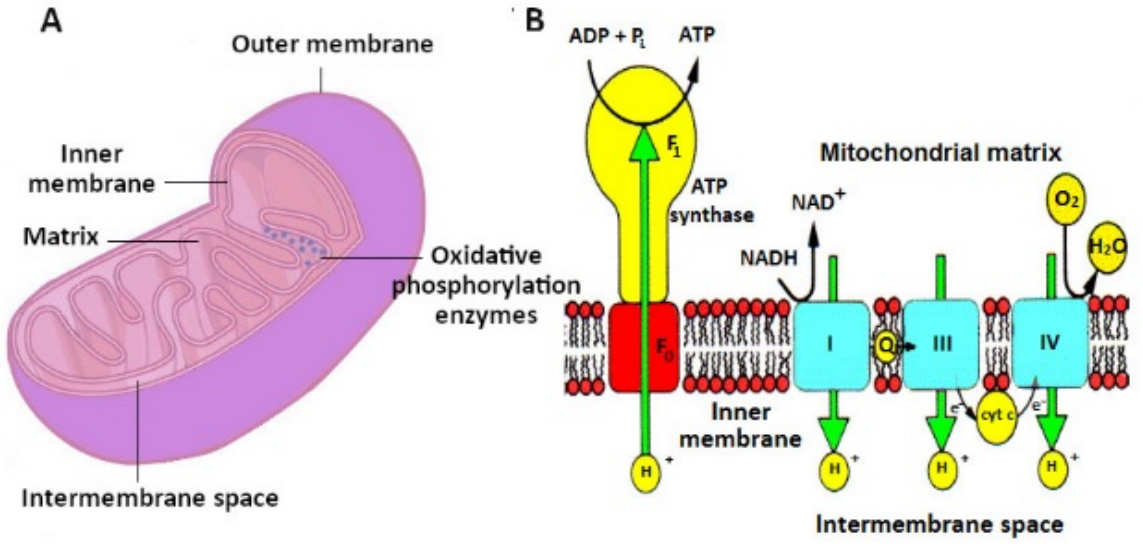

Figure 9. A. An illustration of the structure of mitochondria. Mitochondria are enclosed by two membranes: the outer and the inner mitochondrial membranes, which are separated by the intermembrane space. The inner membrane encloses the plasmatic mitochondrial matrix, which contains most of the enzymes participating in oxidative phosphorylation. **B** A schematic representation of the electron transport chain. While electrons are passed through protein complexes (colored in cyan), protons are pushed out of the mitochondrial matrix. ATP synthase uses the energy of proton gradient to produce ATP molecules out of ADP and phosphate.

Mitochondria play also a crucial role in Ca^{2+} signaling because they regulate the concentration of calcium ions in the cytosol of the cell by taking up Ca^{2+} by means of mitochondrial calcium uniporter complex ([73] - [75]) and by transporting Ca^{2+} into the cytosol via antiporters, exchanging Ca^{2+} with Na^{+} or H^{+} ([76], [77]). Moreover, accumulation of Ca^{2+} in mitochondria regulates the ATP production by oxidative phosphorylation through modulation of three Ca^{2+}-sensitive dehydrogenases of the Krebs cycle [78]. Under pathological conditions of mitochondrial Ca^{2+} overload, Ca^{2+} uptake by mitochondria might lead to cell death [79].

Additionally, mitochondria play a central role in the intrinsic apoptotic pathway: they release cytochrome c that together with apoptotic protease activating factor 1 (Apaf-1) forms the cytosolic ‘apoptosome’, which, by activation of caspase 9, triggers the caspase cascade, leading to apoptotic cell death [80].

Mitochondria have their own genome that in humans presents a circular 16,569 bp long DNA (mtDNA). Human mitochondrial DNA contains 37 genes coding for 13 protein components of the oxidative phosphorylation system, 22 transport RNA (tRNA) and 2 ribosomal RNA (rRNA) [81]. Human cells contain thousands of mitochondrial DNA copies.

Accumulation of mtDNA defects in the form of point mutations, deletions or depletion may cause so-called mitochondrial diseases that in humans affect organs strongly dependent on mitochondrial functionality, such as heart, skeletal muscles, brain and kidneys [82]. Due to the essential roles of mitochondria in cell metabolism, failure of mtDNA replication has been also related with premature aging [83] and some forms of cancer ([84], [85]).

The occurrence of such diseases is associated with the accuracy and effectiveness of mitochondrial DNA replication (see the next section), hence understanding the molecular processes governing mtDNA replication may help to determine the molecular bases of mitochondrial pathology.

2.1.2 Human mitochondrial DNA replication

2.1.2.1 Human mitochondrial DNA replication complex

The so-called human mitochondrial 'minimal replisome', a complex that is capable of processive DNA synthesis, is composed of three proteins: Human mitochondrial polymerase γ holoenzyme (Pol γ), human mitochondrial DNA helicase (TWINKLE) and human mitochondrial single-stranded DNA binding proteins (Hm mtSSB) [86].

Polymerase γ is the only known polymerase, working at the human mitochondrial DNA replication fork [87]. Pol γ holoenzyme is a heterotrimer that contains one catalytic subunit (Pol γA) and two accessory subunits (Pol γB). Pol γA possesses both, polymerase and exonuclease activities, the last one needed for proofreading the newly synthesized DNA primer. Pol γB increases the processivity of Pol γ by increasing the enzyme's affinity to the DNA template, increasing the polymerization rate and diminishing the exonuclease activity of Pol γ [88]. The domains for polymerase and exonuclease in the catalytic subunit are separated by a linker. Pol γA adopts the canonical polymerase 'right-hand' configuration with the 'finger', 'palm' and 'thumb' subdomains that bind template DNA and substrate nucleotide triphosphate [89] (Figure 10). The process of nucleotide incorporation is coupled with cyclic conformational changes (between open and closed conformations) in the catalytic subunit. A nucleotide incorporation cycle starts with the polymerase binding an incoming nucleotide, which leads to rotation of the fingers from open to closed conformation undergoing a number of intermediate states. Finger-closing, which results in the formation of a tight binding pocket, allows the exclusion of incorrectly bound nucleotides ([90], [91]). Then, the polymerase catalyzes the formation of a phosphodiester bond between the incoming deoxynucleoside triphosphate and the terminal primer nucleotide with the release of a pyrophosphate, which provokes another conformational change in the polymerase, from closed to open state. Then the polymerase translocates to the next 3′-OH primer terminus and the whole system is ready to a new nucleotide incorporation cycle ([92], [93]).

The catalytic subunit of Pol γ, Pol γA, contains 3′-5′ exonuclease domain connected to the polymerase domain through a spacer region [94]. The exonuclease domain eliminates (mainly) mispaired nucleotides during mtDNA replication by reversing the direction of the polymerase. The incorporation of an incorrect nucleotide during replication by Pol γ disrupts the interactions with the polymerase active site which provokes shuttling of the primer strand to the exonuclease site ([95], [96]). The proofreading ability of Pol γ via its exonuclease activity contributes to the high average fidelity of the polymerase (e.g. pig liver and chick embryo Pol γ commit one error in ~ 500,000 and 260,000 incorporated nucleotides respectively ([97], [98])).

As for many other replicative DNA polymerases ([99] - [102]), Pol γ presents a limited strand displacement activity *in vitro* (1-2 nt, [103]), it cannot use dsDNA as template for DNA synthesis. At a nick, Pol γ has been shown to idle at the 5' end of the primer; the nucleotides added during strand displacement are subsequently degraded by the 3'-5' exonuclease activity until the polymerase returns to the nick position. The *pol-exo* balance prevents extensive strand displacement at a nick and ensures in this way the generation of ligatable ends upon completion of H-strand synthesis ([103], [104]). Interestingly, as reported for several other DNA polymerases ([105] - [108]), mutations that impede exonuclease activity disrupt the *pol-exo* balance of Pol γ, which results in significant strand displacement activity of exonuclease deficient mutant (up to 30-40 for Pol γ exo-, ([109], [110]). These observations indicate that Pol γ presents an intrinsic ability to catalyze strand displacement, which is masked by the exonuclease contribution. Therefore, at the fork junction, modulation of the *pol-exo* balance of Pol γ by the other components of the replication machinery would be absolutely required to promote efficient DNA synthesis without compromising fidelity. In addition, this modulation facilitates the intrinsic strand displacement synthesis of Pol γ, which would contribute to the unwinding of the fork. In fact, the poor *in vitro* DNA unwinding activity of the mitochondrial helicase TWINKLE ([86], [111]), suggests a significant contribution of Pol γ to the strand displacement reaction during leading strand synthesis.

The mitochondrial DNA helicase (**TWINKLE**) forms a stable ring-shaped hexamer that adopst a compact two-level arrangement surrounding a central channel (Figure 10) [112]. During replication, TWINKLE uses the energy of nucleotides hydrolysis to translocate unidirectionally (in the 5' to 3' direction) along single-stranded DNA and helps in the unwinding of the duplex DNA fork [113]. The exact mechanism by which TWINKLE loads onto DNA is unclear, however a recent study has demonstrated that TWINKLE oligomers exist in both, open- and closed-ring conformations, which suggests that the helicase loads onto DNA in an open-ring configuration [114]. Like T7 gene 4 protein, TWINKLE needs both, 5' and 3' stretches of single-stranded DNA to be able to efficiently initiate unwinding ([115], [116]). The minimal length of the 5' tail that permits efficient DNA unwinding by TWINKLE is 15 nucleotides [113]. It has been demonstrated that TWINKLE can also load onto circular ssDNA without the assistance of any special loader and it can support initiation of DNA synthesis on a closed circular

dsDNA substrate together with Pol γ ([117], [114]). TWINKLE can bind ssDNA in two different sites: in the central channel of the ring and on its outer surface [118]. This data suggests that TWINKLE unwinds dsDNA by steric exclusion mechanism, in which the helicase threads one of the DNA strands through its central channel, while the other strand is displaced away from the outer surface of the hexamer by steric exclusion ([119], [120]).

In the absence of other components of the replisome (Pol γ, mtSSB), the human mitochondrial DNA helicase has a very poor unwinding activity: *in vitro* studies have shown that TWINKLE unwinds only DNA duplexes shorter than 20 bp ([113], [111], [121]). The poor helicase activity of an isolated TWINKLE might prevent a possible extensive DNA unwinding when the helicase is uncoupled from the polymerase.

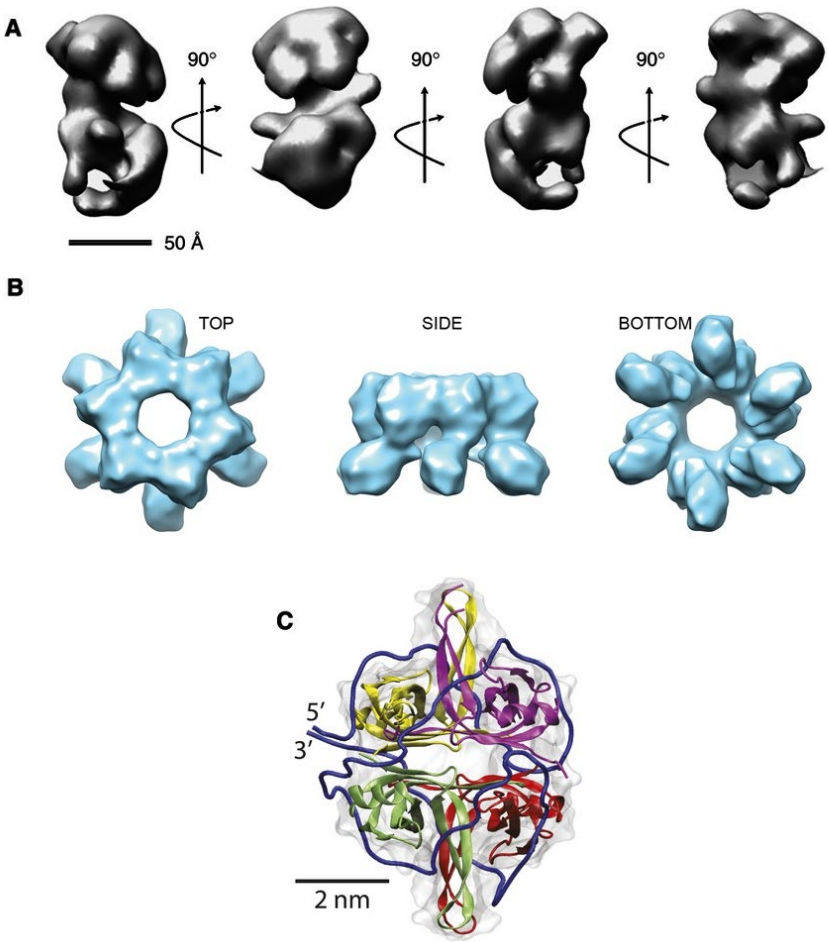

Figure 10. A The EM structure of the pol γ holenzyme. Each of the four images is rotated by 90^0 in respect to its neighbours (taken from [122]) **B** The 3D reconstruction of the structure of the TWINKLE hexamer (from EM and SAXS data, [112]). The top, side and bottom views. **C** Crystal structure of the *E. Coli* SSB tetramer wrapped by ssDNA (taken from [123]).

In addition to its helicase activity, TWINKLE has shown an ability to anneal two complementary DNA strands [124]. It was demonstrated in [118] that the annealing function of TWINKLE is important for strand exchange between an unwinding substrate and a homologous single DNA strand. It was also shown in that work that TWINKLE possesses the ability to catalyze branch migration by resolving a four-way Holiday Junction DNA. These results may indicate the involvement of this protein in the recombinational repair of the human mtDNA. The low processivity (the number of unwound nucleotides) of the helicase might be explained by the annealing activity of the protein, which might compete with the unwinding. While TWINKLE needs the energy of nucleotides hydrolysis, its annealing activity is independent of NTP [118].

The human mitochondrial single-stranded DNA binding protein (**mtSSB**) is structurally similar to SSB from *Escherichia coli* (EcoSSB) (see Figure 10), and as its prokaryotic homolog, it forms stable homotetramers in solution and binds ssDNA with great affinity (2 nM) and in a sequence independent manner ([125] - [127]). During the process of mitochondrial DNA replication, human mtSSB covers the parental heavy single-stranded DNA (see below), which is gradually displaced during mtDNA replication, protecting it against degradation and preventing secondary structure formation. ([128], [121], [129]).

In our lab, we have shown that the human mtSSB can bind DNA in two modes: in a low binding site size mode, it wraps ~30 nucleotides ($mtSSB_{30}$) of single-stranded DNA, and in a high binding site size mode, each SSB tetramer binds 60 nucleotides of ssDNA ($mtSSB_{60}$) [53]. The mtSSB binding mode is modulated by the concentration of magnesium and sodium ions, as well as by the protein concentration in a very similar way to that shown for EcoSSB ([130], [131]): low salt and/or high SSB concentrations favor the low binding mode, whereas high salt and/or low SSB concentrations favor the high binding mode. We also have shown that when SSB binding occurs concomitantly with DNA replication the low binding site size mode ($mtSSB_{30}$) is selected for all mtSSB concentrations tested, suggesting this mode as the relevant mode for DNA replication. This behavior was later proposed to occur for the EcoSSB too [132].

It is known that human mtSSB has a stimulatory effect on the unwinding activity of TWINKLE ([113], [121]). The primer extension activity of Pol γ is also stimulated by mtSSB: mtSSB enhances primer recognition and binding by Pol γ, decreases non-specific binding of the polymerase to the DNA template, increases processivity [133] and promotes the maximum replication rate of the holoenzyme by eliminating the secondary structure of the template ([134], [135], [121]). However, to date, little is known about the effect of mtSSB on strand-displacement activity of Pol γ.

2.1.2.2 Mitochondrial DNA replication and disease

Mutations in any of the components of mtDNA replication machinery may result in mitochondrial dysfunction:

1. Defects in Pol γA are associated to a number of disorders, such as autosomal dominant progressive external ophthalmoplegia (adPEO), a disease related to a progressive accumulation of mtDNA deletion in post-mitotic tissue [136], Alpers syndrome and other infantile hepatocerebral syndromes, ataxia-neuropathy syndromes and idiopathic parkinsonism ([137], [138]). Mutations in Pol γB, which affect the processivity of the catalytic subunit, are also known to be associated with PEO [139].

2. Mutations in TWINKLE are related to deletions or depletion of mtDNA, which may cause autosomal dominant PEO, cardiomyopathy, ataxia and parkinsonism ([140], [141]).

3. Mutations in human mtSSB cause deletions in mtDNA [142]. MtSSB deficiency has been shown to be associated with human breast cancer [143].

2.1.2.3 Models of mitochondrial DNA replication

Currently, there is no consensus regarding the mechanism by which mammalian mtDNA is replicated. The model most supported by experimental observations is the *strand displacement model*. According to this model, the synthesis of the two DNA strands is continuous, unidirectional, asymmetrical and unsynchronized ([144], [145]). The synthesis of the leading (heavy) strand begins at a site denominated as O_H by the coordinated action of Pol γ, TWINKLE and mtSSB (Figure 11). As the DNA synthesis progresses, mtSSB gradually binds the displaced parental (heavy) strand. When the replication fork has advanced approximately two-thirds of the genome, it exposes the origin of the lagging (light) strand synthesis, O_L, and forms a stem-loop structure that blocks SSB binding in this region [146]. Then, POLRMT synthetizes a 25 bp primer, so a new Pol γ can initiate the lagging strand synthesis [147]. A strong *in vivo* evidence for the strand displacement mechanism of mtDNA replication was reported by the group of Maria Falkenberg in 2014 [148]. In that work, it was demonstrated that during mtDNA replication, mtSSB binds exclusively the heavy strand and that the protein is not equally distributed over the genome: the levels of mtSSB are higher just downstream of the D-loop region and the mtSSB occupancy decreases towards the O_L.

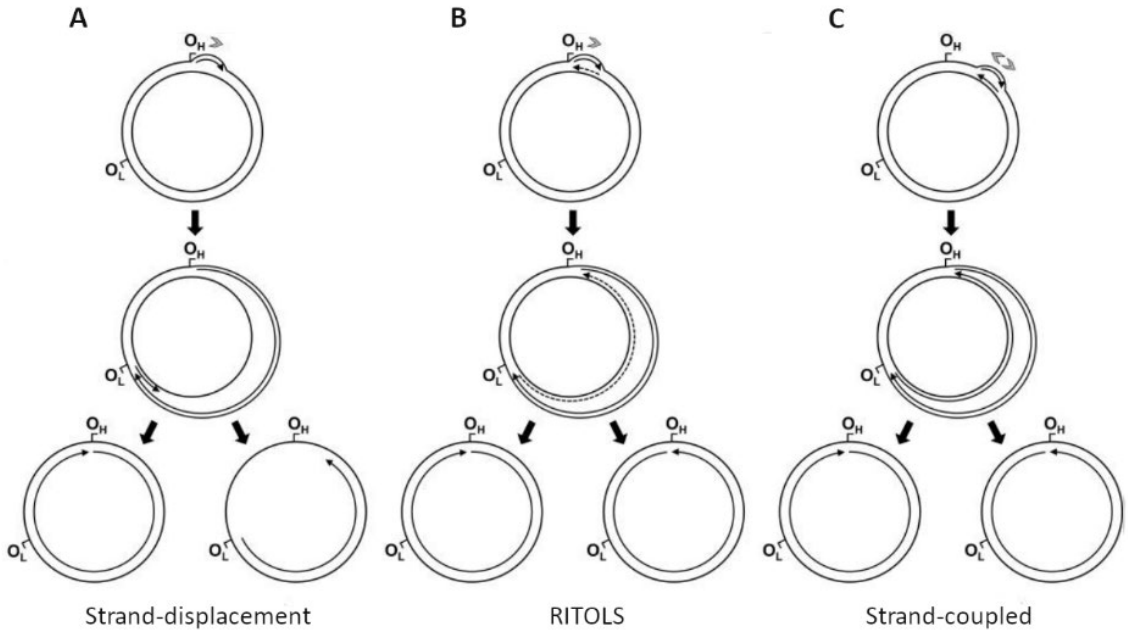

Figure 11. Different models for mitochondrial DNA replication. **A** The strand displacement model. **B** The RNA incorporated throughout the lagging strand model (RITOLS) **C** The strand-coupled model (The image is taken from [149]).

30 years after the introduction of the strand displacement model, two other models for mitochondrial DNA replication have been suggested: the RNA Incorporated Throughout the Lagging Strand model (RITOLS) [150] and the strand-coupled model [151]. Both of these models are primarily based on mtDNA replication intermediates observed using neutral 2D agarose gel electrophoresis (aka 2d-AGE).

According to the RITOLS model, the DNA synthesis, as in the strand displacement model, is unidirectional and asymmetric and it starts at two origins of replication, the origin of the leading strand synthesis (O_H) and the origin of the lagging strand synthesis (O_L), but in this model, during the leading strand synthesis, the parental heavy strand is covered with RNA fragments (Figure 11B), which are replaced or converted to DNA during the lagging strand synthesis [150].
In the strand-coupled model, the synthesis of the leading and the lagging strands is coupled. The replication begins at multiple sites across a broad initiation region and it progresses bidirectionally (Figure 11C) till the fork is arrested at O_H [152] .

It has been proposed that all these mechanism may occur depending on cell type, cell cycle and environmental conditions.

2.2. Open questions and objectives

To date, little is known about how the three main constituents of the mtDNA replication machinery orchestrate their activities at the replication fork. In order to understand the molecular basis of the synergy and coordination between the mitochondrial polymerase, helicase and SSB during leading strand synthesis we propose to address the following questions: How does the helicase couple its single- and double- stranded DNA binding activities with translocation and unwinding of the DNA? What is the effect of Pol γ on the real-time kinetics of the helicase? What is the mechanism used by Pol γ to destabilize the fork junction? Which protein destabilizes the fork junction to a greater extent? How do the two individual enzymes assist each other? How does the mtSSB modulate the real-time kinetics of Pol γ and TWINKLE at the replication fork? What is the specific role of the mtSSB on the reaction? Answering these questions is relevant for a better understanding of the mitochondrial biogenesis and, it will also shed light into the general mechanisms by which related replication systems work at the molecular level. Please, see Methodology section for the experiments specifically designed to answer these questions.

In order to answer these questions, in this thesis, we proposed the aim to characterize the functional coupling between the mitochondrial replication proteins during leading strand DNA synthesis.

Our specific objectives were:

1. To characterize the real-time kinetics of Pol γ activity during strand displacement synthesis, determine the mechanism used by the polymerase to couple DNA replication and DNA unwinding, and to quantify the energy applied by the polymerase at the fork junction to unwind the DNA helix.

2. To determine the effect of mtSSB proteins on the strand displacement activity of Pol γ,

3. To characterize the DNA unwinding activity of the mitochondrial helicase, TWINKLE, to determine the 'real-time' kinetics of helicase translocation and unwinding and quantify the DNA unwinding mechanism of the helicase.

4. To determine the effect of mtSSB on the activity of TWINKLE

5. To characterize the coupling between the polymerase and the helicase activities at the replication fork.

6. To establish the conditions to measure at the single-molecule level the coordinated activity of the constituents of the minimal mitochondrial replisome: Pol γ, TWINKLE and mtSSB.

2.3 Materials and methods

2.3.1. Overexpression and purification of the protein components of the human mitochondrial replisome

All protein components used in this thesis were overexpressed and purified in the laboratory of Prof. L.S. Kaguni (Michigan State University, USA). Briefly, recombinant catalytic (Pol γA) and accessory (Pol γB) subunits of human Pol γ were prepared from S*f9* and bacterial cells. Pol γA was purified by phosphocellulose chromatography and Ni-NTA affinity chromatography followed by glycerol gradient sedimentation. Pol γB was purified by nickel-nitrilotriacetic acid (Ni-NTA) chromatography and sedimentation in a glycerol gradient [153]. The Pol γA exo- variant was purified following the same procedure as in the case of the wild-type bn catalytic subunit.

Recombinant mtSSB proteins were overexpressed in *E. coli* cell cultures and purified in two steps: by affinity chromatography using Blue Sepharose and sedimentation in a glycerol gradient [153].

Recombinant mitochondrial DNA helicase, TWINKLE, was prepared from S*f9* cells. The helicase was purified via Ni-NTA chromatography followed by heparin sepharose chromatography and glycerol gradient sedimentation [154].

2.3.2. Preparation of functionalized polystyrene beads

It was mentioned above that in experimental assays of this thesis we used plastic beads of two types: polystyrene beads functionalized with streptavidin (~2 μm in diameter) and beads functionalized with anti-digoxigenin (~3 μm in diameter).
The beads functionalized with streptavidin were purchased from Spherotech. The anti-digoxigenin-coated beads were prepared in the following way:

1. 750 μl of polystyrene beads coated with protein G (purchased from Kisker Biotech) were added to a 1.5 ml micro-centrifuge tube and centrifuged for 6 minutes at 3,000 rpm and after the centrifugation the supernatant was discarded.

2. The remaining pellet was diluted in 750 μl of crosslinking buffer (containing 100mM NaCl and 100mM Na_2HPO_4).

3. Afterwards, 22.5 μl of DMP (50 μg/ μl) and 45 μl of α-dig antibody (1 μg/μl) were added to the diluted beads. The obtained solution was mixed thoroughly and incubated for 1 hour at room temperature on a micro-centrifuge tube shaker set at

1,000 rpm. The crosslinking reaction ensures covalent bonds between the α-dig antibody and the protein G-covered polystyrene beads.

4. After the incubation, the solution was centrifuged for 6 minutes at 1,000 rpm and, after that, the supernatant was discarded.

5. 750 µl of Tris-HCl pH 7.5 were added to the remaining pellet and the obtained mixture was incubated for 2 hours on a micro-centrifuge tube shaker set at 1,000 rpm to quench the crosslinking reaction.

6. Then, the total volume of the sample was divided into two different 1.5 ml micro-centrifuge tubes and 750 µl of ultra-pure water were added to each of them.

7. The two micro-centrifuge tubes were centrifuged for 6 minutes at 3,000 rpm. Afterwards, the supernatant was discarded and the pellet containing the beads was eluted with 750 µl of PBS 7.4. The step number 7 was repeated 3 times.

8. The content of the two tubes was mixed in a single tube and centrifuged again for 6 minutes at 3,000 rpm. Afterwards, the supernatant was discarded.

9. The remaining pellet was eluted in 1 ml PBS 7.4, divided into 50 µl aliquots and stored at 4 ºC.

2.3.3 DNA hairpin preparation

To study the strand displacement activity of Pol γ and unwinding activity of TWINKLE we used DNA hairpins (Figures 12 and 13), which we prepared in the following steps:

2.3.3.1 Preparation of the unwinding segment

The main unwinding segment containing one, two and three repetitions of the GCC cluster separated by 97 bp of a low GC content sequence was prepared by PCR amplification of a 410 bp long fragment of the pUC57 vector using the following protocol:

1. In a 250 µl PCR tube, 1 µl of the dNTP mix (10 mM of each dNTP) was mixed with 2 µl of each of the oligonucleotide primers (5'-AACATCCGCCGCCGTCGACTTATGATACATTC-3' and 5'-GCGGCCAGTGAATTCATGTTCATTCTAATC-3'), 5 µl of the 10x PCR

buffer, 1 µl of pUC57 DNA and 0.5 µl of Taq DNA polymerase (5 U/ µl) and filled to 50 µl with ultra-pure water.

2. The thermal cycler was configured as follows: **step 1**: 3 minutes, 94 ºC. **Step 2**: 1 minute, 94 ºC. **Step 3**: 1 minute, 57 ºC. **Step** 4: 2.5 minutes, 72 ºC. The steps 2-4 were repeated 30 times. **Step 5**: 10 minutes at 72 ºC.

3. After the PCR, the amplified DNA was purified using a commercial DNA purification column and it was eluted in a final volume of 30 µl.

4. 500 ng of the PCR product were digested with 1.5 µl of *EcoRI* (20 U/ µl) in a final reaction volume of 30 µl containing 3 µl of 10x *EcoRI* restriction buffer for 2 hours at 37 ºC.

5. The product of the digestion was purified in a final volume of 30 µl using a commercial DNA purification column.

6. Then, the purified DNA was digested with 1.5 µl of *SalI* (20 U/ µl) in a final reaction volume of 50 µl containing 5 µl of 10x *SalI* restriction buffer for 2 hours at 37 ºC.

7. The unwinding segment, digested with the restriction endonucleases *EcoRI* and *SalI*, was purified in a final volume of 30 µl using a commercial DNA purification column.

2.3.3.2 Preparation of digoxigenin-labelled dsDNA handles

The digoxigenin-labelled dsDNA handles were prepared by PCR amplification of an 827 bp long fragment of the PUC18 vector in the presence of Digoxigenin-11-dUTP using the following protocol:

1. The dNTP-DIG-mix for the PCR was prepared as follows: In a 1.5 ml micro-centrifuge tube, 6 µl of dATP, 6 µl of CTP, 6 µl of dGTP and 3 µl dTTP (all dNTPs at 10mM) were mixed with 3 µl of digoxigenin-labeled dUTP (DIG-dUTP 10 mM) and the obtained mixture was filled up to the volume of 75 µl with ultra-pure water.

2. In a 250 µl PCR tube, 25 µl of the dNTP-DIG-mix were mixed with 2 µl of each of the PCR oligonucleotide primers (1 mM, 5'-CCTCTGACACATGCAGCTCC-3' and 5'-CGCGGCCTTTTTACGGTTCC-3'), 10 µl of the 10x PCR buffer, 1 µl of PUC18 DNA (100 ng/ µl) and 2 µl of

Taq DNA polymerase (5 U/ µl), and the obtained mixture was filled to 100 µl with ultra-pure water.

3. The thermal cycler was configured as follows: **step 1**: 3 minutes, 94 ºC. **Step 2**: 1 minute, 94 ºC. **Step 3**: 1 minute, 60 ºC. **Step 4**: 2 minutes, 72 ºC. The steps 2-4 were repeated 29 times. **Step 5**: 10 minutes at 72 ºC.

4. The PCR product was purified using a commercial DNA purification column and eluted in a final volume of 30 µl.

5. The purified PCR product was digested with 1 µl of *BamHI* (20 U/ µl) in a final reaction volume of 40 µl containing 4 µl of 10x *BamHI* restriction buffer and 5 ml of ultra-pure water. The digestion was carried out at 37ºC for 2 hours.

6. The product of the digestion was purified in a final volume of 30 µl using a commercial DNA purification column.

7. Afterwards, the resulting DNA products were checked by agarose gel electrophoresis.

2.3.3.3 Preparation of a dsDNA spacer

A DNA segment of 2,664bp, used as a spacer to separate the two polystyrene beads and to facilitate the manipulation and identification of single DNA hairpins, was prepared via the following protocol:

1. 600 ng of the PUC19 DNA vector were digested with 1.5 µl of *BamHI* (20 U/ µl) in a final volume of 30 µl containing 3 µl of *BamHI* 10x reaction buffer for 1 hour at 37 ºC.

2. The product of the digestion was purified in a final volume of 30 µl using a commercial DNA purification column.

3. Then, the purified DNA was digested with 1.5 µl of *PstI* (20 U/ µl) in a final reaction volume of 50 µl containing 5 µl of 10x *PstI* restriction buffer for 2 hours at 37ºC.

4. The obtained *BamHI-PstI* PUC19 DNA was purified in a final volume of 30 µl using a commercial DNA purification column.

2.3.3.4 Preparation of a linker DNA segment

The DNA linker was prepared by annealing two partially complementary DNA oligonucleotides (5'-Biot $(dT)_{30}$CAATCACTTCAGGTAGCATC-3' and 5'-AATTGATGCTACCTGAAGTGATTGGCTGATGCA-3'). The DNA product of the annealing reaction contains two distinctive ends (Figure 12): one end, contains a 5' protruding terminus complementary to *EcoRI* restriction sequence, whereas the other end contains a 3' protruding terminus complementary to *PstI* restriction sequence and a $(polydT)_{30}$ 5' tail labeled with biotin. The annealing was carried out as follows:

1. In a 1.5 ml micro-centrifuge tube, the equimolar concentrations of the two partially complementary oligonucleotides were mixed with the annealing buffer to reach the final volume of 100 µl.

2. The annealing reaction was carried out at 95 ºC for 10 minutes in a thermo-shaker, then the heating was switched off and the reaction mixture was left for ~2 hours to cool down to the room temperature.

3. Afterwards, the sample was diluted 1/500 and stored at -20 ºC in 20 µl aliquots.

2.3.3.5 Preparation of a DNA loop for hairpin apex

To prepare a DNA loop for hairpin apex, a self-annealing DNA oligonucleotide (5'-[Phos]-TCGAGCCGATGCACG[abasic]ATAACGTGCATCGGC-3') was diluted to a final concentration of 100 ng in annealing buffer. The self-annealing was carried out at 95 ºC for 10 minutes in a thermo-shaker, then the heating was switched off and the reaction mixture was left for ~2 hours to cool down to the room temperature. The obtained sample was diluted 10 times and stored at -20 ºC in aliquots.

2.3.3.6 Preparation of the final DNA hairpin constructs

The final hairpin constructs were produced after two consecutive ligation steps (Figures 12 and 13):

Ligation I:

The first ligation was carried out following this protocol:

1. In a 1.5 ml micro-centrifuge tube, 230 ng of the unwinding segment (digested with *BamHI* and *EcoRI*, see 2.3.3.1) were mixed with 1.5 µl of the linker DNA segment (2.3.3.4), 2 µl of the DNA loop (2.3.3.5), 3 µl of 10x T4 reaction buffer and 1.5 µl of T4 ligase. The obtained mixture was filled with ultra-pure water to reach the final reaction volume of 30 µl.

2. The reaction was carried out at 16 ºC overnight.

3. Then, the DNA product of the ligation was purified using a commercial DNA purification column, eluted in 30 µl of water and stored at -20 ºC.

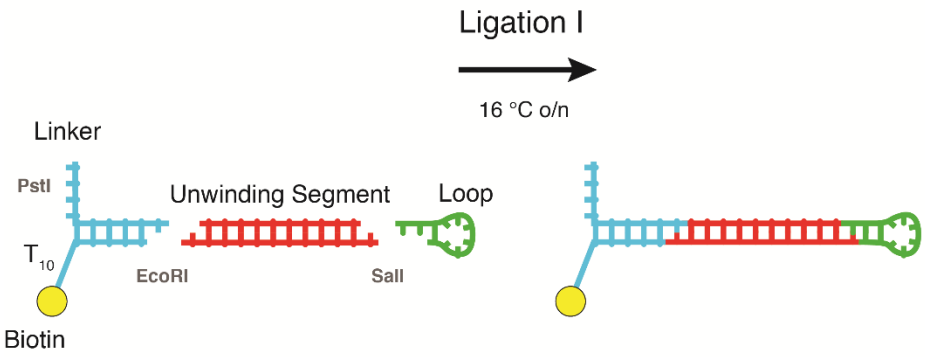

Figure 12. In the first step of the hairpin construct preparation, the unwinding segment digested with *EcoRI* and *SalI* restriction endonucleases is ligated to the loop segment and the linker segment labelled with biotin.

Ligation II:

The second ligation step was carried out as follows:

1. In a 1.5 ml micro-centrifuge tube, 15 µl of the Ligation I were mixed with 7 ng of the DNA spacer (2.3.3.3), 0.5 µl of the digoxigenin-labelled DNA handles (section 2.3.3.2), 3 µl of 10x T4 reaction buffer and 1.5 µl of T4 ligase. The mixture was filled with ultra-pure water to reach the final reaction volume of 30 µl.

2. The reaction was carried out at 16 ºC overnight.

3. Afterwards, the DNA product of the ligation was purified using a commercial DNA purification column, eluted in 30 µl of water and stored at -20 ºC.

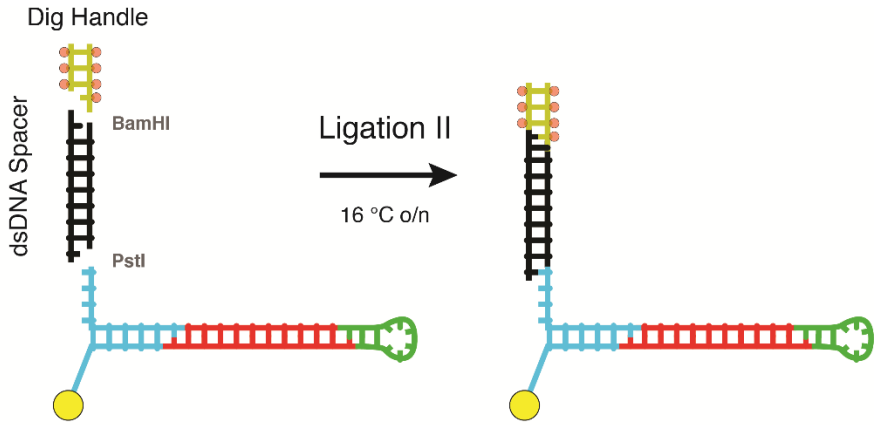

Figure 13. In the second step, the dsDNA spacer digested with *BamHI* and *PstI* restriction enzymes is ligated to the product of Ligation I and the digoxigenin-labelled DNA handle (Dig Handle, section 2.3.3.2).

2.3.4 Preparation of hybrid single-double-stranded DNA (ssdsDNA) molecules for manipulation with optical tweezers

All procedures for ssdsDNA preparation were carried out at room temperature unless otherwise specified. Figure 14 shows a schematic diagram of the preparation protocol.

2.3.4.1 Preparation of hybrid single-double-stranded DNA molecules (ssdsDNA)

ssdsDNA hybrid molecules containing ~1000 nt ssDNA segment were prepared as follows:

1. In four 1.5 ml micro-centrifuge tubes, 2 µg of pBacgus11 DNA plasmid were mixed with 3 µl of 10x *NBbvCI* reaction buffer and 1.8 µl of the *NBbvCI* (10 U/ µl) nicking enzyme. The mixture was filled with ultra-pure water to a final volume of 30 µl and the obtained solution was mixed gently.

2. Then, the mixture was incubated at 37 ºC for 1 h.

3. Afterwards, *NBbvCI* was inactivated by heating the sample for 20 minutes at 80 ºC

4. After the inactivation of the nicking enzyme, 0.5 µl of *Exonuclease III* (100 U/ µl) were added to the reaction mixture and it was incubated for 6 minutes at room temperature.

5. Afterwards, EDTA was added to the reaction solution (the final EDTA concentration: 40 mM) to stop *Exonuclease III* reaction.

6. Then, *proteinase K* was introduced to the reaction solution (the final *proteinase K* concentration: 50 µg/ml) and the mixture was incubated at 55 ºC for 1 hour and 30 minutes. Further, the sample was allowed to cool down to room temperature.

7. The content of the four micro-centrifuge tubes was combined and the obtained ssdsDNA was purified using one column of a commercial DNA purification kit. Then, ssdsDNA was eluted in a final volume of 30 µl.

8. Then, the purified ssdsDNA was digested with 0.8 µl of *HindIII* (20 U/ µl) and 0.8 µl of *BamHI* (20 U/ µl) restriction enzymes at 37ºC during 2 hours in a final volume of 50 µl.

9. The product of the digestion was purified using a commercial DNA purification column and stored at -20 ºC.

10. The length of the ssDNA gap generated by the *Exonuclease III* activity was estimated by alkaline agarose gel electrophoresis.

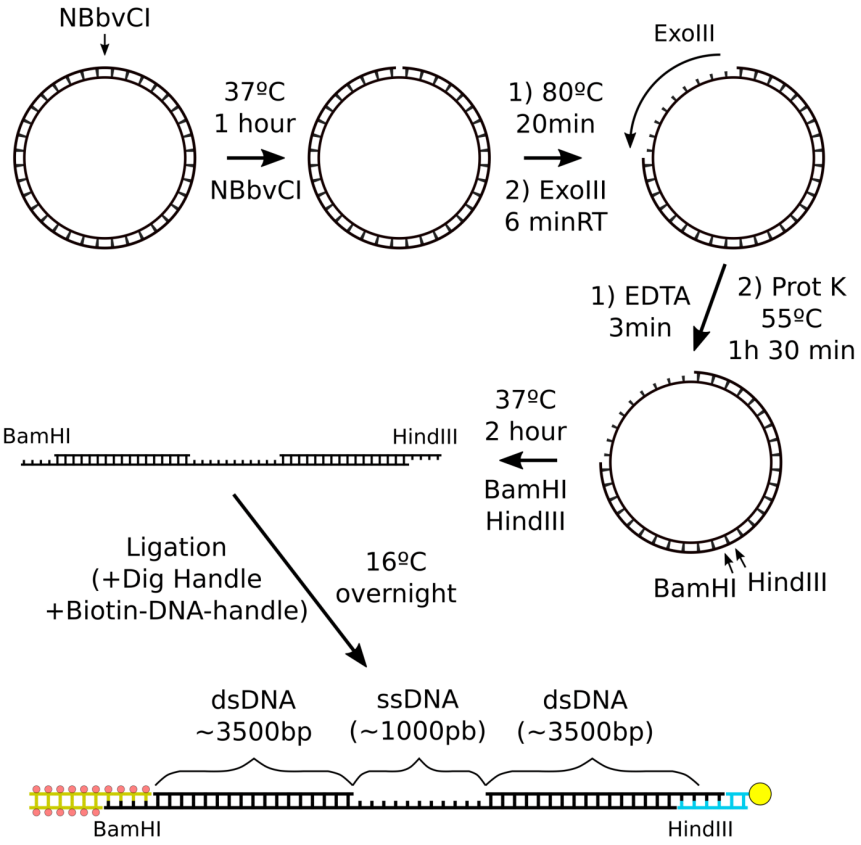

Figure 14. A schematic diagram of preparation of hybrid single-double-stranded DNA (ssdsDNA) molecules for manipulation with optical tweezers. First, pBacgus11 DNA plasmid (8041 bp) is cut with *NBbvCI* nicking enzyme. After the nicking enzyme is deactivated (at 80 ºC for 20 minutes), the DNA is incubated with *Exonuclease III* enzyme for 6 minutes at room temperature. Over this time, *Exonuclease III* generates a fragment of ssDNA of a size of ~1000 nt. Then, *Exonuclease III* is deactivated with EDTA and is digested with *proteinase K* (at 55 ºC for 1 hour 30 minutes). After the elimination of *Exonuclease III,* the DNA is purified and subsequently cut with two restriction enzymes, *HindIII* and *BamHI*, during 2 hours at 37 ºC. Next, the resulting DNA is purified and ligated the digoxigenin-labelled dsDNA handle (Dig Handle, see section 2.3.3.2) and the biotin-labelled DNA handle (see below) at 16 ºC overnight. The resulting DNA construct two segments of dsDNA of a size of ~3500 bp each, separated by a segment of ssDNA of a size of ~1000.

2.3.4.2 Preparation of a biotin-labelled DNA handle

The biotin-labeled DNA handle was prepared by annealing two complementary DNA oligonucleotides (5'-Biot-G-Biot-GGTTTGTAAGCCTGAT-3' and 5'-[Phos]-AGCTATCAGGCTTACAAAC-3') as described above:

The equimolar concentrations of the complementary oligonucleotides were mixed in a 1.5 ml micro-centrifuge tube with the annealing buffer to reach the final volume of 100

µl. The annealing reaction was carried out at 95 ºC for 10 minutes in a thermo-shaker and, after switching off the heating, the reaction solution was left to cool down to room temperature (for ~2 hours). Afterwards, the sample was diluted to the concentration of 1 ng/ µl, divided into aliquots and stored at -20 ºC.

2.3.4.3 DNA ligation

The final ssdsDNA construct for manipulation with optical tweezers was obtained via ligation as described above (the final step shown in Figure 14):

50 ng of ssdsDNA (2.3.4.1) were mixed with 0.5 µl of biotin-labeled DNA handle (2.3.4.2), 0.4 µl of DIG-DNA handle (2.3.3.2), 3 µl of 10x T4 reaction buffer and 1.5 µl of T4 DNA ligase (400 U/ µl) in a 1.5 ml micro-centrifuge tube. The obtained mixture was filled with ultra-pure water to reach the final volume of 30 µl. The ligation was carried out at 16 ºC overnight and the product of the reaction was purified using a commercial DNA purification column and eluted in 30 µl of water.

2.3.5 Preparation of reaction buffers

Replication reaction buufer:

The reaction buffer for replication assays (primer extension or strand displacement) contained 50 µM of dNTP, 50 mM of Tris pH 7.5, 30 mM of KCl, 10 mM of Dithiothreitol (DTT), 4 mM of $MgCl_2$ and 0.2 mg/ml bovine serum albumin. To test the effect of mtSSB on the strand displacement activity of Pol γ wild-type and exo-, 50 nM of mtSSB were added to the replication reaction buffer.

Unwinding reaction buffer:

The reaction buffer for TWINKLE unwinding assays contained 4 mM of ATP, 50 mM of Tris pH 7.5, 30 mM of KCl, 10 mM of Dithiothreitol (DTT), 4 mM of $MgCl_2$ and 0.2 mg/ml bovine serum albumin. In the unwinding assay in the presence of mtSSB, the reaction buffer also contained 5 nM of mtSSB.

Cooperative strand displacement activity of Pol γ and TWINKLE:

The reaction buffer to measure cooperative strand displacement activity of Pol γ wild-type and TWINKLE contained 50 µM of dNTP, 4 mM of ATP, 50 mM of Tris pH 7.5, 30 mM of KCl, 10 mM of Dithiothreitol (DTT), 4 mM of $MgCl_2$ and 0.2 mg/ml bovine serum albumin.

2.3.6 Data analysis

2.3.6.1 Calculation of processivity and mean polymerization and unwinding rates

The number of nucleotides incorporated by Pol γ and Pol γ exo- during primer extension and strand displacement DNA synthesis, can be obtained by dividing the change in distance between the two beads by the change in extension of the molecule that corresponds to the conversion of one nucleotide into a base pair (for primer extension) or the change in extension due to liberation of two nucleotides (one of which is converted into a base pare) as a result of the unwinding of one base pair of the hairpin (for strand displacement).

The number of base pairs unwound by TWINKLE can be calculated by dividing the change in distance between the two beads by the change in extension of the molecule due to liberation of two nucleotides.

During primer extension DNA synthesis, Pol γ elongates the 3' end of the DNA primer, incorporating corresponding nucleotides to the DNA template (converting ssDNA gap into dsDNA). Under these conditions, the number of incorporated nucleotides, $\boldsymbol{Processivity}\ (\boldsymbol{PE})$, can be calculated as follows:

$$\boldsymbol{Processivity}\ (\boldsymbol{PE}) = \frac{\boldsymbol{\Delta x_{Exp}}\,(\boldsymbol{f})}{\boldsymbol{x_{ds}}(\boldsymbol{f}) - \boldsymbol{x_{ss}}(\boldsymbol{f})} \qquad (eq.4),$$

where $\boldsymbol{\Delta x_{Exp}}(\boldsymbol{f})$ is the change in molecular extension measured with optical tweezers at a given tension, $\boldsymbol{x_{ds}}(\boldsymbol{f})$ and $\boldsymbol{x_{ss}}(\boldsymbol{f})$ are extensions per base pair or nucleotide at a given force for dsDNA and ssDNA correspondingly.

During strand displacement DNA synthesis, Pol γ unwinds the duplex DNA ahead of it, displacing one strand and using the other as a template to incorporate the corresponding complementary nucleotides at the 3' end of the primer. Under these conditions the change in DNA's extension corresponds to the sum of the extension of the displaced single strand (ssDNA) and the extension of the newly synthesized dsDNA.

The number of incorporated nucleotides, $\boldsymbol{Processivity}\ (\boldsymbol{SD})$, during strand displacement DNA synthesis , at a given force can be calculated as:

$$\boldsymbol{Processivity}\ (\boldsymbol{SD}) = \frac{\boldsymbol{\Delta x_{Exp}}\,(\boldsymbol{f})}{\boldsymbol{x_{ds}}(\boldsymbol{f}) + \boldsymbol{x_{ss}}(\boldsymbol{f})} \qquad (eq.5),$$

During the helicase activity of TWINKLE, the observed change in the molecular extension corresponds to the extension of the two unwound single DNA strands. The number of unwound base pairs during the helicase activity of TWINKLE, $\boldsymbol{Processivity\ (Unw)}$, at a given force can be calculated as follows:

$$\boldsymbol{Processivity\ (Unw)} = \frac{\boldsymbol{\Delta x_{Exp}\,(f)}}{\boldsymbol{2 \cdot x_{ss}(f)}} \qquad (eq.6).$$

The extension per base pair of dsDNA, $\boldsymbol{x_{ds}(f)}$ is calculated using *Extensible Worm-like chain model (WLC)* ([155] - [157]), according to which, the extension of a dsDNA molecule under tension is given by:

$$\boldsymbol{x_{ds}(f) = L \cdot \left[1 - \frac{1}{2} \cdot \left(\frac{k_B T}{FP}\right)^{\frac{1}{2}} + \frac{F}{S}\right]} \qquad (eq.7),$$

where $\boldsymbol{S}$ is the elastic stretch modulus of dsDNA (the value for $\boldsymbol{S}$ used in our calculations is 1200 pN [158], $\boldsymbol{L}$ is the contour length of 1 base pair of a dsDNA molecule ($\boldsymbol{L} = 0.34$ nm, [159], $\boldsymbol{P}$ **t**he persistence length of dsDNA (we used $\boldsymbol{P} = 53$ nm, [158], $\boldsymbol{k_B}$ is the Boltzmann constant**,** $\boldsymbol{T}$ is the absolute temperature and $\boldsymbol{F}$ is the applied force.

The extension per nucleotide of ssDNA,$\boldsymbol{x_{ss}}$, was calculated as the average of 5 experimental FECs (force-extension curves) of ssDNA, normalized to 1 nt, under the conditions used in our experiments (see Figure 15).

Figure 15 shows that mtSSB binding leads to compaction of ssDNA. At tensions relevant to the strand displacement and unwinding assays (<11 pN) mtSSB-bound ssDNA has similar extension at 5 nM and 50 nM of mtSSB.

The mean polymerization or unwinding rate is calculated as the number of incorporated nucleotides or unwound base pairs divided by the total time of an activity:

$$\boldsymbol{V_{mean}} = \frac{\boldsymbol{Processivity}}{\boldsymbol{t}} \qquad (eq.8).$$

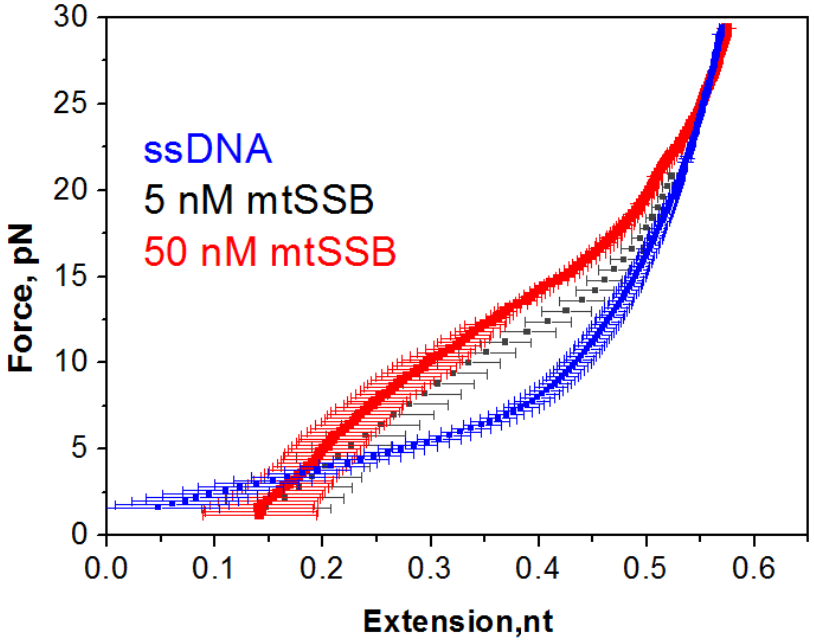

Figure 15. Averaged force-extension curves (with errors), normalized to 1 nt: naked ssDNA (blue curve), mtSSB-ssDNA, 5 nM mtSSB (black curve) and mtSSB-ssDNA, 50 nM (red curve). All the FECs were measured under the buffer conditions of the replication and unwinding assays.

2.3.6.2 Identification of the maximum replication and unwinding rates

To compute the average velocity without pauses, we used the method described in [134]. In this method, a variable time window is used to calculate the instantaneous replication rate of the polymerase, thus enabling the identification of the optimal time window range to calculate the maximum replication rate of the enzyme.

2.3.6.3 Quantification of the strand displacement mechanism of Pol γ

We have extended the physical framework ([160], [161]), where the unwinding activeness of a nucleic acid unwinding motor depends on the interaction energy ($\boldsymbol{\Delta G_{int}}$) between the motor and the DNA fork to quantify the strand displacement mechanism of Pol γ and Pol γ exo- (in the absence and presence of mtSSB). In our model, the polymerase could move forward with a rate $\mathbf{k_+}$ favored by a dNTP incorporation step, or backwards with a rate **k-**, due its exonuclease activity. In the presence of saturating dNTP concentrations, any factor opposing the forward movement of the polymerase (as fork stability) will trigger successive cycles of polymerization and exonuclease at the fork. This process, known as idling, will be observed as a pause with our current experimental resolution. During strand displacement activity, one or more base pairs ahead of the

polymerase should be open for the polymerase to move forward (Figure 16). Therefore, any factor that control the height of the DNA unwinding activation barrier, such as DNA sequence or external mechanical tension applied to the fork, may affect the strand displacement behavior of the polymerase. In general, the contributors to decrease the activation energy ($\boldsymbol{B}$) of dsDNA unwinding can be written as:

$$\boldsymbol{B = N(\Delta G_{bp} - \Delta G_{int} - \Delta G_F)} \qquad (eq.9),$$

where $\boldsymbol{N}$ is the number of unwound bp in the transition state, $\boldsymbol{\Delta G_{bp}}$ is the free energy of bp formation ($\boldsymbol{\Delta G_{GC}}$~2.9 kBT, $\boldsymbol{\Delta G_{AT}}$~1.5 kBT, [162]) and $\boldsymbol{\Delta G_{int}}$ and $\boldsymbol{\Delta G_F}$ present the reduction in that free energy due to the polymerase and the external unzipping force, respectively (see equation 12).

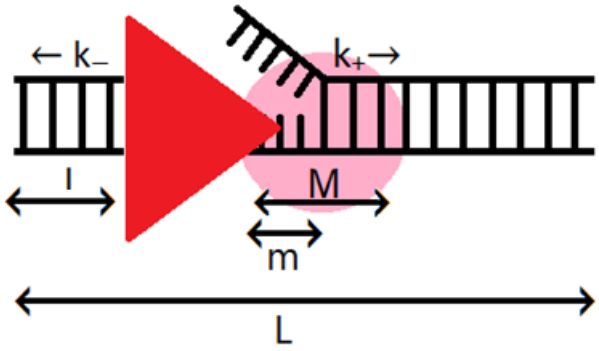

Figure 16. A scheme showing the polymerase γ interacting with the replication fork during strand displacement**.** The polymerase is situated at the position $\boldsymbol{l}$ on the DNA template and can move forward and backwards with the rates $\boldsymbol{k_+}$ and $\boldsymbol{k_-}$ correspondingly. $\boldsymbol{M}$ is the number of base pairs destabilized by the polymerase and $\boldsymbol{m}$ is the number of open bases ahead of the polymerase. $\boldsymbol{L}$ is the total length of the chain being replicated (the image adapted from [163]).

According to the model, the maximum replication rate at the position $\boldsymbol{l}$, $\boldsymbol{V_{max}}$, can be expressed as:

$$\boldsymbol{V_{max}(l,f) = \sum_{m=0}^{L-l} k_+(l,m,f) \cdot P_0(l,m,f)} \qquad (eq.10),$$

where $\boldsymbol{f}$ is tension, applied to the DNA hairpin and $\boldsymbol{P_0(l,m,f)}$ is the probability of finding the polymerase at the $\boldsymbol{l}$ th position on the template with $\boldsymbol{m}$ base pairs ahead open.

This probability is defined by the energy needed to open $\boldsymbol{m}$ base pairs of the DNA duplex ahead of the polymerase, $\boldsymbol{\Delta G\left(l,\ m,\ f\right)}$:

$$\boldsymbol{P_0(l,m,f)} = \frac{\boldsymbol{exp}[-\frac{\boldsymbol{\Delta G\left(l,\ m,\ f\right)}}{\boldsymbol{k_B T}}]}{\sum_{\boldsymbol{m=0}}^{\boldsymbol{L-l}} \boldsymbol{exp}[-\frac{\boldsymbol{\Delta G\left(l,\ m,\ f\right)}}{\boldsymbol{k_B T}}]} \qquad (eq.11)$$

$\boldsymbol{\Delta G\left(l,\ m,\ f\right)}$ is determined by several components:

$$\boldsymbol{\Delta G\left(l,\ m,\ f\right)} = \sum_{\boldsymbol{i=l+1}}^{\boldsymbol{l+m}} \boldsymbol{\Delta G_{bp}\,(i)} - \boldsymbol{2m}\int_{\boldsymbol{0}}^{\boldsymbol{f}} \boldsymbol{x_{nt}(f')df'} - \begin{cases} \boldsymbol{m\Delta G_d,\ 0 < m \le M} \\ \boldsymbol{M\Delta G_d,\ m > M} \end{cases} (eq.12),$$

where $\boldsymbol{\Delta G_{bp}}$ is the stability of the base pairs, calculated as described in [163], $\boldsymbol{2m\int_0^f x_{nt}(f')df'}$ is the contribution of the external force to destabilize $\boldsymbol{m}$ base pairs, calculated as an integral of extension of two nucleotides (obtained after a base pair unwinding) at a given force $\boldsymbol{f'}$ from zero to applied force, and $\boldsymbol{\Delta G_d}$ parameterizes the intensity of the interaction between the polymerase and the duplex DNA ahead of it, and $\boldsymbol{M}$ is the range of this interaction.

The rate for the forward step of the length $\boldsymbol{\delta}$ = 1 bp during strand displacement polymerization is now given by $eq.13$:

$$\boldsymbol{k_+(l,m,f)} =$$

$$\begin{cases} \boldsymbol{0\,, m < \delta} \\ \boldsymbol{k_0 \cdot exp\left[-a \cdot min(M,\delta) \cdot \frac{\Delta G_d}{k_B T}\right] \cdot exp\left[-\delta \cdot f \cdot \frac{\left(x_{nt}(f) - x_{bp}(f)\right)}{k_B T}\right], \delta \le m < max(M,\delta)} \\ \boldsymbol{k_0 \cdot exp\left[-a \cdot (M + \delta - m) \cdot \frac{\Delta G_d}{k_B T}\right] \cdot exp\left[-\delta \cdot f \cdot \frac{\left(x_{nt}(f) - x_{bp}(f)\right)}{k_B T}\right], max(M,\delta) \le m < M + \delta'} \\ \boldsymbol{k_0 \cdot exp\left[-\delta \cdot f \cdot \frac{\left(x_{nt}(f) - x_{bp}(f)\right)}{k_B T}\right], M + \delta \le m} \end{cases}$$

Where $\boldsymbol{a\,(0 < a < 1)}$ is a coefficient associated with the relative location of the activation barrier for a replication step, which equals 0.01 [163], $\boldsymbol{k_0}$ is the maximum replication rate during primer extension at zero tension ($\boldsymbol{f = 0}$) in the absence of the

secondary structure of the template ssDNA (it has a value 23.04 for Pol γ and 27.10 for Pol γ exo-), and $\boldsymbol{exp}\left[-\boldsymbol{\delta}\cdot\boldsymbol{f}\cdot\left(\boldsymbol{x_{nt}}(\boldsymbol{f})-\boldsymbol{x_{bp}}(\boldsymbol{f})\right)\right]$ is the work of converting 1 nucleotide of the template ssDNA into a base pair, $\boldsymbol{x_{nt}}(\boldsymbol{f})$ and $\boldsymbol{x_{bp}}(\boldsymbol{f})$ are extensions of ssDNA and dsDNA per nucleotide at a given force (obtained from experimental force-extension curves), $\boldsymbol{k_B}$ is the Boltzmann constant and $\boldsymbol{T}$ is the absolute temperature**.**

In the case of the strand displacement activity of the polymerase in the presence of mtSSB, instead of $\boldsymbol{\Delta G_d}$ **,** we used another parameter, $\boldsymbol{\Delta G_{d,eff}}$ ('eff' – for the effect of SSB), which includes the energy of interaction between the polymerase and the fork in the presence of mtSSB and the energy gain due to the mtSSB binding to the displaced single strand.

In this model, two variables determine the maximum strand displacement rate of the DNA polymerase: the intensity of interaction between the polymerase and the fork, $\boldsymbol{\Delta G_d}$ and the range of this interaction, $\boldsymbol{M}$. These two free parameters were fixed by the least squared errors fit of the model to the strand displacement $\boldsymbol{V_{max}}$ data.

2.3.6.4 Model for moving probabilities

The probability of finding the polymerase in the active state (where net polymerization occurs) can be calculated as the ratio between the average polymerization rate and the polymerization rate without pauses:

$$\boldsymbol{MP}=\frac{\boldsymbol{V_{mean}}}{\boldsymbol{V_{max}}} \qquad (eq.14),$$

The average residence time per nucleotide, $\boldsymbol{T}$, can be calculated as an inverse of the average polymerization rate, $\boldsymbol{V_{mean}}$, and the time the polymerase spends in the active state per nucleotide, $\boldsymbol{T_a}$, can be found as an inverse of $\boldsymbol{V_{max}}$. Therefore, the moving probability can be also expressed as follows:

$$\boldsymbol{MP}=\frac{\boldsymbol{T_a}}{\boldsymbol{T}} \qquad (eq.15),$$

Besides, the residence times per nucleotide for primer extension and strand displacement conditions (see section 2.4) can be defined respectively as:

$$\boldsymbol{T_{PE} = T_{a,PE} + T_{p,PE}} \quad (eq.15),$$

$$\boldsymbol{T_{SD} = T_{a,SD} + T_{p,PE} + T_{p,SD}} \quad (\text{eq. } 16),$$

where $\boldsymbol{T_{p,PE}}$ and $\boldsymbol{T_{p,SD}}$ denote paused time per nucleotide during by primer extension and strand displacement, respectively.

Then, the moving probability of the polymerase during primer extension can be found as follows:

$$\boldsymbol{MP_{PE} = \frac{T_{a,PE}}{T_{PE}} = \frac{T_{a,PE}}{T_{a,PE} + T_{p,PE}} = \frac{1}{1 + \frac{T_{p,PE}}{T_{a,PE}}}} \quad (\text{eq. } 17).$$

It is known from our experimental data that, during primer extension (see section 2.4), the moving probability of Pol γ and Pol γ exo-, $\boldsymbol{MP_{PE}}$, does not change significantly with the tension applied to the template and is ~ 65%, hence the ratio $\boldsymbol{T_{p,PE}/T_{a,PE}}$ should be constant too (here, we define this ratio as $\boldsymbol{K_{PE}}$). Therefore, the moving probability during primer extension can now be expressed as:

$$\boldsymbol{MP_{PE} = \frac{1}{1 + K_{PE}}} \quad (\text{eq. } 18).$$

The moving probability of the polymerase during strand displacement, in turn, can be found as follows:

$$\boldsymbol{MP_{SD} = \frac{T_{a,SD}}{T_{SD}} = \frac{T_{a,SD}}{T_{a,SD} + T_{p,PE} + T_{p,SD}} = \frac{1}{1 + \frac{T_{p,PE}}{T_{a,SD}} + \frac{T_{p,SD}}{T_{a,SD}}} = \frac{1}{1 + K_{PE}\frac{T_{a,PE}}{T_{a,SD}} + \frac{T_{p,SD}}{T_{a,SD}}}}$$
$$\boldsymbol{= \frac{1}{1 + K_{PE}\frac{V_{max,SD}}{V_{max,PE}} + \frac{T_{p,SD}}{T_{a,SD}}} = \frac{1}{1 + K_{PE}V_{max,SD/PE} + \frac{T_{p,SD}}{T_{a,SD}}}} \quad (\text{eq. } 18),$$

where $\boldsymbol{V_{max,SD}}$ and $\boldsymbol{V_{max,PE}}$ are average replication rates without pauses in strand displacement and primer extension conditions respectively, and $\boldsymbol{V_{max,SD/PE} = V_{max,SD}/V_{max,PE}}$.

Here we consider that during replication, the polymerase can be found only in two possible states, moving state and pause state. The equilibrium constant for the process of switching from the active state to the pause state during strand displacement (we denote it here as $\boldsymbol{K_{SD}}$) can be found as $\boldsymbol{k_{ent,SD}/k_{exit,SD}}$, where $\boldsymbol{k_{ent,SD}}$ and $\boldsymbol{k_{exit,SD}}$ are the rates of entering and exiting the pause state correspondingly. The number of entries into pauses, $\boldsymbol{N_{ent}}$, during the time the polymerase spends in the active state, $\boldsymbol{T_a}$, is given by:

$$\boldsymbol{N_{ent} = T_a \cdot k_{ent}} \quad \text{(eq. 19)}.$$

If a single pause has a mean duration of $\boldsymbol{\overline{T}_P = 1/k_{exit}}$, where $\boldsymbol{k_{exit}}$ is the rate of exit from the pause state, then the total time in pause $\boldsymbol{T_p}$ is given by:

$$\boldsymbol{T_p = \overline{T}_P \cdot N_{ent} = T_a \cdot \frac{k_{ent}}{k_{exit}}} \quad \text{(eq. 20)}.$$

Therefore, $\boldsymbol{T_{p,SD}/T_{a,SD} = k_{ent,SD}/k_{exit,SD} = K_{SD}}$.

The equilibrium constant for the process of switching from the active to the pause state during strand displacement, $\boldsymbol{K_{SD}}$, depends exponentially on external tension, $\boldsymbol{F}$, and can be expressed as:

$$\boldsymbol{K_{SD} = K_{SD}^{\dagger}(0) exp(-f \cdot d)} \quad \text{(eq. 20)},$$

where $\boldsymbol{K_{SD}^{\dagger}(0)}$ is the equilibrium constant for the process of switching from the active to the pause state in the strand displacement conditions in the absence of tension. $\boldsymbol{f}$ is applied tension and $\boldsymbol{d}$ is the conformational change along the pulling coordinate that favors an exist from pause state.

Accordingly, eq. 18 can be now written as:

$$\boldsymbol{MP_{SD} = \frac{1}{1 + K_{PE} V_{max}^{SD/PE} + K_{SD}^{\dagger}(0) exp(-f \cdot d)}} \quad \text{(eq. 21)}.$$

Now, if we define $\boldsymbol{MP_{SD/PE}}$ as the ratio of the moving probabilities during strand displacement and primer extension (at a given tension), $\boldsymbol{MP_{SD}/MP_{PE}}$, and taking into account equations 21 and 18, it can be expressed as:

$$\boldsymbol{MP_{SD/PE}} = \frac{\mathbf{1}}{\mathbf{1} + \boldsymbol{K_{PE}V_{max,SD/PE}} + \boldsymbol{K_{SD}^{\dagger}}(\mathbf{0})\boldsymbol{exp}(-\boldsymbol{f}\cdot\boldsymbol{d})} \cdot \left(\frac{\mathbf{1}}{\mathbf{1} + \boldsymbol{K_{PE}}}\right)^{-\mathbf{1}} = \\ = \frac{\mathbf{1} + \boldsymbol{K_{PE}}}{\mathbf{1} + \boldsymbol{K_{PE}V_{max,SD/PE}} + \boldsymbol{K_{SD}^{\dagger}}(\mathbf{0})\boldsymbol{exp}(-\boldsymbol{f}\cdot\boldsymbol{d})} \qquad \text{(eq. 22).}$$

Eq. 22 was used to fit the moving probability data (see below) with $\boldsymbol{K_{SD}^{\dagger}}(\mathbf{0})$ and $\boldsymbol{d}$ being free variables.

2.4 Results

2.4.1 Strand displacement activity of Pol γ

Experimental set-up and detection of individual DNA strand displacement activities

With optical tweezers, we applied mechanical tension to the ends of the two strands of a 440 bp long DNA hairpin attached between two functionalized plastic beads (see Figure 17). The DNA hairpin contained a single loading site for the polymerase and 1 to 3 repetitions of the GCC sequence separated by ~100 nucleotides of high-AT content. To monitor strand displacement activities of individual wild-type (Pol γ) and exonuclease-deficient variant $D_{198}AE_{200}A$ (Pol γ exo-) [164] of the Pol γ holoenzyme (both at 2 nM) in the presence and absence of human mtSSB (50 nM), we held individual DNA hairpins at constant tensions (under 12 pN) where the hairpin is closed. An individual strand displacement activity was monitored as an increment in the end-to-end distance seprating the two beads as a result of an elongation of the 3'- end of the dsDNA handle by a single holoenzyme that incorporates corresponding complementary nucleotides (50 μM dNTP in the reaction buffer) to the template DNA and displaces the complementary strand (Figure 17). The resulting change in the DNA extension was converted to the number of replicated nucleotides at each moment in time at a given force, considering that each catalytic step results in an increase of the tether extension by an amount equal to the addition of a single base pair plus a single free-nucleotide or a single mtSSB-bound nucleotide, in the absence or presence of mtSSB respectively. The corresponding extensions per nucleotide at each force of free- and mtSSB-bound ssDNA were obtained from the force-extension curves recorded under the buffer conditions of the DNA unwinding assay (50 mM Tris–HCl, pH 7.5, 30 mM KCl and 4 mM $MgCl_2$) (see section 2.3.6.1).

Primer extension replication assay

The kinetics of primer extension replication by DNA polymerases is modulated by mechanical tension applied to the DNA template ([165] - [170], [134]). Hence, in order to determine the effect of mechanical tension on the kinetics of strand displacement replication by Pol γ, we should also consider the effect of mechanical tension on the polymerase primer extension activity, since in strand displacement configuration the DNA template strand is also under mechanical tension.

To measure the effect of mechanical tension on the real-time replication kinetics of the wild-type polymerase and the exonuclease deficient variant during primer extension under the same experimental condition as those of the strand displacement experiments, we held a DNA molecule with ~1000 nt ssDNA gap under mechanical tensions below 20 pN (Figure 18). A single primer extension activity was followed as a decrease in the end-to-end distance between the two beads as a result of elongation the 3' end by a single

holoenzyme that incorporates corresponding complementary nucleotides to the template and converts ssDNA gap into dsDNA.

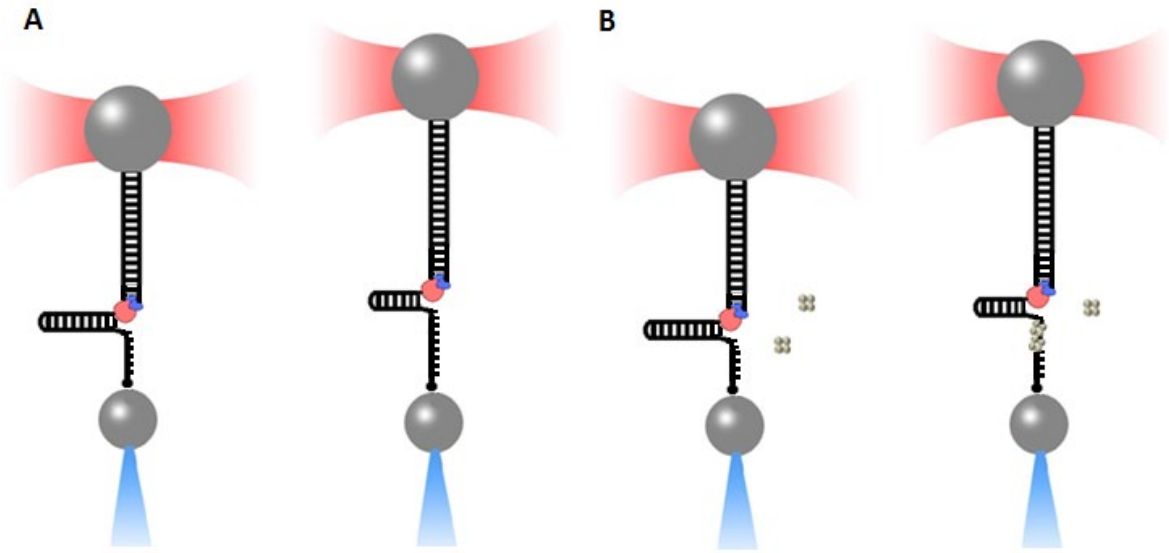

Figure 17. A schematic representation of the strand displacement replication assay (not to scale). A In a strand displacement replication assay in the absence of mtSSB, the hairpin is held at constant tensions below 12 pN. Pol γ loads at the 3' end of the dsDNA handle. During strand displacement, Pol γ elongates the 3' end incorporating corresponding complementary nucleotides to the DNA template, unwinding the DNA duplex of the hairpin and displacing the opposite DNA strand. This leads to the increment of the DNA extension. **B** In a strand displacement replication assay in the presence of mtSSB, SSB tetramers gradually bind the displaced single DNA strand.

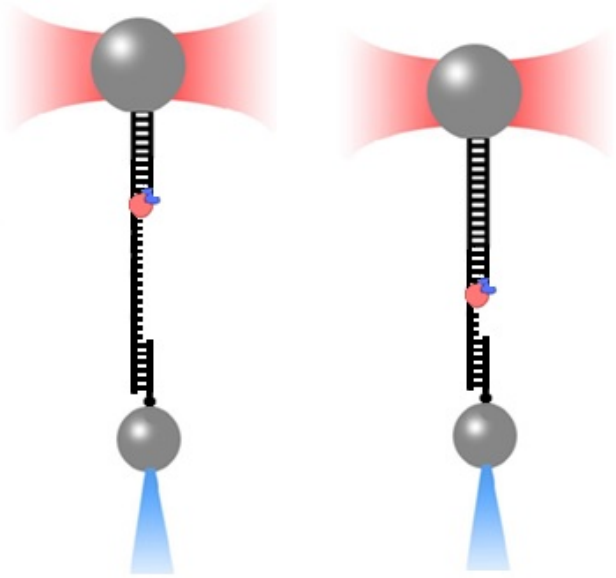

Figure 18. A schematic representation of the primer extension replication assay (not to scale). A single polymerase elongates the 3' end of a dsDNA handle converting ssDNA gap into dsDNA, which results in a decrease in the end-to-end distance between the two beads.

The effect of the stability of fork on strand displacement replication kinetics and processivity of Pol γ and Pol γ exo-

Strand displacement activities of Pol γ and its variant, Pol γ exo-, were detected, as we applied tension favoring destabilization of the hairpin DNA duplex. For both enzymes, varying the polymerase concentration 50-fold (from 0.2 nM to 10 nM) did not significantly change the number of replicated nucleotides (or processivity), neither did it affect their moving probabilities (see below). The time interval between replication events was 5-10 times longer than the duration of an individual event. These observations suggest that each replication event is a result of an operation of a single polymerase. We did not observe any backward movements which, in the case of Pol γ wild-type, could be considered as processive exonuclease events, previously measured for T4 and T7 DNA polymerases [171].

For Pol γ, processive replication events were detected at F ≥ 6 pN and as the applied tension increased, the replication rate increased, reaching values similar to those of primer extension conditions (Figures 19A and 21A). The processivity of Pol γ also increased with applied tension: while at 6 pN, Pol γ on average replicated only 45% of the length of the hairpin, at the highest force, the holoenzyme was able to replicate ~80% of the hairpin. On the contrary, in the case of Pol γ exo-, processive replication events were detected at lower tensions, F≥ 2.5 pN (Figure 19A and 21A). At tensions <9 pN, the replication rate of Pol γ exo- increased with applied force towards the rate of primer extension conditions with values significantly higher than those of the wild-type polymerase. These results are in agreement with the higher ability of Pol γ exo- to perform strand displacement replication in bulk ([103] , [172]). At tensions above 9 pN, the processivity of the exo- variant decreased, which indicates a damaging effect of high tensions on the strand displacement mechanism of the mutant enzyme.

Determination of the effect of exonuclease activity on strand displacement activity of Pol γ

Next, we studied the effect of tension and exonuclease contribution to the reaction active (where the polymerase actively replicates DNA) and inactive (where the polymerase pauses) states. The presence of short inactive phases (or pauses) was typical for strand displacement activity of both, Pol γ and Pol γ exo- at all tensions (Figure 20). To differentiate the effect of force on the active and inactive (pause) states during replication and to determine the contribution of the exonuclease activity to the pause states, we calculated for each polymerase the average replication velocity without pauses, $\boldsymbol{V_{max}(f)}$, which quantifies the maximum replication rate and can be used to quantify the unwinding mechanism of each polymerase (see [134]).

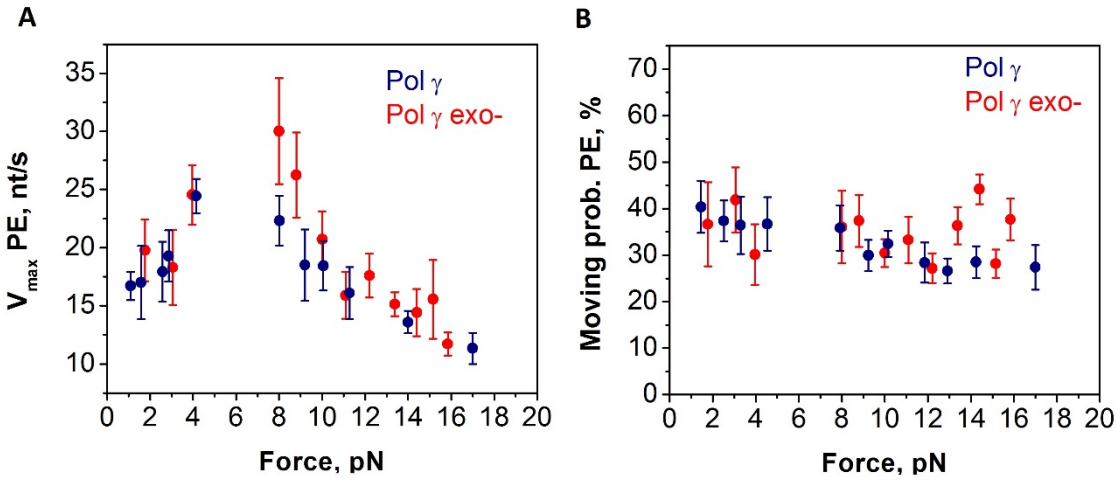

Figure 19. Effect of tension on: **A** Change of maximum replication rate (the replication rate in the absence of pauses, $\boldsymbol{V_{max,PE}}$) in the primer extension conditions; **B** Change of the probability of finding a polymerase in the active, or pol competent, state (Moving probability, $\boldsymbol{MP_{PE}}$) in the primer extension conditions. Navy dots correspond to the Pol γ data and red dots correspond to the Pol γ exo- data.

We also calculated the moving probability (as a ratio between the average replication velocity and $\boldsymbol{V_{max}}$), which represents the percentage of time the polymerase spends in the polymerization competent state in each run at each tension. To determine the effect of tension and fork stability particularly on strand displacement activity of Pol γ and Pol γ exo-, we normalized the strand displacement moving probabilities and $\boldsymbol{V_{max}}$ by their corresponding values under primer extension conditions (Figures 19A and 21C). By comparing the values of $\boldsymbol{V_{max}}$ and moving probabilities of Pol γ and Pol γ exo-, we can extract the information about the exonuclease activity contribution to the strand displacement replication reaction kinetics.

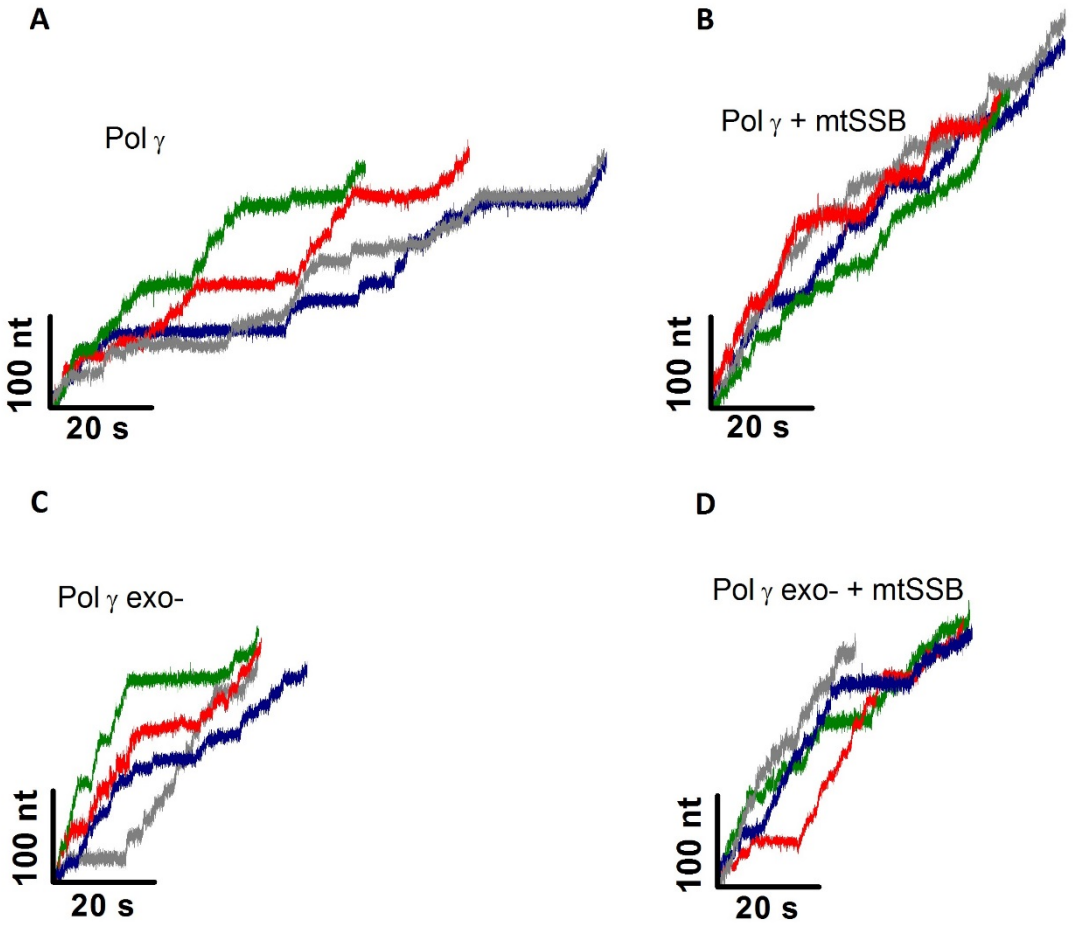

Figure 20. Examples of traces of strand displacement activities (the number of replicated nucleotides vs. time) of the two holoenzymes at 7-8 pN: **A** Pol γ wild-type in the absence of mtSSB; **B** Pol γ wild-type in the presence of mtSSB; **C** Pol γ exo- in the absence of mtSSB; **D** Pol γ exo- in the presence of mtSSB. A typical activity of Pol γ wild-type or Pol γ exo- is characterized by the presence of transitory inactive events (pauses) that follow active (pol competent) states of a polymerase.

First, we calculated the average strand displacement replication rate without pauses (normalized by the corresponding primer extension values) for the two holoenzymes, $\boldsymbol{V_{max,SD/PE}}$ $(\boldsymbol{f})$. Figure 21D shows that Pol γ and Pol γ exo- presented almost identical $\boldsymbol{V_{max,SD/PE}}$ values, which incremented rapidly with applied force until they reached the rates similar to those exhibited by the enzymes under primer extension conditions ($\boldsymbol{V_{max,SD/PE}}$ **(11 pN)** ~1 and $\boldsymbol{V_{max,SD}}$ **(11.5 pN)** ~15 nt/s, Figures 19A and 21B). The similarities of the force dependencies of $\boldsymbol{V_{max,SD/PE}}$ of Pol γ and Pol γ exo- indicate that, for the two enzymes, DNA unwinding is a rate-limiting step, and that the two polymerases present identical DNA unwinding mechanisms.

To quantify the unwinding activity of Pol γ and Pol γ exo-, we extended the theoretical model proposed by Betterton and Jülicher [160], which quantifies the unwinding activeness of DNA helicases. For DNA polymerases, replication occurs in one nucleotide steps [173], and slippage (observed for DNA helicases) can be neglected in the presence of nucleotides. Actually, as we indicated above, we did not detect any polymerase backward movements. Hence, the maximum replication rate during strand displacement activity of the polymerase is defined by two free variables in this model (see section 2.3.6.3): the energy of interaction between the polymerase and the fork, $\boldsymbol{\Delta G_{int}}$ and the range of this interaction, $\boldsymbol{M}$. These two parameters were found by the least squared error fits of the strand displacement model for the $\boldsymbol{V_{max}}$ data of Pol γ and Pol γ exo- (Figure 21C).

The fits (Figure 21C) yielded $\boldsymbol{\Delta G_{int}}$ = 0.9 ± 0.2 k_BT and $\boldsymbol{M}$ = 1 bp for wild-type Pol γ and $\boldsymbol{\Delta G_{int}}$ = 1.0 ± 0.2 k_BT and $\boldsymbol{M}$ = 1 bp for the exo- mutant. The similarity of the interaction potential of two holoenzymes suggests that the exonuclease contribution does not affect the innate strand displacement activity of Pol γ, which is able to lower the activation energy of the closest base pair by approximately 1 k_BT. The obtained values of $\boldsymbol{\Delta G_{int}}$ are substantially lower than the average $\boldsymbol{\Delta G}$ of melting of a base pair in the hairpin ($\boldsymbol{\Delta G_{bp}}$ = 1.8 k_BT), hence an additional destabilization of the fork is needed for DNA unwinding. This explains the effect of tension (and therefore fork stability) on $\boldsymbol{V_{max}}$ of the two polymerases.

Determination of the effect of exonuclease activity on moving probabilities

Both enzymes present comparable DNA unwinding mechanisms, however the exo- mutant was able to start processive DNA synthesis at tension significantly lower than that of wild-type Pol γ (2.5 pN for Pol γ exo- vs. 6 pN for Pol γ wild-type). This difference can be explained by the analysis of their moving probabilities, which represent the percentage of time the polymerase spends in the active state during an activity. We should point out that the probability of finding Pol γ and Pol γ exo- in the active (pol competent) state in primer extension conditions was ~ 35%, and it was practically force-independent within in the range of tensions from 1 to 12 pN (Figure 19B). It means that the two holenzymes are paused during ~ 65% of the time even when there is no fork ahead of them. Thus, to specifically determine the effect of fork on the moving probability of Pol γ and Pol γ exo-, the strand displacement moving probability at each force should be normalized by the corresponding moving probability during primer extension, $\boldsymbol{MP_{SD/PE} = MP_{SD}/MP_{PE}}$.

For the two enzymes, their moving probability during strand displacement was significantly lower than that of primer extension and it increased with force to reach values similar to those found in primer extension conditions, when $\boldsymbol{MP_{SD/PE}}$ = 1 (Figure 21D).

These results point out that the stability of the fork favors the occupancy of the pause state of the polymerase during strand displacement. Pol γ wild-type and Pol γ exo- present very similar moving probabilities in primer extension conditions, however in strand displacement conditions, the probability of finding the exonuclease deficient enzyme in the active (moving) state was higher than the moving probability of Pol γ in the whole range of applied tensions. These results indicate that the lack of the exonuclease contribution favors probability of finding Pol γ in the active state, allowing the exo- Pol γ mutant to start processive strand displacement synthesis at tensions significantly lower than those of the wild-type enzyme.

Individual exonuclease events cannot be detected with our current resolution and they would be observed as part of the inactive pause states. Thus, we considered the two holoenzymes alternating between two possible states: the moving or pol competent state (active) and the pause or pol incompetent state (inactive). We note that the pause state may include different inactive polymerization states, which cannot be solved with our current resolution. In the simplified two-state scenario, the effect of force on moving probability of Pol γ and Pol γ exo-, $\boldsymbol{MP_{SD/PE}}$, can be defined by $eq.22$ (see section 2.3.6.4):

$$\boldsymbol{MP_{SD/PE}(f)} = \frac{\mathbf{1} + \boldsymbol{K_{PE}}}{\mathbf{1} + \boldsymbol{K_{PE}V_{max,SD/PE}} + \boldsymbol{K_{SD}^{\dagger}(0)e^{-df}}},$$

where $\boldsymbol{K_{PE}}$ is the equilibrium constant for the process of switching from the active to the pause state during primer extension. $\boldsymbol{K_{PE}}$ can be obtained by transforming eq.18 and it is constant since the moving probabilities of Pol γ and Pol γ exo- during primer extension were very similar and practically force-independent (see Table 2). $\boldsymbol{V_{max,SD/PE}(f)}$ is determined by the strand displacement model (section 2.3.6.3, Figure 21C). $\boldsymbol{K_{SD}^{\dagger}(0)}$ is the equilibrium constant for the process of switching from the active to the pause state during strand displacement for each enzyme at zero force. $\boldsymbol{f}$ is applied tension and $\boldsymbol{d}$ is the conformational change along the pulling coordinate, favoring an exit from the pause state. The moving probability in this model is defined by two free variables, $\boldsymbol{K_{SD}^{\dagger}(0)}$ and $\boldsymbol{d}$, which were found with the least squared error fit of $eq.22$ to the force dependent $\boldsymbol{MP_{SD/PE}}$ data of each holoenzyme (see Figure 21D).

Fit	K_{PE}	$K_{SD}^{\dagger}(0)$	d , nm/k_BT
Pol γ wild-type, no mtSSB $MP_{SD/PE}$	1.9 ± 0.2	55 ± 34	0.4 ± 0.1
Pol γ wild-type in the presence of mtSSB $MP_{SD/PE}$	1.9 ± 0.2	7 ± 3	0.3 ± 0.1
Pol γ exo-, no mtSSB $MP_{SD/PE}$	1.9 ± 0.2	14 ± 7	0.3 ± 0.1
Pol γ exo- in the presence of mtSSB $MP_{SD/PE}$	2.1 ± 0.2	3 ± 1	0.11 ± 0.05

Table 2. Best parameters for the equation 22, which was fit to the normalized moving probability data. The confidence intervals were calculated for 1σ.

The values yielded by the fits were $K_{SD}^{\dagger}$ = 55 ± 34 and d = 1.64 ± 0.41 nm for Pol γ wild-type and $K_{SD}^{\dagger}$ = 14 ± 7 and d = 1.23 ± 0.41 nm for Pol γ exo- . Extrapolation of the two fits to f = 0 pN gave the values of $MP_{SD/PE}$ ~10% for wild-type Pol γ and ~20% for Pol γ exo-. Note that these values correspond to the normalized moving probabilities. Since during primer extension, the two holoenzymes already spent about 65% of the time in the pause state (MP_{PE} ~ 35%), the absolute probability of finding Pol γ and Pol γ exo- in the active state during their strand displacement activity without assisting external force destabilizing the replication fork is ~ 3.5% and ~ 7% respectively. These results indicate that, while Pol γ and Pol γ exo- present the exact same DNA unwinding mechanism, the Pol γ exonuclease activity however decreases the moving probability of the enzyme by two times as compared to that of the exonuclease-deficient variant. We should note that both, Pol γ and Pol γ exo-, spent similar amounts of time in the active state and it practically did not depend on force (T_a~20-30 s, Figure 22A). The time spent in the pause state for both polymerases however decreased gradually with tension and was approximately two times higher for Pol γ than for Pol γ exo-, Figure 22B. These data suggest that tension and exonuclease activity affect the moving probability of Pol γ by modulating the time the enzymes spent in the pause state and not the time in the active state.

Effect of mtSSB on the strand displacement replication kinetics and processivities.

To determine the effect of mtSSB on the real-time replication kinetics of wild-type Pol γ under strand displacement conditions, we followed the experimental assay described above in the presence of 50 nM mtSSB. In this case, mtSSB binds the displaced strand in the low binding site size mode [53], ~ 35 nucleotides per mtSSB tetramer. We should note that mtSSB binding to the 5' tail of the hairpin in the absence of Pol γ did not results in hairpin unwinding (detectable with our experimental resolution).

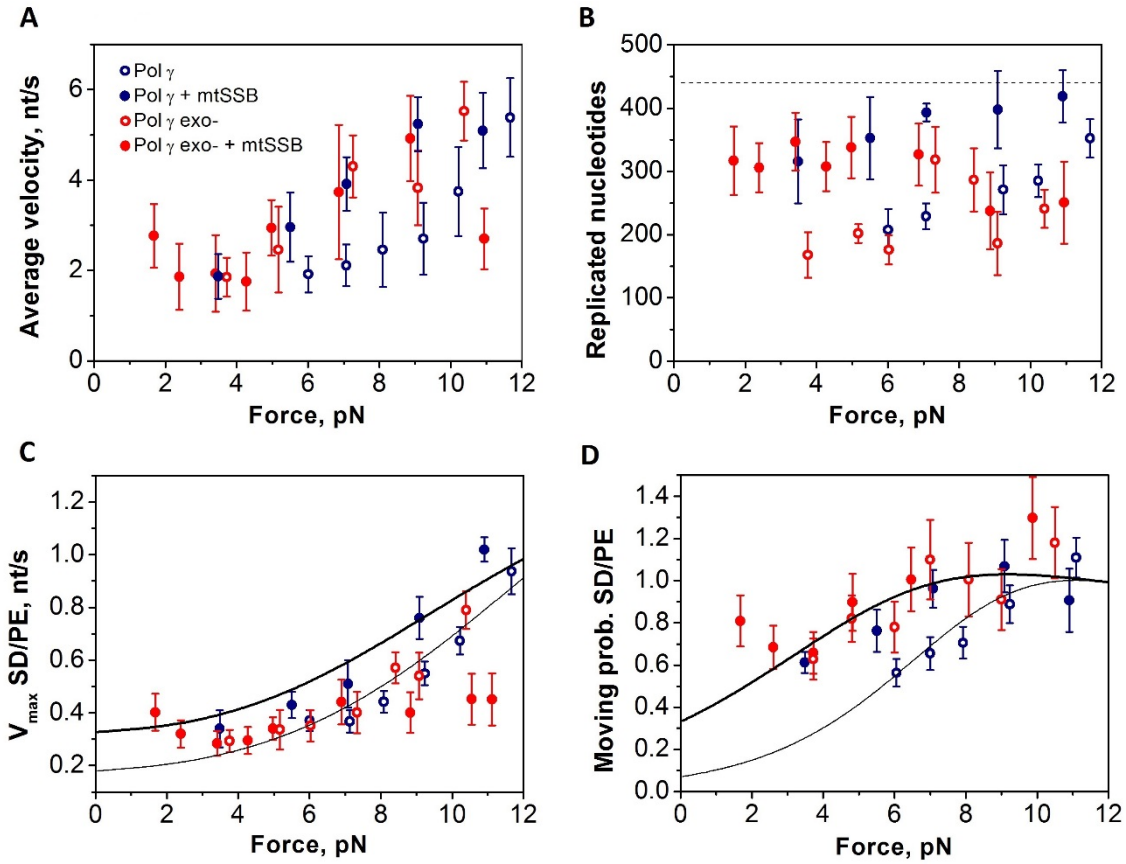

Figure 21. Effect of tension on strand displacement activity of the wild-type Pol γ and Pol γ exo- in the absence and in the presence of mtSSB. Here, empty blue circles correspond to the Pol γ wild-type data in the absence of mtSSB, filled blue circles correspond to the Pol γ wild-type data in the presence of mtSSB, empty red circles represent the Pol γ exo- data in the absence of mtSSB and filled red circles are the Pol γ exo- data in the presence of mtSSB. The data is presented as a mean ± standard error. **A** Change of average replication rate with tension **B** Change of processivity (the number of replicated nucleotides) with tension. **C** Tension dependence of the normalized average replication rate without pauses ($\boldsymbol{V_{max,SD/PE}}$) with the fits of the strand displacement model in the absence and in the presence of mtSSB (thin and thick black lines correspondingly). **D** The effect of tension on the normalized moving probability ($\boldsymbol{MP_{SD/PE}}$) with the fits of the equation 22 to the moving probability data of Pol γ wild-type in the absence and in the presence of mtSSB (thin and thick black lines correspondingly).

Co-replicational binding of mtSSB had an important effect on the strand displacement activity of the two variants, comparing to the conditions without mtSSB: the force required to promote processive strand displacement replication activities decreased from 6 and 2.5 pN (in the absence of mtSSB) to 3 and 1 pN for Pol γ and Pol γ exo- respectively. For the wild-type Pol γ, processivity and strand displacement rate were approximately two times higher than those found under conditions with no mtSSB at all forces, and increased with tension till they reached values found under primer extension conditions (see Figure 21, A and B). In contrast, strand displacement rate and processivity of Pol γ exo- did not increase gradually with applied force in the presence of mtSSB: at the lowest

force, mtSSB binding stimulated the average replication rate of the exo- mutant, however, as tension increased to 3 pN, the replication rate decreased to values similar to those found in the absence of mtSSB. Then, at F > 3 pN, the average replication rate increased with applied force as it was found in the absence of mtSSB, however at tensions higher than 8pN, it decreased again to the values lower than those measured with no mtSSB (Figure 21A). Within the tension range of 1-8 pN the processivity of Pol γ exo- was stimulated by mtSSB similarly to what was for the wild-type polymerase (Figure 21B), however, above 8 pN, the continuous increment in processivity was interrupted (as observed for Pol γ exo- in the absence of mtSSB). These results indicate that the detrimental effect of high forces on strand displacement activity of Pol γ exo- cannot be compensated by the trapping of the displaced strand with mtSSB.

Determination of the mtSSB binding the destabilization of the fork

To determine the contribution of mtSSB binding to the strand displacement activity of Pol γ and Pol γ exo-, we quantified the effect of mtSSB and increasing force on $\boldsymbol{V_{max}}$ and moving probabilities (both normalized by their respective values under primer extension condition) of the two variants.

In the presence of mtSSB, the force dependencies of the normalized $\boldsymbol{V_{max}}$ were different from those measured with no mtSSB (Figure 21C). For Pol γ wild-type, the values of $\boldsymbol{V_{max,SD/PE}}$ at all tensions were slightly higher than those found in the absence of mtSSB, and they increased with applied force until reaching the values matching those found under primer extension conditions (Figure 19A). The interaction energy of Pol γ wild-type and the mtSSB with the fork was obtained with the least-squares fits of the strand displacement model to the $\boldsymbol{V_{max,\ SD/PE}}$ data (Figure 21C) and yielded $\boldsymbol{\Delta G_{int}^{SSB}}$= 1.6 ± 0.3 k_BT (with the range of interaction, $\boldsymbol{M}$= 1). The obtained $\boldsymbol{\Delta G}$ is approximately two times higher than the one found for Pol γ in the conditions with no mtSSB ($\boldsymbol{\Delta G_{int}}$ = 0.9 k_BT, $\boldsymbol{M}$= 1).

For Pol γ exo-, $\boldsymbol{V_{max,\ SD/PE}(f)}$ did not increase in a continuous manner with applied force, instead presenting three different tension-dependent regimes. At the lowest tension (~ 1 pN), $\boldsymbol{V_{max,\ SD/PE}}$ had a value of 0.40 ± 0.07 which is in agreement with the predictions of the strand displacement model for Pol γ and mtSSB (Figure 21C, thick black line), however as tension increased, $\boldsymbol{V_{max,\ SD/PE}}$ of the exo- invariant decreased continuously to the values found under conditions with no mtSSB (Figure 21C). As the applied tension further increased till 7 pN, $\boldsymbol{V_{max,SD/PE}}$ of Pol γ exo- was similar to that measured for the enzyme in the absence of mtSSB. At the highest tension range (F > 7 pN), the values of $\boldsymbol{V_{max,\ SD/PE}}$ decreased even below the values found for the mutant in the absence of mtSSB, indicating again the detrimental combined effect of mtSSB binding and high tension on the strand displacement activity of Pol γ exo-. Regardless the sensitivity of the performance of Pol γ exo- to high tension, the stronger ability of the

exonuclease-deficient variant to perform strand displacement replication made it possible for us to probe the effect of mtSSB on the strand displacement activity at very low tensions (approximately 1 pN). Interestingly, the decrease of $\boldsymbol{V_{max,\ SD/PE}}$ form 1 pN to 3 pN suggests that the energy of interaction between the polymerase and the fork in the presence of mtSSB, $\boldsymbol{\Delta G_{int}^{SSB}}$, may be tension dependent.

Determination of the effect of the mtSSB binding on moving probabilities

Next, we studied the effect of the mtSSB binding and tension on strand displacement moving probabilities, normalized by their corresponding primer extension values, $\boldsymbol{MP_{SD/PE}^{SSB}}$, of Pol γ and Pol γ exo-. In the presence of mtSSB, the normalized moving probability of Pol γ wild-type was higher than that measured in the absence of mtSSB in the whole range of applied forces. As it can be seen in Figure 21D, $\boldsymbol{MP_{SD/PE}^{SSB}}$ of Pol γ increased gradually with applied force approaching the value of 1 at the highest forces, which means that the absolute (non-normalized) strand displacement moving probability, $\boldsymbol{MP_{SD}}$, reached the values characteristic of primer extension conditions, $\boldsymbol{MP_{PE}}$. The least squared error fit of $eq.22$ to this data gave $\boldsymbol{MP_{SD/PE}^{SSB}}(0pN)$~30% and $\boldsymbol{d}$=1.23 ± 0.41 nm, indicating that mtSSB binding increased the moving probability Pol γ wild-type during strand displacement by approximately three times as compared to the conditions where mtSSB was absent ($\boldsymbol{MP_{SD/PE}}(0pN)$~10%). Interestingly, the stimulation of the moving probability of Pol γ by mtSSB can be associated with two opposite effects mtSSB binding has on the times the polymerase spends in active and pause states: at tensions below 6 pN, mtSSB binding increased the time Pol γ spends actively moving through the fork, and, conversely, the binding of mtSSB consistently decreased the average duration of pauses.

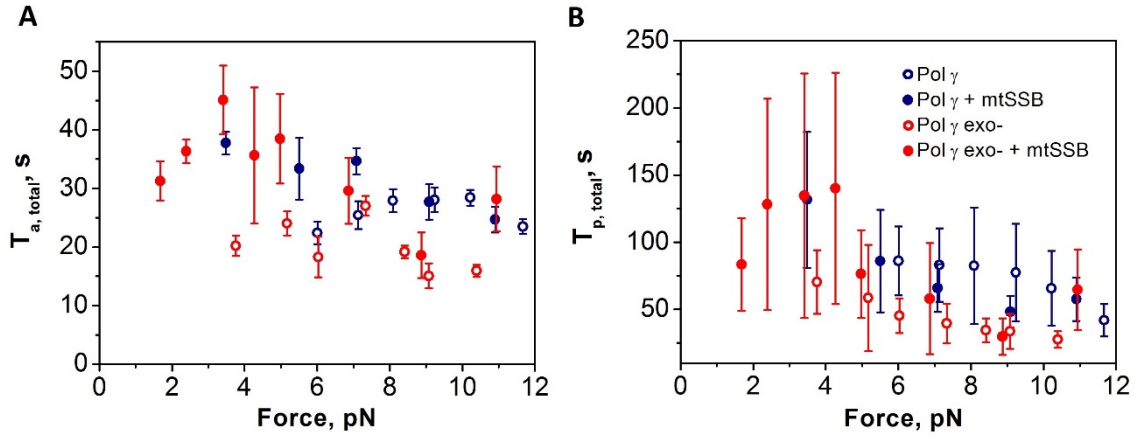

Figure 22. Effect of tension on average total times Pol γ wild-type and Pol γ exo- spent **A** in a state where next DNA synthesis occurs (active state) and B in a state with no net DNA replication (pause state). In **A** and **B**, empty blue circles correspond to the Pol γ wild-type data in the absence of mtSSB, filled blue circles correspond to the Pol γ wild-type data in the presence of mtSSB, empty red circles represent the Pol γ exo- data in the absence of mtSSB and filled red circles are the Pol γ exo- data in the presence of mtSSB. The data is presented as mean ± standard error.

For Pol γ exo-, the normalized moving probability in the presence of mtSSB, $\boldsymbol{MP_{SD/PE}^{SSB}}$, presented force dependency similar to that observed for the maximum replication rate, $\boldsymbol{V_{max,SD/PE}}$ (Figure 21, C and D). At the lowest tension (~1 pN), the moving probability of Pol γ exo- in the presence of mtSSB was roughly two times higher than that predicted by our model (see above) for the conditions in the absence of mtSSB at this tension (thick line Figure 21D), however with the increment of tension, $\boldsymbol{MP_{SD/PE}^{SSB}}$ decreased gradually to reach values similar to those measured in the absence of mtSSB, and F > 3 pN, the moving probability increased gradually with tension (similarly to what we observed in the absence of mtSSB, see Figure 21D). This behavior can be explained by analyzing the average times Pol γ exo- spent in active and pause states in the presence of mtSSB (Figure 22, A and B): at the lowest force, mtSSB binding increased the time the polymerase spends in the active state and decreased the time in the pause state. Also, as applied force increased to 3 pN, the duration of pauses increased drastically. Interestingly, we did not observe this behavior in the case of Pol γ wild-type, where as it was said above, the presence of mtSSB decreased average pause duration, increasing the moving probability of Pol γ at all tensions (> 3 pN).

Altogether, the stimulating effect of mtSSB binding on moving probabilities of Pol γ and Pol γ exo- (in this case at low tensions) promoted average replication rates of the two variants, which allowed us to detect strand displacement activities at lower tensions as compared to the conditions where the mtSSB was absent.

2.4.2 Unwinding activity of TWINKLE

Experimental set-up and detection of individual DNA unwinding activities

To study the real-time kinetics of DNA unwinding by the TWINKLE helicase in the presence and absence of mtSSB, we used optical tweezers to apply mechanical tension to the ends of the two strands of individual DNA hairpins attached between two functionalized polystyrene beads (Figure 23A)**.** We held individual DNA hairpins at constant tensions below 12 pN at which the hairpin remains stably closed. In these experiments, the helicase loads at the protruding 5'-end tail $(dT)_{40}$ of the hairpin, which is attached to the bead placed on top of the micropipette. The unwinding activity of TWINKLE (5 nM hexamers in a reaction buffer containing 4 mM ATP) was tracked as an increase in the end-to-end distance between the polystyrene beads, as the helicase translocates in the 5'→3' direction along the encircled single DNA strand and unwinds the DNA duplex ahead of it, excluding the opposite DNA strand (Figure 23B). The change in distance was converted to a number of unwound base pairs as a function of

time at a given constant force, taking into account that a single catalytic step results in the increase of the tethered molecule's extension equivalent to the extension of two single stranded nucleotides (or two SSB-bound nucleotides when the experiments are conducted in the presence of mtSSB) at a given force (see methods section 2.3.6.1.). The corresponding extensions per nucleotide at each force of SSB-free and SSB-bound ssDNA were obtained from the force-extension curves recorded under the buffer conditions of the DNA unwinding assay (50 mM Tris–HCl, pH 7.5, 30 mM KCl and 4 mM $MgCl_2$, section 2.2.3.1).

We note that the following results are still preliminary. Additional data and a detailed modeling of the results are absolutely required to understand the mechanism of DNA unwinding by the mitochondrial replicative DNA helicase.

Effect of fork stability on the real-time kinetics of DNA unwinding

To characterize the effect of the mechanical stability of the replication fork on the unwinding activity of TWINKLE, we monitored the change in extension of individual DNA hairpins at increasing constant tensions below 12 pN. In the whole range of tensions, at which DNA unwinding was detected, we observed two types of activities:

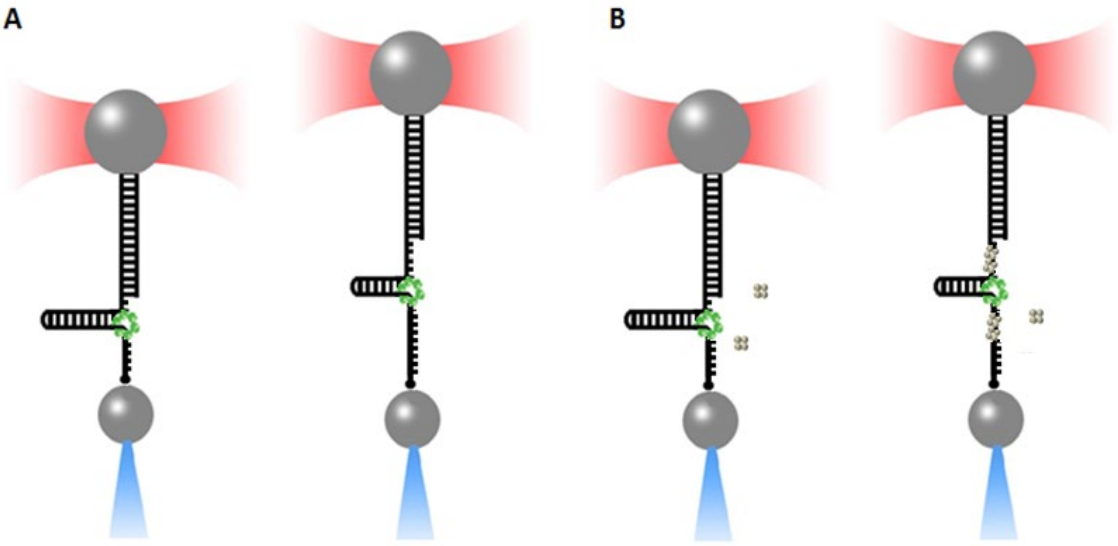

Figure 23. **A** In a DNA unwinding assay, the hairpin is held at constant tensions below 12 pN. The helicase encircles the protruding 5'-end tail $(dT)_{40}$ of the hairpin, translocates in the 5'→3' direction, unwinding the hairpin. The unwinding of the hairpin results in the increment of the DNA extension. **B** In a DNA unwinding assay in the presence of mtSSB, SSB tetramers gradually bind the displaced single DNA strand as well as the encircled strand behind the helicase.

DNA unwinding events followed by a long pause with no subsequent annealing (the total number of observed unwinding events of this type, N=37) and unwinding events followed by re-annealing of the hairpin (the total number of observed re-annealing events, N=33), leading to a decrease in the extension of the DNA tether (Figure 24, A and B). The kinetics of the re-annealing reaction (Figure 24, A and B and Figure 26) argues against a sudden re-zipping of the hairpin due to helicase dissociation (an instantaneous extension drop would be expected in this case). Instead, this behavior suggests that the extension recovery, following the unwinding, is a result of the annealing of the hairpin in the presence of the helicase. This observation is compatible with the annealing activity described previously *in vitro* for this helicase [111].

In our experimental assay, unwinding activities were detected at $\boldsymbol{f} \geq 5$ pN (Figure 25). The average number of unwound nucleotides per event (unwinding processivity) was 35 base pairs, consistent with the average number of nucleotides unwounded by the helicase in *in vitro* studies in the absence of tension, ~20-30 bp ([86], [111]). Interestingly, the unwinding processivity did not present a consistent dependence on the applied force in contrast to what has been observed and predicted for other replicative DNA helicases ([174] - [176]), (Figure 25). Also, the processivity of the DNA re-annealing reaction did not present any clear dependence on applied tension (Figure 25).

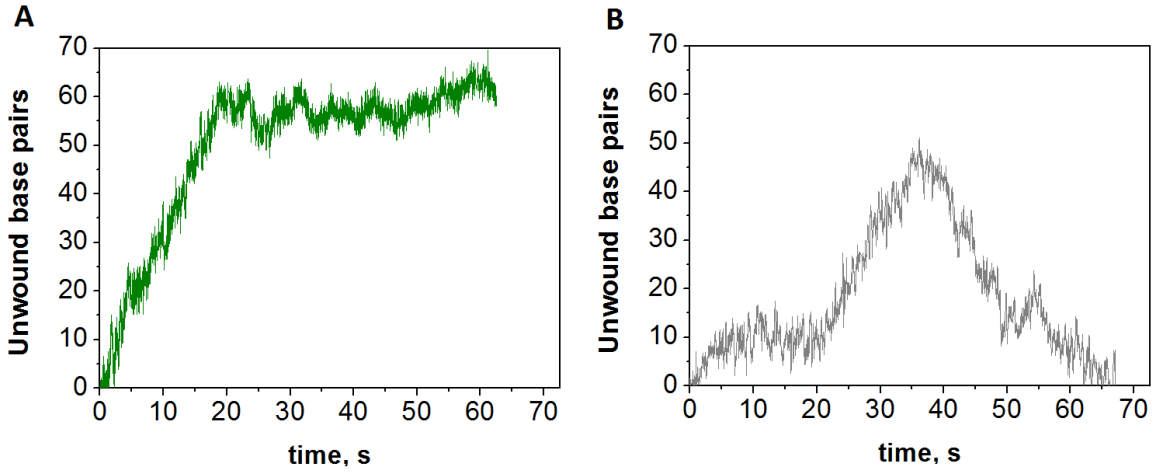

Figure 24. A An example of a trace of an individual unwinding activity followed by a long pause (no subsequent DNA annealing is observed). **B** An example of a trace of an individual unwinding activity with subsequent annealing of the hairpin, which results in the recovery of the initial extension.

The average unwinding and annealing velocities were calculated by dividing the total number of unwound or annealed base pairs by the total time of the activity. The obtained values of average unwinding and annealing velocities at different tensions are shown in Figure 26A. On average, we did not observe significant differences between the average velocities of each reaction, which suggests that the annealing rate is limited by the

helicase translocation rate on ssDNA. For the two types of TWINKLE activity, the average velocities did not present any clear dependence on applied tension.

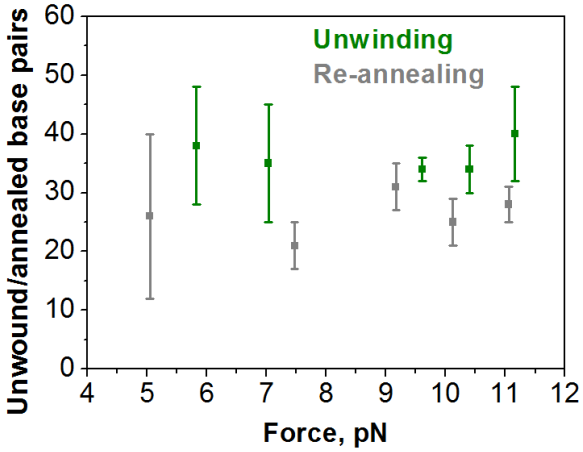

Figure 25. The average processivity of unwinding (the average number of unwound nucleotides of the DNA duplex) at different tensions is represented by the green dots. In our experimental assay, the helicase unwinds an average number of 35 base pairs. The processivity of the helicase is not affected by applied tension. On average, the processivity of re-annealing (grey dots) was ~23% lower than the processivity of DNA unwinding. The number of re-annealed base pairs does not show any evident dependence on force.

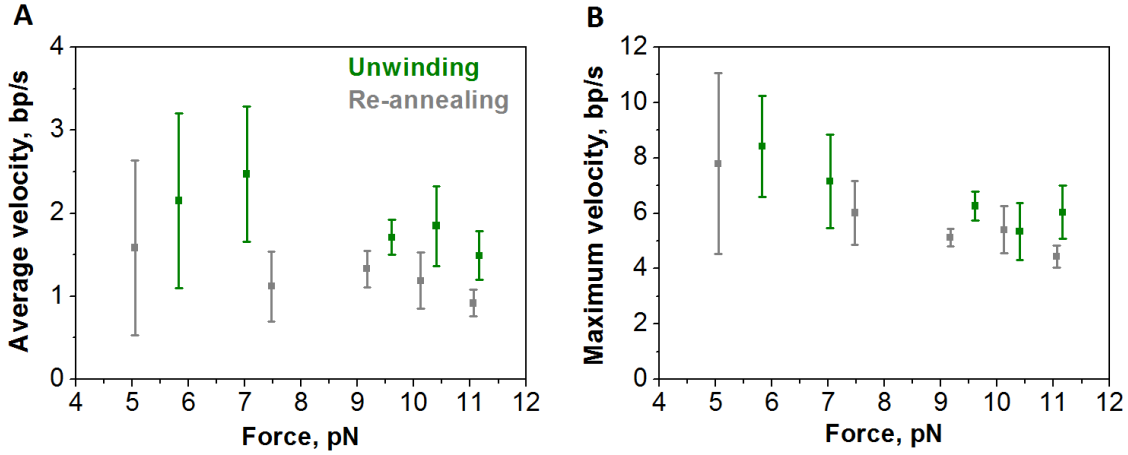

Figure 26. **A** The effect of tension on the average velocities of TWINKLE during its unwinding (green dots) and annealing (grey dots) activities. **B** The effect of tension on the pause-free unwinding velocity ($\boldsymbol{V_{max}}$) for DNA unwinding (green dots) and annealing (grey dots).

Overall, these results contrast with the strong force dependencies measured in previous single-molecule manipulation studies for the unwinding processivities and unwinding rates of other replicative DNA helicases ([174] - [176]) and suggest that the DNA unwinding mechanism of TWINKLE may be significantly different from that reported for other replicative hexameric helicases.

During a typical unwinding or annealing activity, time intervals in which the helicase is actively moving with constant velocity are followed by time intervals during which, within our resolution, the helicase does not present any significant activity (so-called paused states, see Figure 24). To differentiate the effect of force on the active and paused states of TWINKLE, we calculated the average unwinding and re-annealing velocities without pauses at each force, $\boldsymbol{V_{max}(f)}$, following the procedure described in section 2.3.6.2. We found that the maximum rates for the two reactions are similar and force independent. During the re-annealing reaction, the fork is behind the helicase and the helicase rate under these conditions would correspond to the translocation rate of TWINKLE on ssDNA. The similarity between the unwinding and re-annealing rates may indicate that TWINKLE is moving at its maximum rate on the fork, which in turn would explain the absence of force dependencies (see discussion).

Effect of mtSSB binding on the DNA unwinding reaction

To determine the effect of mtSSB on the real-time unwinding kinetics of TWINKLE, we performed the experiments described above in the presence of 5 nM mtSSB. In this case, as the DNA unwinding proceeds, the mtSSB gradually covers the displaced ssDNA as well as the encircled ssDNA strand behind the helicase.

Overall, binding of mtSSB to ssDNA had a significant effect on the unwinding activity of TWINKLE in comparison to the conditions in the absence of mtSSB:

1) In the presence of mtSSB, all unwinding activities were followed by a long pause and re-annealing events were no longer observed (Figure 27). This is consistent with the mtSSB binding to ssDNA and preventing the re-annealing reaction.

2) Binding of mtSSB to ssDNA allowed us to detect helicase activities at force as low as 2.6 pN, which is consistently lower than the minimal force at which we detected DNA unwinding in the absence of mtSSB (5.5 pN).

3) At the lowest force (2.6 pN), the helicase unwinds, on average, 110 base pairs in the presence of mtSSB, which is three times higher than the number of base pairs unwound by TWINKLE in the absence of mtSSB at 5.5 pN. This result contrasts with previous *in vitro* assays in which mtSSB seemed not to affect the processivity of the helicase [113], see discussion. Interestingly, the stimulatory effect of mtSSB on

unwinding processivity decreased gradually with tension to reach the processivity values measured in the absence of SSB, see discussion (Figure 28).

As compared to the results in the absence of mtSSB, binding of mtSSB to the excluded strand and to the strand encircled by the helicase had a small effect on $\boldsymbol{V_{max}}$ (Figure 28B). At 2.6 pN, TWINKLE unwinds the DNA duplex with the same rate as it does it at 6-7 pN in the absence of mtSSB. Similarly to the case of DNA unwinding in the absence of mtSSB, the obtained $\boldsymbol{V_{max}}$ values for the DNA unwinding in the presence of mtSSB did not show any consistent dependence on force (they only slightly decreased from ~8 bp/s at 2.6 pN to ~6 bp/s at 9 pN). This is consistent with TWINKLE moving at its maximum rate already, as mention above.

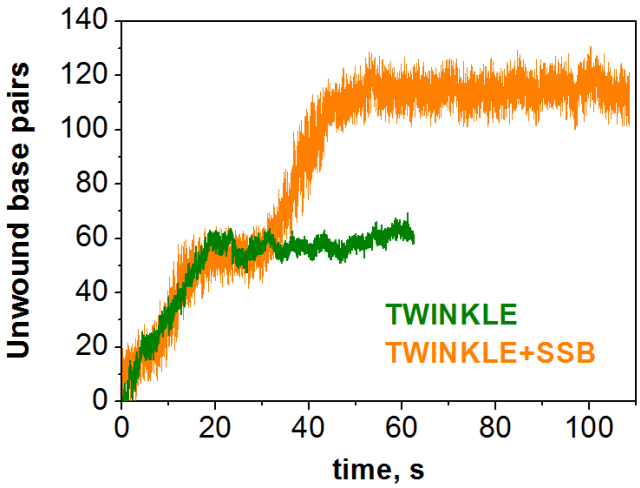

Figure 27. Examples of traces of individual unwinding activities in the presence of mtSSB (orange) and in the absence of mtSSB (green). In both cases, the helicase activity is followed by a long pause.

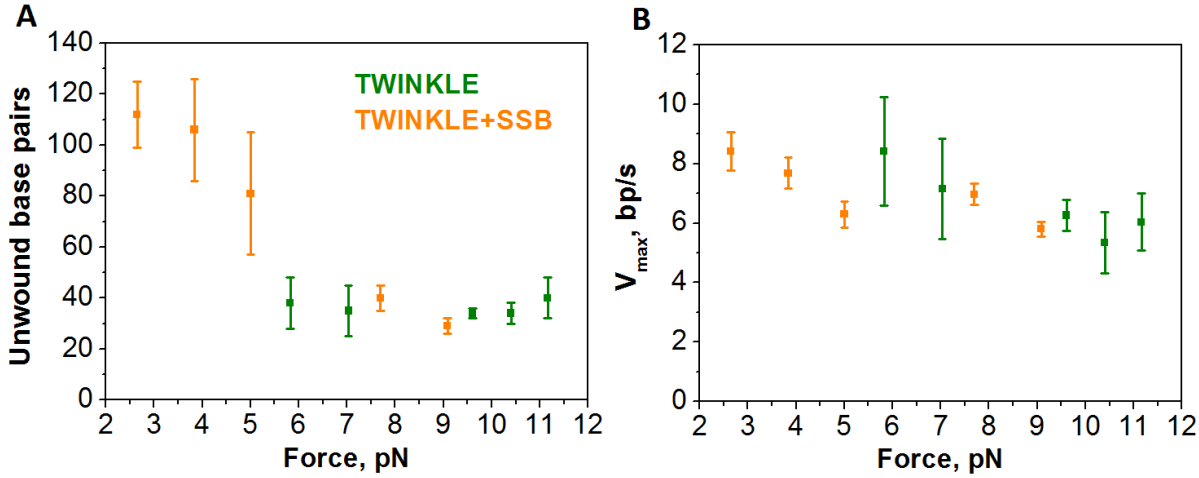

Figure 28. A Effect of external tension on the processivity (the number of unwound base pairs) of TWINKLE in the presence of 5 nM mtSSB (orange dots) and in the absence of mtSSB in (green dots). **B** Effect of applied tension on the maximum unwinding velocity in the presence of 5 nM mtSSB (orange dots) and in the absence of mtSSB (green dots).

2.4.3 Coordinated activity of Pol γ and TWINKLE

Experimental set-up and detection of individual Pol γ strand-displacement activities in the presence of TWINKLE

Next we aimed to measure strand displacement activity of the wild-type Pol γ when it works together with the helicase at the replication fork. To study the real-time kinetics of Pol γ in the presence of TWINKLE, we held individual DNA hairpins under tensions below 12 pN and monitored individual strand displacement activities in the presence of 2 nM polymerase and 5 nM helicase hexamers in the replication buffer (see section 2.3.5.1) that additionally contained 4 mM ATP needed for the helicase activity of TWINKLE. An individual activity was tracked as an increase of the end-to-end distance of the tethered DNA molecule as TWINKLE/Pol γ unwind the hairpin and a single Pol γ elongates the 3' end of the dsDNA handle incorporating corresponding complementary nucleotides to the template DNA, displacing the complementary strand. The change in distance was converted to the number of replicated nucleotides as a function of time at a given force as it was done for strand displacement activities of individual Pol γ wild-type and Pol γ exo-.

Effect of fork stability on the coupled activity of Pol γ and TWINKLE

In the presence of both, Pol γ and TWINKLE, processive replication events were detected at $F \geq 3$ pN (Figure 29), whereas when the enzymes work solo, they can initiate DNA unwinding at $F \geq \sim 6$ pN. At 3 pN, the two enzymes were able to replicate ~100 bp. The number of replicated nucleotides (processivity) increased with tension and, at $F \geq \sim 6$ pN, it reached values ~8 times higher than the values characteristic of the helicase activity of TWINKLE, and similar to those displayed by Pol γ (Figure 29A). These results indicate that the two enzymes worked in a coordinated manner at the replication fork. Interestingly, at tensions above 7 pN, the replication processivity of the two enzymes started to decrease with applied force till, at the highest tension, it dropped to the values even lower than those of Pol γ working alone. These results reflect the negative effect of tension on the coordination between the polymerase and the helicase.

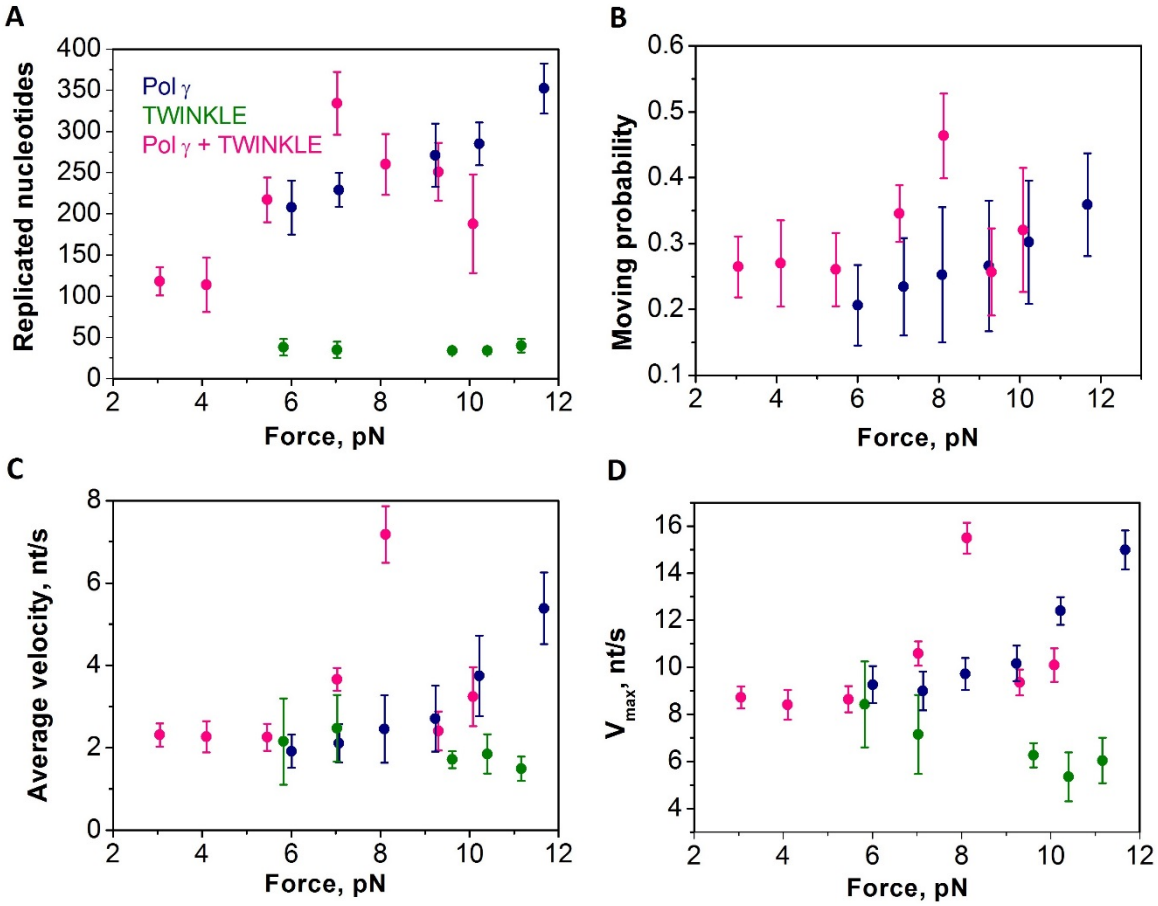

Figure 29. Effect of tension on: **A** processivity of coordinated activity of Pol γ and TWINKLE (pink dots), activities of individual Pol γ (blue dots) and individual TWINKLE (green dots); **B** moving probability in the conditions of coordinated activity of Pol γ and TWINKLE (pink dots) and when Pol γ replicates alone (blue dots); **C** average replication velocity and **D** average replication rate in the absence of pauses, $\boldsymbol{V_{max}}$, during coordinated activity of Pol γ and TWINKLE (pink dots), activities of individual Pol γ (blue dots) and individual TWINKLE (green dots).

Overall, the ability of the two enzymes to initiate processive strand displacement synthesis at significantly lower tensions as compared to the conditions where Pol γ operates alone can be explained by analyzing the probability of finding Pol γ in the active (polymerase competent) state (its moving probability, defined by eq. 14). As it can be seen in Figure 29B, coupling with the helicase favors the moving probability of the polymerase through the fork: in the whole range of tensions below 8 pN, the moving probability of Pol γ coupled with TWINKLE is higher than that of Pol γ working without the assistance of the helicase. Curiously, at tensions above 8 pN, the moving probability drops to the values found in the conditions of Pol γ operating solo, which again demonstrates the detrimental effect of tension on the ability of the two enzymes to coordinate their activities.

Furthermore, the coordination of activities of Pol γ and TWINKLE was also reflected in the observed replication rates: below 9 pN, the average replication rate and $\boldsymbol{V_{max}}$ increased rapidly with applied tension, reaching the values similar to those of primer extension activity of Pol γ at 8 pN (Figure 29, C and D). In contrast, to promote strand displacement activity of Pol γ to this extent, when the holoenzyme operates alone, the fork needs to be destabilized by significantly higher tensions (>11 pN). These results again point out that, when working at the replication fork, Pol γ and TWINKLE couple their activities, dramatically decreasing the activation energy of DNA unwinding. Interestingly, at tensions above 8 pN, the average replication rate and $\boldsymbol{V_{max}}$ dropped to the values similar to that of Pol γ working alone, which once again reflects the negative effect of high tension on the coordinated activity of the two enzymes.

2.5 Discussion

Pol γ vs. Pol γ exo-

Human mitochondrial DNA replication is carried out by a minimal replication complex that includes Pol γ holenzyme, the TWINKLE helicase and the mtSSB. In isolation, none of these three components is able to efficiently unwind the replication fork during leading strand synthesis.

Wild-type Pol γ has a very limited strand displacement activity and it is unable to use dsDNA as a template. In our strand displacement assays, a substantial destabilization of the fork (≥ 6 pN) was required to detect processive activity of individual Pol γ. The replication rate and the processivity of the enzyme were sensitive to applied tension, indicating the negative effect of the fork stability on strand displacement activity of Pol γ (Figure 21, A and B). The replication rates in the absence of pauses, $\boldsymbol{V_{max}}$, also presented strong dependency on tension: at the lowest force, the maximum replication rate of Pol γ presented ~40% of its maximum replication rate during primer extension (Figure 21C) and, $\boldsymbol{V_{max}}$ increased gradually with applied tension till they reached values showed by the holoenzyme during primer extension DNA synthesis. The moving probability of Pol γ during under strand displacement conditions also drastically increased applied tension. Our model predicted that in the absence of tension the probability of finding the polymerase in active state is only ~ 10% of the moving probability of Pol γ during primer extension (Figure 21D). The moving probability increased as we applied tension and, at F ~ 6 pN, it reached ~56% of the primer extension moving probability, which allowed us to detect processive Pol γ activity. The further increment of tension promoted the moving probability till it saturated at ~1 at high tensions, meaning that Pol γ displayed the same moving probability as found during primer extension. This strong force dependence of the probability of finding the polymerase performing an active strand displacement replication moving probabilities of both enzymes also increased with tension (Figures 21D), again, points out the negative effect of the fork stability on the advance of the polymerase.

As it was shown for several other polymerases ([105] - [108]), inactivation of 5'-3' exonuclease site in Pol γ stimulates its strand displacement activity [172], indicating that the ability to catalyze strand displacement is an intrinsic property of the polymerase and it is masked in the wild-type Pol γ by the exonuclease contribution. The successive cycles of polymerization and exonuclease at the fork are known as idling and it has been observed as a pause of Pol γ with our current experimental resolution. During replication, the strand displacement activity of Pol γ should be downregulated by polymerase-exonuclease balance (idling) to avoid uncoupling with the helicase and to prevent the creation of 5'-flaps that impair normal mtDNA ligation. With our current resolution, we did not detect any processive exonuclease activity of wild-type Pol γ, which is in agreement with idling reaction.

Overall, our data on strand displacement activity of the exonuclease-deficient variant of Pol γ, suggests that the absence of exonuclease contribution favors the ability of the polymerase to initiate DNA unwinding at the stably closed fork (by preventing idling). At highest tensions, the maximum replication rate is expected to be similar to that of primer extension conditions (as it is found for Pol γ wild-type, Figure 19A), however, in the case of the exo- mutant, at the highest tension, the $\boldsymbol{V_{max}}$ of Pol γ exo- is lower than in primer extension conditions. Furthermore, at tensions above 7 pN, the processivity of the exonuclease deficient Pol γ is no longer promoted by force, as opposed to what we observed for the wild-type holoenzyme (Figure 21B).

As it has been shown for yeast Pol δ [177], the interaction with long 5'-flaps of displaced DNA may inhibit strand displacement activity of Pol γ and disruption of this interaction by tension should promote strand displacement. However, the strand-displacement activity of Pol γ exo- is less inhibited by the displaced strand (the enzyme is able to initiate processive DNA synthesis at lower forces). This indicates that the interaction with the displaced strand may be important for strand displacement activity of Pol γ.

Pol γ + mtSSB

Single stranded DNA binding proteins bind ssDNA with high affinity and in a sequence-independent manner ([178], [179], [127]), preventing ssDNA from degradation and stimulating DNA replication. Under primer extension conditions, mtSSB stimulates DNA synthesis by removing the template secondary structure and by facilitating primer recognition [180] and processivity of Pol γ [135]. In addition, mtSSB establishes functional interaction with Pol γ that promotes its release from ssDNA during primer extension [134].

SSB binding is also known to play an important role during strand displacement synthesis (e.g. Eco SSB promotes strand displacement synthesis by T7 DNA polymerase and DNA polymerase I ([181], [105]) and gp32 protein stimulates strand displacement ability of T4 DNA polymerase [105]). Little is known about the effect of mtSSB on the strand displacement activity of Pol γ.

According to our results, mtSSB increases the moving probability of Pol γ and lower the force required to promote processive strand displacement DNA synthesis (form 6 to 3 pN, see Figure 21). These results suggest that the mtSSB binding modulates the polymerase-exonuclease equilibrium and promotes the polymerase function of Pol γ over its exonuclease function, preventing idling. A possible explanation of this stimulation of the polymerase function is that the mtSSB binding eliminates the secondary structure of the displaced ssDNA strand, which may hinder the advance of the polymerase. Additionally, mtSSB binding to the displaced strand prevents its re-annealing to the template, which makes the process of exonucleolysis less energetically favorable.

MtSSB binding slightly stimulates the $\boldsymbol{V_{max}}$ of Pol γ (Figure 21C), which according to the strand displacement model, means that mtSSB contribute to the destabilization of the fork. We found that this additional destabilizing effect is due to the energy gain as a result of mtSSB binding to the displaced strand. On the other hand, in the presence of mtSSB, the processivity of Pol γ increased two times in comparison to the conditions in the absence of mtSSB (Figure 21B). These results point out the role of mtSSB in promoting Pol γ stability at the replication fork.

As we have shown here, Pol γ exo- is able to initiate processive strand displacement synthesis at low forces (3 pN). The presence of mtSSB lowered the initiation force to 2.5 pN. We found that at low forces mtSSB greatly stimulates $\boldsymbol{V_{max}}$ and its stimulatory effect decreases with applied tension. These findings may indicate the existence of functional interaction between the polymerase and mtSSB.

Unwinding and annealing activity of TWINKLE

TWINKLE, as many replicative helicases [182], is able to unwind only short stretches of DNA. *In vitro* the helicase can unwind just up to ~25 base pairs ([86], [111]). The average processivity of TWINKLE that we observed in our experiments (~35 bp, Figure 25) is in agreement with these previous findings *in vitro*.

The force independency of the processivity of TWINKLE might be relevant to the determination of its mechanism of DNA unwinding. Overall, depending on the mechanism of coupling translocation to unwinding helicases are considered to behave as passive or active unwinding motors. On one hand, optimally active helicases greatly destabilize the fork, lowering the activation energy of base pairs melting, which promotes DNA unwinding. On the other hand, the unwinding activity of passive helicases relies on transient thermal fraying of the base pairs ahead. Most of the helicases display a behavior between that characteristic of ideal optimally active and optimally passive helicases. One of the ways to classify a helicase as active or passive is to estimate the energy of interaction between the enzyme and the fork, which results in disruption of base pairs stability, for example, by using Bretterton and Jülicher framework [183]. An optimally active helicase would unwind dsDNA at velocity close to its translocation rate on ssDNA [160], whereas the unwinding velocity of a passive helicase should depend greatly on the stability of the fork (which is ultimately dictated by sequence, and in our experiments on the external force destabilizing the fork), [183].

It has been suggested that, for passive helicases, the binding time (time of activity) is independent of tension, while the velocity of unwinding would increase rapidly with force. To the contrary, in the case of optimally active helicases, the helicase binding time would increase with tension, while the unwinding rate remains constant [184]. Hence, for the two types of helicases, the processivity should increase when the force increases.

The unwinding velocity of some other hexameric helicases, like T7 and T4 helicases, is known to be strongly force dependent ([161], [175]). Accordingly, basing on different criteria, the T7 helicase was defined as either passive or partially active helicase ([183], [161]), and the unwinding mechanism of the T4 helicase was classified as passive [175]. In contrast to what has been observed for the T7 and T4 helicases, according to our findings, the unwinding velocity of TWINKLE is force independent. Moreover, in our experiments the helicase binding time did not present any evident dependency on force either, and as a result, the unwinding processivity of TWINKLE was also tension-independent. With the obtained data, we cannot classify TWINKLE as rather active nor passive helicase, but we can say that it presents an unwinding mechanism that may be different from those proposed for other ring-shaped helicases.

A possible explanation for the force independence of TWINKLE unwinding velocity lies in the ability of the helicase to interact with the displaced DNA strand. It is known that TWINKLE can bind ssDNA within the central hole of the hexamer as well as on its outer surface, and this ability may confer the protein its annealing activity [111], which we also observed in our experiments. We hypothesize that by binding the occluded and the displaced strands, TWINKLE may shield the fork junction from the effect of tension. In fact, the ability to hold on both RNA strands during unwinding was previously demonstrated for the non-ring shaped hepatitis C NS3 helicase [60], and the insensitivity of its unwinding rate to external tension [185] was proposed to be attributed to the enzyme's ability to shelter the fork junction. Such ability of TWINKLE would give a reason for the force independence of the helicase unwinding rate, and it would also explain why the unwinding velocity is not affected by mtSSB binding (see below).

~47% of all observed hairpin unwinding events were followed by DNA re-annealing. The kinetics of the re-annealing reaction argues against a sudden re-hybridization of the hairpin as a result of helicase dissociation, because, in the latest case, an instantaneous change in extension would be observed. As it was said above, these findings are in agreement with previously described *in vitro* annealing activity of TWINKLE [111]. We found that TWINKLE anneals two complementary strands of the hairpin at the same rate as it unwinds dsDNA. During re-annealing the helicase does not encounter the fork ahead of it (the fork is behind TWINKLE), therefore during re-annealing the helicase may move at its translocation rate. Unless TWINKLE can reverse its translocation polarity, which is highly improbable, its annealing activity involves strand switching, which requires close contact with both DNA strands, in agreement again with observed force independence.

Modulation of TWINKLE activity by mtSSB binding

As it was said above, we found that mtSSB binding promotes the initiation of DNA unwinding by TWINKLE: in the presence of mtSSB we were able to detect unwinding activities at tension as low as 2.6 pN, whereas in the absence of mtSSB the helicase is able to initiate unwinding only when the DNA hairpin is subjected to tensions higher than

5.5 pN. At low tensions (≤ 5 pN), mtSSB binding increased the helicase binding time which resulted in the incremented unwinding processivity of TWINKLE, while the helicase unwinding rate was unaffected by the presence of mtSSB and remained virtually constant at all forces (Figure 28, A and B).

In the presence of mtSSB, we did not observe any annealing activity of TWINKLE at all forces. MtSSB binding stabilizes the two unwound strands, hindering hairpin re-annealing. Besides, mtSSB binding may impede strand switching by the helicase and therefore prevent TWINKLE from shifting to DNA annealing. In fact, binding of mtSSB to ssDNA hinders helicase loading: at mtSSB concentration used in the strand displacement replication assay (50 nM) we did not observe any unwinding by TWINKLE, and only after we had decreased the mtSSB concentration ten-fold, the helicase was able to initiate unwinding.

As it was discussed above, the insensitivity of the helicase unwinding rate to external force may be explained by the ability of TWINKLE to shelter the fork by holding on both unwound DNA strands. In this case, the mtSSB binding would not have any destabilizing effect on the fork since it is protected by TWINKLE from external disruptions. Consequently, mtSSB would not have any effect on $\boldsymbol{V_{max}}$, which is in agreement with our findings (see Figure 28B).

At the lowest tensions (2-5 pN), mtSSB had a marked effect on TWINKLE unwinding activity. According to our findings, the processivity of TWINKLE was stimulated approximately five-fold by mtSSB in comparison to what was observed *in vitro* experiments ([86], [111]). Similar stimulatory effect of SSBs was found for other helicases (e.g. for NS3 [186] and RecQ [187]), but not for TWINKLE. One of the possible explanations for the stimulatory effect of mtSSB is that mtSSB traps the excluded strand, which as discussed above, in the absence of mtSSB might interact with the helicase. This, in turn, may decrease its binding time in an unwinding-competent conformation. Besides, mtSSB binding may prevent TWINKLE from sliding back due to the fork pressure, which would also increment unwinding processivity. Interestingly, as tension increases, the effect of SSB disappears. To explain this phenomenon, among other possibilities, we propose two hypothesis: our findings might indicate that mtSSB interacts (specifically or nonspecifically) with TWINKLE, promoting the helicase processivity. This hypothesis is supported by observed sensitivity of the stimulating effect of mtSSB to tension: the applied force might disrupt the interaction between TWINKLE and mtSSB, resulting in decrease of the helicase processivity to the values similar to those found in the absence of mtSSB. Overall, the enhanced processivity of TWINKLE arises from the longer binding times of the helicase in the presence of mtSSB at low tensions. This means that mtSSB might stabilize the attachment of TWINKLE at the fork.

Pol γ and TWINKLE

In this thesis we studied real-time kinetics of coordinated activity of Pol γ and TWINKLE at the replication fork. Overall, our data suggests that, the presence of the helicase facilitates the initiation of the DNA unwinding and replication (working together, the polymerase and the helicase are able to initiate processive DNA replication at 3 pN, whereas when the two proteins operate independently, they can unwind the fork at F ≥ 6 pN, see Figure 29). This can be explained by analyzing the probability of finding the polymerase in the active state (moving probability, $\boldsymbol{MP}$, Figure 29B) in the presence and absence of the helicase: TWINKLE increased the probability of finding Pol γ in the active state at all tensions below 7 pN, meaning that the helicase lowers the pause occupancy of Pol γ, promoting the polymerase function of Pol γ over its exonuclease activity. While the processivity (the average number of replicated nucleotides) remained similar to that found in the conditions when the polymerase operated alone (Figure 29A), at tension below 8 pN, the average polymerization rate and the average polymerization rate without pauses, $\boldsymbol{V_{max}}$, were significantly higher when Pol γ and TWINKLE worked together as compared to the conditions when the polymerase worked independently (Figure 29, C and D). Thus, the increment in the average replication velocity in the presence of the helicase is a result of two factors: on one hand, the decrease in the duration of pauses (reflected in the higher moving probability) and, on the other hand, the increment of $\boldsymbol{V_{max}}$. Also, it is worth nothing that Pol γ drastically promotes the unwinding activity of TWINKLE. During replication, the polymerase stabilizes the template strand converting it into dsDNA, impeding the annealing activity of TWINKLE, which leads to the dramatic increment in helicase processivity (Figure 29A). Overall, these results point out that the polymerase and the helicase couple their activities when working at the replication fork.

The existence of functional coupling between replicative polymerases and helicases was observed for many replicative complexes ([171], [188] - [190]), including mitochondrial DNA replisome [86]. In particular, it is well known that the interactions between the T7 DNA helicase (gp4) and T7 DNA polymerase (gp5) are essential for initiation and realization of effective leading strand DNA synthesis performed by the T7 replisome [191]. The two proteins connect through charge-charge interactions: the negatively charged acidic C-terminal tail of the helicase interact with the basic residue on the polymerase ([192], [191]). The recent cryo-EM visualization of the structures of the T7 replisome revealed how the T7 helicase and polymerase are organized at the replication fork to work in a coordinated manner [193]. It was found that the two proteins form a T-shape structure with the replication fork: the helicase and the polymerase, each one on its strand, translocate in opposite directions, which are tangential to the direction of DNA duplex. Overall, similar organization of TWINKLE and Pol γ at the replication fork would explain the assisting effect of tension on the strand displacement replication as tension favors the 'correct' geometry of the replication fork (the two unwound strands being perpendicular to the direction of the DNA duplex ahead of the fork). Actually, it was proposed that TWINKLE and Pol γ could interact via charge-charge interactions through a highly positively charged C-terminal region in TWINKLE and the large negatively

charged region near the exo domain of Pol γ [96]. Excessive tension applied to the fork however could have deleterious effect on interactions between Pol γ and TWINKLE and/or their interaction with the fork, which would result in disruption of the 'correct' geometry of the fork. Indeed, we found that, at tensions, above 8 pN the strand displacement activity of Pol γ is no longer promoted by the helicase: the values of moving probability, average replication rate and $\boldsymbol{V_{max}}$ are very similar to those found in the conditions when Pol γ replicates alone. These results suggest that Pol γ and TWINKLE interact and couple their activities at the replication fork, and that this coupling is disrupted at high tensions, that affect the interactions between the two proteins and/or their interactions with the fork.

To date, there is no proof of the physical interaction between Pol γ and TWINKLE, although it has been shown that Pol γ subunit is needed for coordination between the holoenzyme and the helicase [194].

2.6 Conclusions

According to the results obtained in this part of the thesis, it can be concluded that:

1. The exonuclease activity of Pol γ modulates strand displacement activity of the holoenzyme. The exonuclease activity of Pol γ leads to idling, which hiders the ability of the polymerase to initiate processive DNA synthesis.

2. The capacity of Pol γ to carry out strand displacement DNA synthesis strongly depends on the stability of the fork. Co-respirational binding of mtSSB promotes strand displacement activity of Pol γ in terms of processivity and replication velocity.

3. We quantified the DNA unwinding activity of Pol γ in the presence and in the absence of mtSSB. According to our results, mtSSB binding adds additional destabilization of the replication fork. Our findings indicate that Pol γ presents the same mechanism of DNA unwinding in the presence and in the absence of mtSSB. MtSSB binding promotes the ability of Pol γ to initiate processive unwinding of the fork by favoring the polymerase activity of the holoenzyme over its exonuclease activity, which prevents idling.

4. MtSSB binding promotes the processivity of TWINKLE and the ability of the helicase to initiate DNA unwinding.

5. Pol γ and TWINKLE coordinate their activities at the replication fork. Pol γ promotes the unwinding activity of TWINKLE, dramatically increasing the processivity of the helicase and the DNA unwinding velocity. The two proteins mutually stimulate each other's ability to initiate the unwinding of the replication fork.

Chapter 3

CONFORMATIONAL DYNAMICS OF INDIVIDUAL MOLECULAR SHUTTLES

3.1 Introduction

Molecular shuttles are now of great research interest, due to their potential applications in different fields, from molecular machinery and electronics to biomedicine ([195] - [197]). These devices are constructed of a dumbbell-shaped component composed by a molecular thread with two bulky 'stoppers' on its ends and a macrocycle that encircles the thread. In these systems, the macrocycle can move between two or more recognition sites on the molecular thread, like a train between stations, as a response to an external stimulus. The term 'molecular shuttle' was first introduced by F. Stoddart in 1991 (Figure 30), [198] for a degenerate donor-acceptor [2] rotaxane. In this rotaxane, the cyclobis-(paraquat-*p*-phenylene) ($CBPQT^{4+}$, blue in Figure 30) ring can move back and forth between two hydroquinone recognition sites.

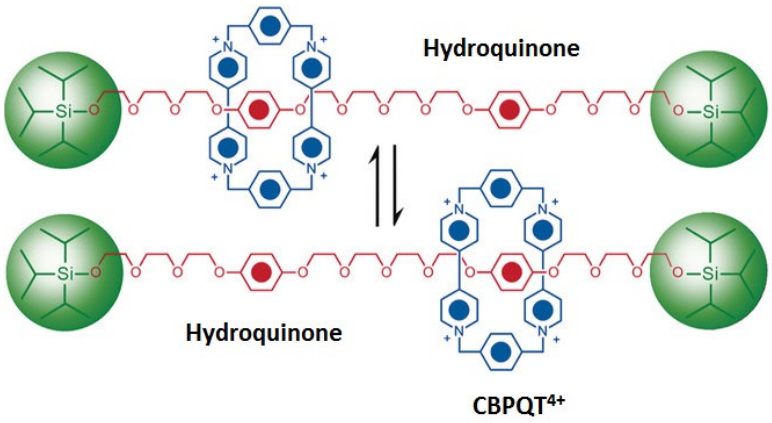

Figure 30. $CBPQT^{4+}$ macrocycle can travel between two hydroquinone 'stations' ([199]).

Since the recognition sites in this rotaxane are identical, the $CBPQT^{4+}$ ring can reside over either of them with an equal probability. This molecular shuttle served as a prototype for further developed rotaxane-based molecular switches.

In a rotaxane-based molecular switch, the two recognition sites on the molecular chain are chemically different and present different affinities to the macrocycle, thus the probability of the macrocycle residing over either of the two recognition sites depends on the strength of the non-covalent interactions that hold the macrocycle over the recognition sites. To create the first rotaxane-based molecular switch, Stoddart and coworkers replaced one of the hydroquinone units in the molecular shuttle with the benzidine unit (Figure 31) and the other hydroquinone was replaced by a biphenol unit. It was found that the $CBPQT^{4+}$ spends 84% of the time residing over the benzidine site and only 16% of the time on the biphenol at room temperature in CD_3CN solution [200]. It was also shown that by protonating the nitrogen atoms on the benzidine site, it is possible to make, as a result of the Coulomb repulsion, the macrocycle switch to the neutral biphenol unit, and this switch can be reset by adding base.

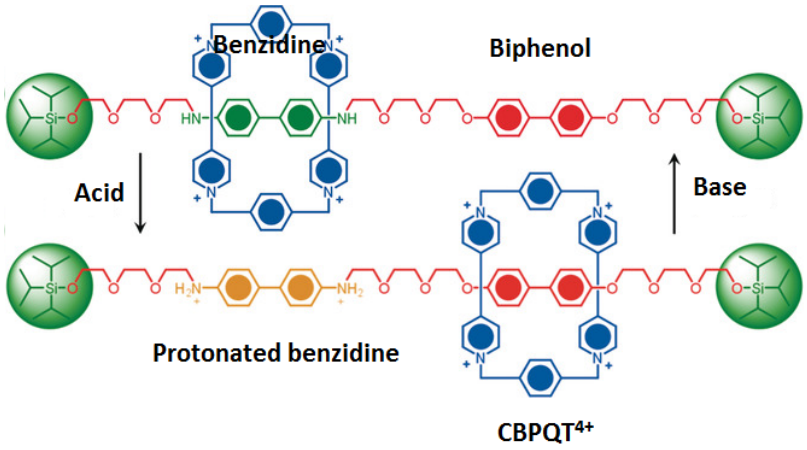

Figure 31. By adding acid to protonate the benzidine site, it is possible to make the $CBPQT^{4+}$ ring switch to the neutral biphenol site. The switch can be reset by adding base [199].

Open questions and objectives

Creating a synthetic molecular device that can perform mechanical work is a particularly challenging goal in the context of modern nanotechnology. For a molecule to perform as a motor it has to include some short of trigger or switch that in response to external stimuli imparts a reversible conformational change affecting function. As described above, one of the most prominent examples of supramolecular systems which can potentially enable a molecular device to perform mechanical work are molecular shuttles. Transitioning from molecules towards molecular machinery, which incorporates different molecular components to generate work, will require good control of the dynamics and mechano-chemical processes that govern the operation of these systems. Although the thermodynamics and kinetics of rotaxanes in bulk are well understood [195], a good

understanding of the operational dynamics and mechanistic properties of these systems at the single-molecule level is still missing. Until recently, Atomic Force Microscopy (AFM) has been the most common tool to probe the mechanical properties of mechanically interlocked macromolecular systems at the single-molecule level (see above), because it permits to interrogate these systems in the organic solvents these molecules are soluble in. Yet classical AFM-based techniques have some drawbacks that hinder the full understanding of the dynamics of the non-covalent interactions governing the operation of molecular motors:

- force resolution is limited by the stiffness of the cantilever to forces above ~20 piconewtons which is higher than the strength of the weak, non-covalent interactions responsible for the remodeling events at the molecular level [201] and higher than the forces characteristic of biological molecular motors ([202], [203]).
- limited force precision and stability makes it difficult to perform near-equilibrium measurements with AFM;
- non-specific adsorption of the sample to the cantilever and the lack of proper reporter can hinder clear identification of single molecule events.

So far, it has been impossible for chemists to study the operational dynamics of molecular devices with single molecule tools, due to a practical gap that exists between the techniques suitable to study the dynamics of molecular machinery and classical synthetic Chemistry. Here we note that very recent advances in the field have improved the force resolution and force stability of AFM 10 times, which makes this technique suitable for future studies of the dynamics of non-covalent interactions ([204], [205]).

Therefore, very basic questions about the operation of molecular motors at the nanoscale have still to be answered: What are the real-time kinetics (dynamics) of the operation of a synthetic motor? How do the motors dynamics respond to external stimuli like mechanical stress, chemical variations, thermal fluctuations, light, etc.? How much force is a particular motor able to exert? What are the mechano-chemical mechanisms governing the motor operation? What are thermodynamic efficiencies of synthetic molecular motors?

Answering these questions is of fundamental importance for the design, use and control of efficient devices based on synthetic molecular machinery able to carry our countless operations continuously. However, to date there is none experimental quantification of the real-time dynamics of synthetic molecular motors, and very little is known about their mechano-chemical properties. In addition, for nano-biotechnological applications synthetic molecular motors should operate in near-physiological conditions. Then, their operational mechanisms should be tested under aqueous, bio-compatible conditions.

As mention in the introduction, the extraordinary force stability and resolution of optical tweezers have been proven highly relevant for the study of the near-equilibrium dynamics of non-covalent interactions responsible for the structure of biological systems ([206] -

[209]). In this thesis, we used optical tweezers to probe the mechanical properties and study the operational dynamics of individual molecular shuttles under near-physiological conditions. This work was done in close collaboration with the group of Emilio M Perez (Supramolecular Chemistry) at IMDEA Nanociencia, which was in charge of the synthesis of the molecular shuttle.

Objectives

To achieve the aim of this part of the thesis to determine the mechanical and dynamic properties of individual molecular shuttles under near-physiological conditions, we needed to reach the following specific objectives:

1. To find a way to interface individual rotaxane molecules with optical tweezers.

2. To probe the mechanical stability of the interaction of the macrocycle with the two stations.

3. To study real-time dynamics of the molecular shuttle in near-equilibrium conditions.

4. To quantify the kinetics and thermodynamics of the shuttling process under near-physiological conditions.

3.2 Materials and methods

3.2.1 Chemical synthesis of a rotaxane molecular shuttle (collaboration)

The synthesis of the rotaxane molecule used in this thesis was done in the laboratory of Emilio M. Pérez (Supramolecular Chemistry) at IMDEA Nanociencia.

The rotaxane molecule is composed of an oligoethyleneglycol molecular thread with two binding sites (stations) for the tetraamide macrocycle (see [210]): fumaramide site, which due to the trans-orientation of its two amide carbonyls, strongly binds the tetraamide macrocycle by forming four hydrogen bonds, and succinic amide ester binding site, which presents less affinity to the macrocycle, than fumaramide, because of the substitution of one of the amides with an ester, a weaker hydrogen bond acceptor. The fumaramide: succinic amide ester occupancy ratio is biased towards the fumaramide station, even in the strongly competing solvent d6-DMSO. Two spacious diphenylethyl groups at the two ends of the thread serve as stoppers to prevent the unlacing of the macrocycle.

The axle for the shuttle was synthesized in 12 steps (Figure 32 and [210]). The rotaxane included additional functionalization for its manipulation in the optical tweezers. On one hand, the diphenylethyl group close to the fumaramide station was functionalized with a biotin group, needed to later attach the rotaxane to a polystyrene bead. On the other hand, the macrocycle encircling the axle at the fumaramide station was synthesized out of 5-azidoisophthaloyl dichloride and N^2,N^6-bis(4-(aminomethyl)benzyl)pyridine-2,6-dicarboxamide. The former leaves azide group that will be later used as an attachment point to connect the macrocycle to the bead in the optical trap via DNA (see below).

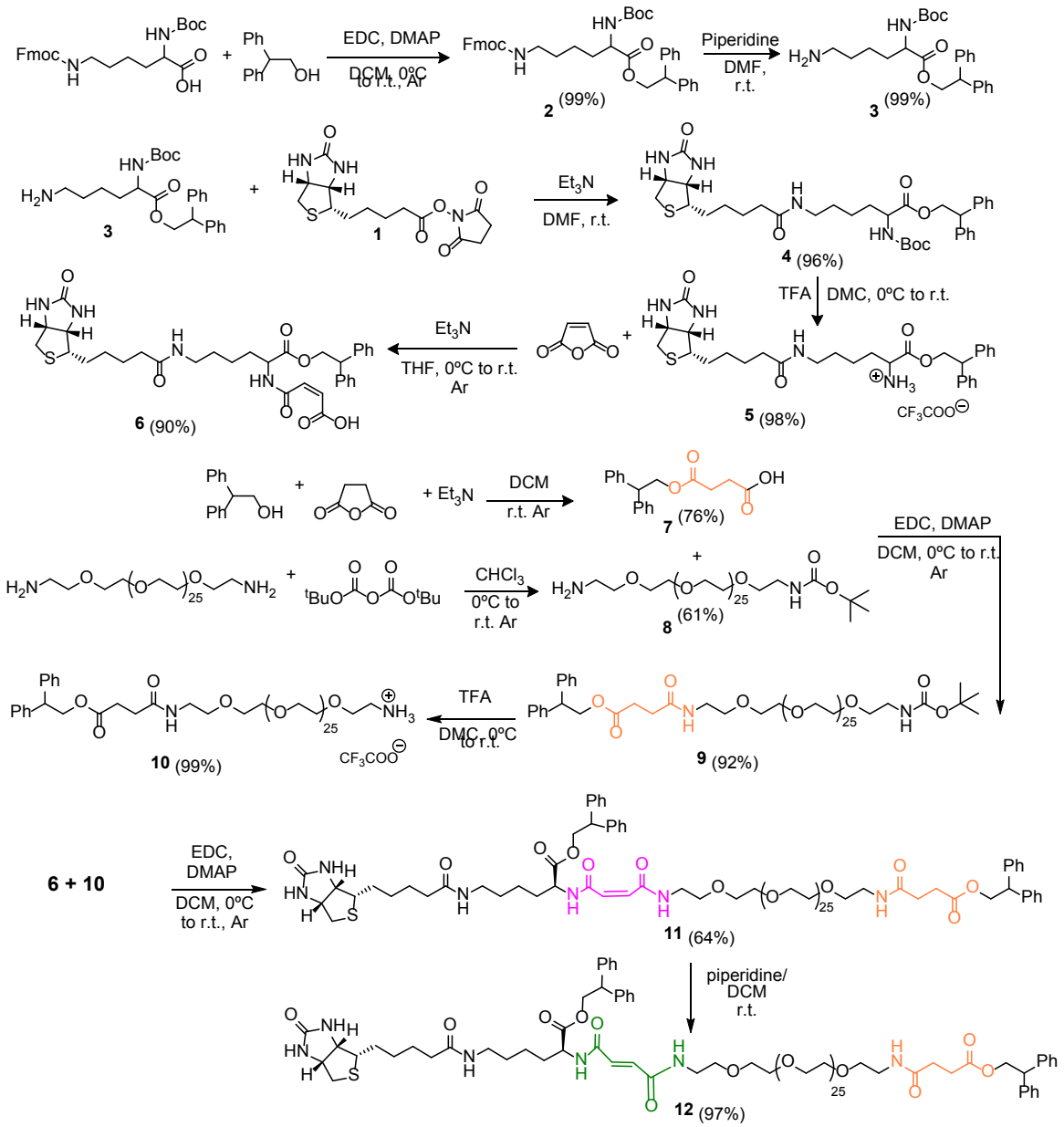

Figure 32. The synthesis of the molecular thread (included in 12 steps) [210]. The thread of the rotaxane (the E-thread, compound 12) is obtained from the (*Z/E* 55/45)-thread, compound 11. The (*Z/E* 55/45)-thread was synthesized from two constructs: compound 6 and compound 10. Compound 10 was obtained in 3 steps from *O,O´*-bis (2-aminoethyl) hexacosaethylene glycol, and compound 6 was synthesized in 3 steps from 2,2-diphenylethyl 6-([((9H-fluoren-9-yl)methoxy)carbonyl]amino)-2-aminohexanoate and *N*-Hydroxysuccinimidobiotin. Each step of the synthesis scheme is indicated by an arrow with the reaction conditions shown above and below it. The figure was taken from [210].

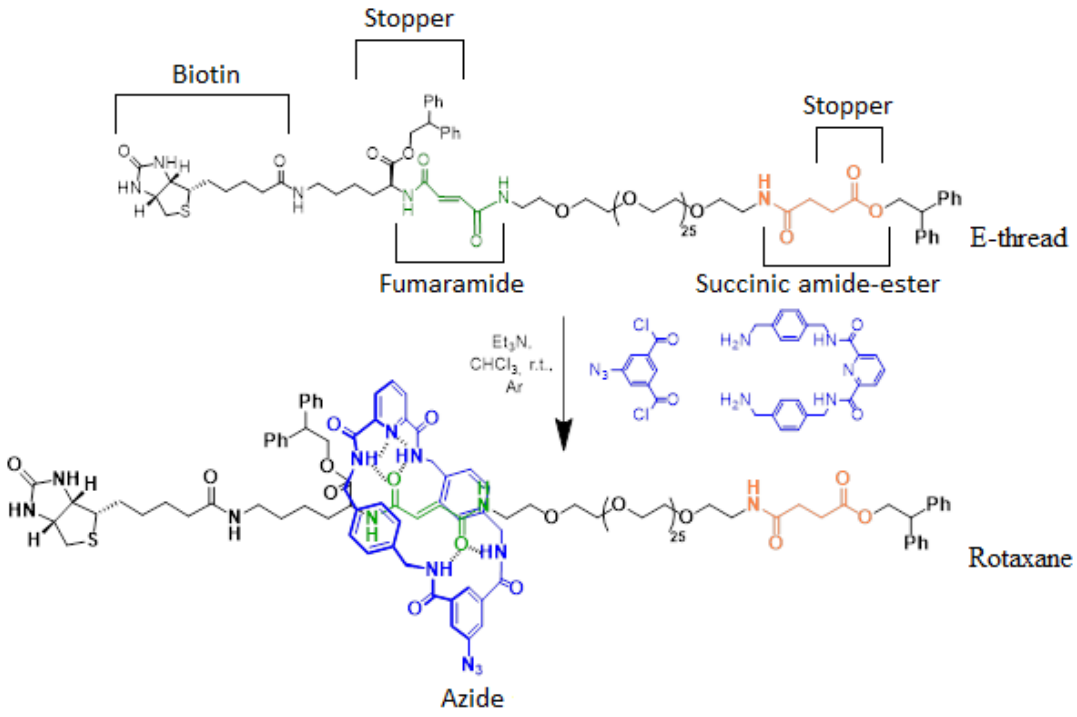

Figure 33. Formation of the macrocycle encircling the fumaramide station on the axle. 5-azidoisophtaloyl and N^2,N^6-bis(4-(aminomethyl)benzyl)pyridine-2,6-dicarboxamide react at room temperature in chlorophorm to form a macrocycle around the fumaramide station of the E-thread (See [210]). Triethylamine (Et_3N) is used in this reaction as a base to remove HCl. The azide group is needed to connect the macrocycle with DNA. The figure is taken from [210] and then modified.

3.2.2 Coupling of the rotaxane with optical tweezers

Coupling the rotaxane with the optical tweezers involved the following sequential steps:

3.2.2.1 Coupling of the macrocycle with ssDNA oligonucleotide via a copper-free 'click' reaction

Two single-stranded DNA (ssDNA) oligonucleotides, R-5'TTTTTTTTTTTTTTAGCT (R-$(dT)_{15}$AGCT) and 3'AAAAAAAAAAAAAAA5'$(dA)_{15}$ (Figure 34) were synthetized with a MerMade 4 synthesizer using phosphoramidite methodology. This methodology is based on the use of DNA phosphoramidite nucleosides, modified with a 4,4'-dimethoxytrityl (DMTr) group, protecting the 5'-OH, a ß-cyanoethyl that protects the 3'-phosphite and appropriate conventional protecting groups on the reactive primary amines in the heterocyclic nucleobase. To be connected to the macrocycle of the rotaxane, one of the oligonucleotides needed to be functionalized with a cyclooctyne, so the synthesis

of the oligo R-$(dT)_{15}$AGCT started from a dibenzoazacycloactyne derivative of a phosphoamidite instead of a phosphoamidite nucleoside. The columns for synthesis of the oligonucleotides were filled with the corresponding Controlled Pore Glass solid support, and anhydrous MeCN was used as solvent. The synthesis cycle included the following steps: deblocking, activation, capping and oxidation. The 5'-DMTr group of the 5'-terminal base was removed by brief exposure to the 3 % trichloroacetic acid in anhydrous DCM, which later was removed by purging with anhydrous MeCN. The activation of the phosphoramidite functionality was achieved by adding a 0.25 M benzylthiotetrazole solution in anhydrous MeCN. The activated species was then reacted with the 5'-OH to give a trivalent phosphite triester. The coupling time for standard phosphoramidites was 2 min, and for the cyclooctyne derivative, it was 5 min. The P(III)-species were oxidized using alkaline iodine solution (20 mM I_2 in THF/Py/water 7/2/1). The unreacted 5'-OH-groups were capped with a mixture of two solutions: the first solution was composed of 10% Ac_2O, 10% pyridine, 80% THF and the second solution contained 10% 1-methylimidazole in THF.

After the synthesis had been completed, the oligonucleotides were cleaved from the solid support with concomitant removal of the Fmoc and β-cyanoethyl protecting groups by adding 28 % aqueous NH_3 at 55 °C. After 20 h the solution was filtered and concentrated in vacuum. The obtained concentrate was dissolved in water.

The synthesized oligonucleotides were purified by gel electrophoresis (1 mm, 20% polyacrylamide). The oligonucleotide-containing segments of the gel were visualized with UV-light (260 nm) and isolated from the rest of the gel, and the oligonucleotides were extracted with elutrap system (3 h, 200 V).

The R-$(dT)_{15}$AGCT oligonucleotide was bound to the macrocycle of the rotaxane via a copper-free 'click' reaction. The term 'click chemistry' was introduced to describe a family of chemical reactions, that are high yielding, simple to perform and allow to quickly obtain chemical compounds by joining small molecular units. Typically, this kind of reactions should lead only to byproducts that can be easily removed, be stereospecific, can be conducted under physiological conditions, be thermodynamically-favored and lead to only one product. This family of reactions includes the sterically promoted alkyne-azide cycloaddition (SPAAC), in which azides and sterically strained cycloalkynes are cobbled together. The driving force of the reaction is the removal of steric stress in cycloalkyne. This reaction was used to connect the azide of the rotaxane macrocycle to the dibenzoazacyclooctyne of the radical (R), attached to the 5' end of the $(dT)_{15}$AGCT oligonucleotide (Figure 34).

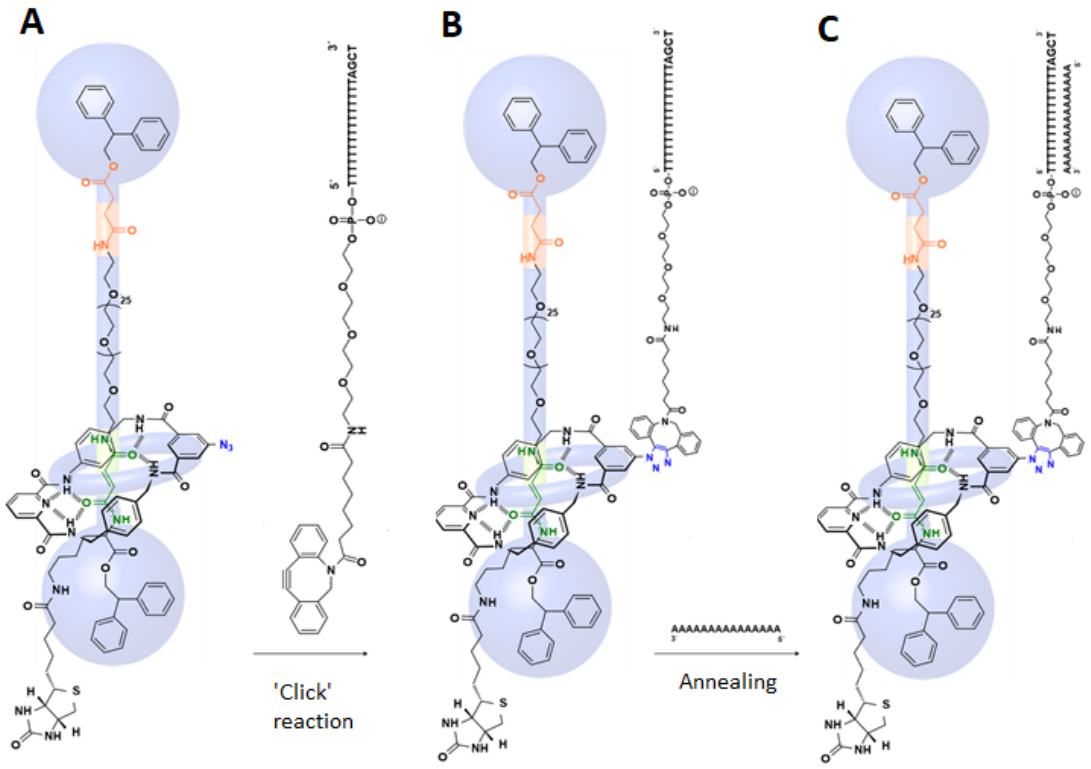

Figure 34. Coupling the rotaxane with DNA. **A** The azide group of the macrocycle interacts with the oligonucleotide functionalized with dibenzoazacyclooctyne in a copper-free 'click' reaction. **B** The product of the 'click reaction' – the R-$(dT)_{15}$AGCT oligonucleotide bound to the macrocycle, posteriorly annealed to the $(dA)_{15}$ oligonucleotide. **C** The product of the annealing with overhanging AGCT 3' end.

To carry out this reaction, the oligonucleotide (50 μM) in H_2O/DMF (0.3 mL, 4/1) was added to a portion of rotaxane (60 μM) in H_2O/DMF (0.3 mL, 4/1), and the obtained mixture was stirred for several hours at room temperature. The product of the reaction was purified by gel electrophoresis (0.2 mm, 20% polyacrylamide). After the purification, the product of the 'click' reaction was added to the solution with previously synthesized complementary oligonucleotide ($(dA)_{15}$). By heating the mixture and then allowing it to slowly cool to room temperature, the two oligonucleotides were annealed, leaving a *rotaxane-oligo* construct with a sticky AGCT 3' end, needed for the subsequent ligations with DNA handles, see below.

3.2.2.2 Coupling the rotaxane-oligo construct with dsDNA molecules

To manipulate individual rotaxane molecules with optical tweezers, they were coupled with two dsDNA molecules: one, used as 'handle' to monitor and manipulate the movement of the macrocycle (*DIG-DNA handle*) and the other, used as a 'spacer' to

separate the rotaxane from the surface of the bead on top of the micropipette (called *spacer-DNA*).

The *DIG-DNA handle* is a 2,686 bp long dsDNA molecule bearing multiple digoxigenines at one end and a protruding TCGA 5' strand at the other end (note that the protruding end is complementary to the *sticky* AGCT 3' end of the rotaxane-DNA construct). This molecule was synthetized as described in [134]. The *DIG-DNA handle* was later ligated to the *rotaxane-oligo* construct using the T4 DNA ligase (NEB), and the resulting molecules (final concentration – 1.8 nM) were incubated with anti-digoxigenin-covered beads for 20 minutes (Figure 35A). In our experimental setup, these beads covered with the rotaxane-dsDNA complexes are held in the optical trap.

The *spacer-DNA* is a dsDNA molecule of 827 bp functionalized with biotin at one end and digoxigenin at the other end. This dsDNA molecule was obtained by PCR amplification of the polylinker segment of the pUC19 vector using two DNA primers labeled either with digoxigenin or biotin at their 5'-ends.The *spacer-DNA* was mixed with an excessive amount of streptavidin and purified with a Promega column. Thus, the final product of these reactions is a dsDNA molecule labeled with digoxigenin at one end and streptavidin at the other.

3.2.2.3 Single-molecule experiments

In order to interface the rotaxane with the optical tweezers, first, the rotaxane-*DIG DNA handle* construct and the *spacer-DNA* were incubated independently for 20 minutes at room temperature with polystyrene beads functionalized with anti-digoxigenin (2 um diameter, Spherotech). In our experiments, the beads incubated with the rotaxane-*DIG DNA handle* construct were held in the optical trap, and the beads incubated with the *spacer-DNA* were placed on top of a micropipette.

In the optical tweezers, the two types of beads were introduced separately into the fluidic chamber through two different channels (Figure 35A), which are connected to a central reaction channel, where the optical trap and the glass micropipette are located. To isolate a single rotaxane molecule, first, a bead containing the *spacer-DNA* was placed on top of the micropipette. Then a bead covered with the rotaxane-*DIG-DNA handle* was trapped and placed close to the bead held on top of the micropipette. To isolate a single rotaxane molecule between the two beads, the optical trap with the bead functionalized with the rotaxane-dsDNA complex was moved in Y direction approaching the bead held on top of the micropipette. The attachment is made when the biotin group situated close to one of the stoppers of the rotaxane binds to the streptavidin molecule at the end of the *spacer-DNA* attached to the bead on top of the pipette. Upon attachment, the force-extension curve of the resulting DNA-rotaxane construct can be obtained, stretching the molecule by moving the optical trap away from the micropipette in the Y direction (Figure 35B).

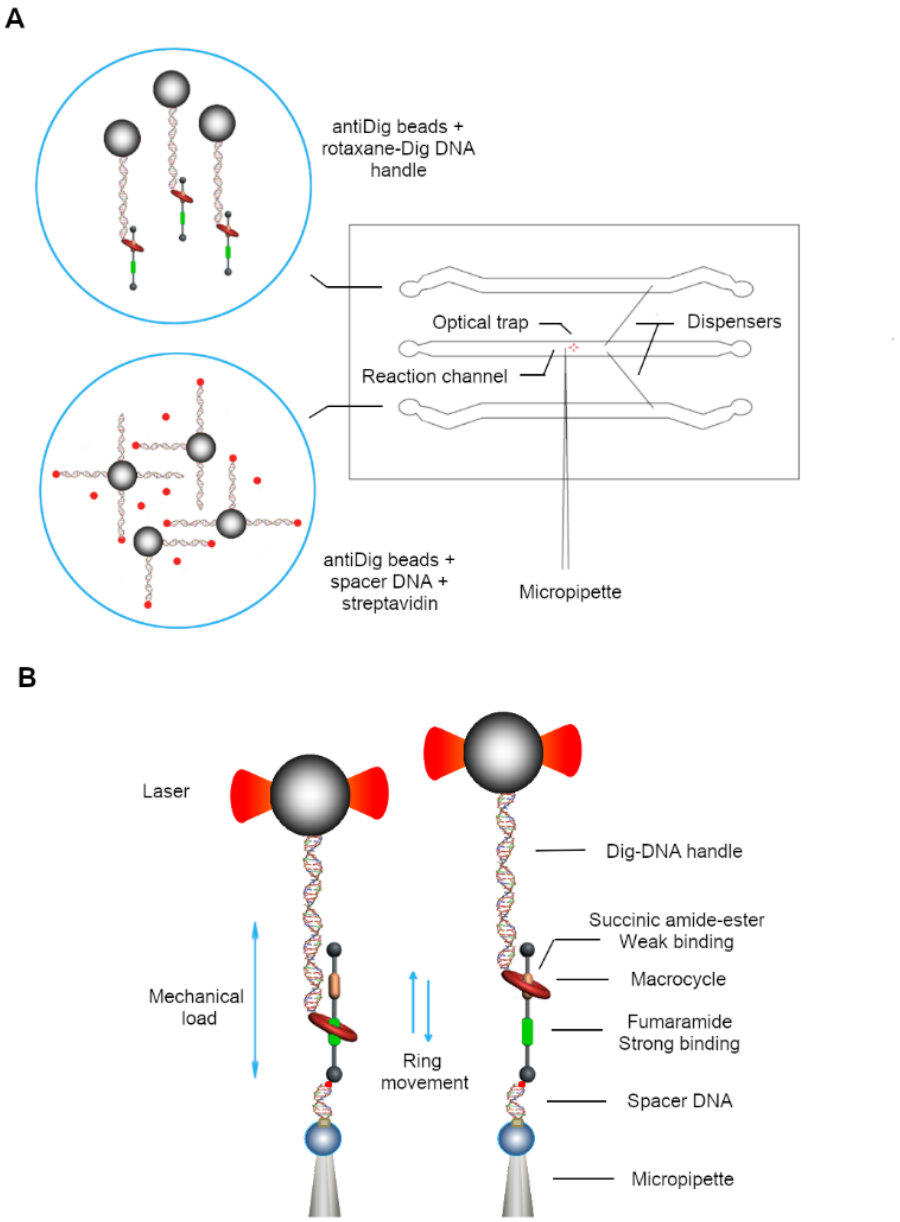

Figure 35. Coupling of the rotaxane with Optical tweezers. **A** Polystyrene beads functionalized with anti-digoxigenin (αDig) are incubated separately with dsDNA-rotaxane constructs (top) or with *spacer-DNA* molecules bearing streptavidin in one end (bottom). After incubations, each set of functionalized beads is introduced to a microfluidic chamber through separate channels, connected to the central reaction channel by means of glass dispensers. Once the polystyrene beads arrive to the central reaction channel, a bead functionalized with *spacer-DNA* is placed on top of the micropipette and a bead containing a dsDNA-rotaxane construct is brought with the optical trap close to the bead on top of the micropipette to make an attachment. **B** Pulling and relaxing a rotaxane molecule connected to two dsDNA handles tethered between two beads. The two dsDNA handles are connected to the polystyrene beads via digoxigenin-anti-digoxigenin (Dig-αDig) connections. The attachment between the dsDNA-rotaxane construct and *spacer-DNA* is made through biotin-streptavidin interaction and the resulting molecule can be pulled and relaxed multiple times by moving the optical trap relatively to the glass micropipette at a constant rate of 200 nm s^{-1}.

3.2.3 Data analysis

3.2.3.1 Crooks Fluctuation Theorem (CFT) and Jarzynski equality (JE)

Crooks Fluctuation Theorem is based on the supposition that processes are microscopically reversible [211]. A consequence of the CFT is Jarzynski equality that relates the equilibrium free energy difference between two states, $\boldsymbol{\Delta G}$, to an exponential average of work, done on the system in an infinite number of non-equilibrium experiments, $\boldsymbol{W}$:

$$\boldsymbol{exp}\left(\frac{-\boldsymbol{\Delta G}}{\boldsymbol{k_B T}}\right) = \langle \boldsymbol{exp}\left(\frac{-\boldsymbol{W}}{\boldsymbol{k_B T}}\right)\rangle \qquad (eq.23)\,.$$

Jarzynski equality has been tested in single-molecule pulling experiments done on RNA hairpins ([212], [213]). By using Crooks Fluctuation Theorem, it is possible to quantify a hysteresis in the values of the irreversible work done on the system (e.g. the work done to unfold and refold an RNA hairpin). According to the CFT, the relation between the probability distributions of the values of work done on the system in infinite number of non-equilibrium experiments along direct and reverse processes is defines as follows:

$$\frac{\boldsymbol{P_D(W)}}{\boldsymbol{P_R(-W)}} = \boldsymbol{exp}\left(\frac{\boldsymbol{W-\Delta G}}{\boldsymbol{k_B T}}\right) \qquad (eq.24)\,,$$

where $\boldsymbol{P_D(W)}$ and $\boldsymbol{P_R(-W)}$ are the probability distributions of the values of work done on the system in a direct and reverse processes, $\boldsymbol{\Delta G}$ is the free energy difference between the final and the initial sates.

In an RNA hairpin folding/unfolding experiment, values of work, $\boldsymbol{W}$, done on the system during pilling-relaxing cycles, can be approximated by force vs. extension integrals:

$$\boldsymbol{W} = \sum_{\boldsymbol{i=1}}^{\boldsymbol{N}} \boldsymbol{F_i \Delta x_i} \qquad (eq.25),$$

where $\boldsymbol{x_i}$ is the extension of the molecule and $\boldsymbol{N}$ is the number of intervals in the sum.

Then, the value of $\boldsymbol{\Delta G}$ can be found when the two probability distributions cross:

$$\boldsymbol{P_D(W) = P_R(-W) \quad \rightarrow \quad W = \Delta G}$$

3.2.3.2 Kinetic rates from experiments under constant force

To determine shuttling kinetic rates at constant force, $\boldsymbol{F}$, the tetraamide macrocycle was manually set to reside over fumaramide (succinic amide ester) station waiting until the macrocycle shuttles to the opposite succinic amide ester (fumaramide) station. The shuttling kinetic rate is then calculated as the inverse of the average residence time at the fumaramide (succinic amide ester station):

$$\boldsymbol{k_{fum} = 1/\tau_{fum}} \qquad (eq.26),$$

$$\boldsymbol{k_{succ} = 1/\tau_{succ}} \qquad (eq.27).$$

In these experiments, the residence times at each station, $\boldsymbol{\tau_{fum}}$ and $\boldsymbol{\tau_{succ}}$ were calculated by partitioning extension traces using a threshold set in the midpoint between the two positions of the two stations (determined as extension histograms peaks). The residence times are defined as it is shown in Figure 35: a residence time is defined by an interval limited by two events of crossing the threshold (direct and reverse shuttling).

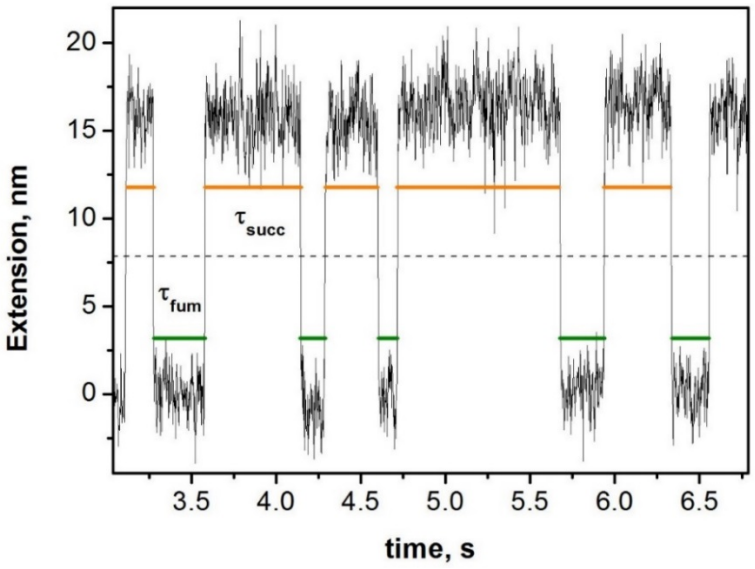

Figure 36. The residence times at the fumaramide ($\boldsymbol{\tau_{fum}}$) and the succinic amide ester ($\boldsymbol{\tau_{succ}}$) stations are defined by time intervals between direct and reverse shuttling events. $\boldsymbol{\tau_{fum}}$ and $\boldsymbol{\tau_{succ}}$ were calculated by dividing extension traces with a threshold set in the midpoint between the position of the two stations (dashed line).

3.2.3.3 Kinetic rates in the Bell-Evans model

According to the Bell-Evans model ([214] - [217]), the shuttling rate from the fumaramide station to the succinic amide ester station, $\boldsymbol{k_{fum}}$, and its reverse, $\boldsymbol{k_{succ}}$, depend on force as follows:

$$\boldsymbol{k_{fum}(f) = k(0)\ exp\left(\frac{f\ x^{\ddagger}_{fum}}{k_B T}\right)} \qquad (eq.28)$$

$$\boldsymbol{k_{succ}(f) = k(0)\ \exp\left(\frac{\Delta G\ - f\ x^{\ddagger}_{succ}}{k_B T}\right)} \qquad (eq.29)\ ,$$

where $\boldsymbol{k(0)}$ is the shuttling rate at zero force, $\boldsymbol{f}$ is the applied external force, $\boldsymbol{x^{\ddagger}_{fum}}$ is the distance between the transition state and the fumaramide station and $\boldsymbol{x^{\ddagger}_{succ}}$ is the distance between the succinic amide ester station and the transition state. Here, $\boldsymbol{\Delta G}$ is the free energy of shuttling at zero force, defined as $\boldsymbol{\Delta G = f_{1/2} \cdot \Delta x}\ (eq.30)$, where $\boldsymbol{f_{1/2}}$ is the so-called coexistence force, at which the rates of direct and reverse shuttling are equal, $\boldsymbol{k_{fum} = k_{succ}}$, and $\boldsymbol{\Delta x}$ is the distance between the two states.

3.2.4.4 Calculation of potential energy profiles

The extension of a rotaxane-DNA hybrid, defined by the position of the tetraamide macrocycle on the molecular thread, obeys Boltzmann distribution, so the potential energy of the system can be computed as:

$$\boldsymbol{\Delta E(x) = -k_B T \cdot ln[\rho(x)]} \qquad (eq. 31)\,,$$

where $\boldsymbol{\rho(x)}$ is the probability distribution of the extension**,** $\boldsymbol{x}$**,** $\boldsymbol{k_B}$ is the Boltzmann constant and $\boldsymbol{T}$ is the absolute temperature.

3.2.4.5 Determination of the free energy of stretching of the rotaxane-DNA hybrid

The force-extension curve of the rotaxane-DNA hybrid after shuttling, when the macrocycle is at the succunic amide ester station, reflects the elastic properties of the dsDNA (the *DIG DNA handle* and the *spacer-DNA*) and those of the rotaxane. The Worm-Like-Chain model (WLC) [155] (see section 2.2.4.1) for polymer elasticity can predict well both, the resulting extension of dsDNA handles [218] and the extension of a linear polymer, like polyethylene glycol [219], as a function of the applied force:

$$\boldsymbol{x(f) = L \cdot \left[1 - \frac{1}{2} \cdot \left(\frac{k_B T}{FP}\right)^{\frac{1}{2}} + \frac{F}{S}\right]} \qquad (eq. 32).$$

The force-extension curve of the rotaxane-DNA hybrid after shuttling can be fit by an expression including the sum of two WLC models: one for the dsDNA, with persistence and contour lengths of $\boldsymbol{P}$ = 50 nm and $\boldsymbol{L}$ = 0.34 nm·bp^{-1} [218], respectively, and another for the rotaxane, with $\boldsymbol{P}$ = 0.9 ± 0.2 nm and $\boldsymbol{L}$ = 21.6 ± 1 nm, under the experimental conditions used in this thesis. The WLC model for the force-extension curve of a rotaxane without dsDNA handles is shown in Figure 37 ($\boldsymbol{P}$ = 0.9 ± 0.2 nm and $\boldsymbol{L}$ = 21.6 ± 1 nm)

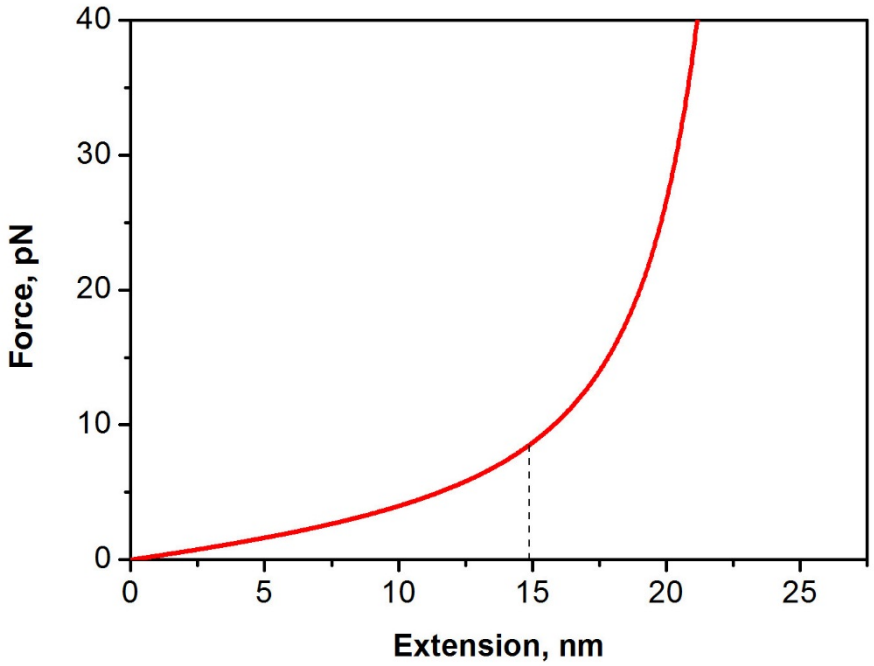

Figure 37. The red line is the simulated force-extension curve of a rotaxane without dsDNA handles under stretching ($\boldsymbol{P}$ = 0.9 ± 0.2 nm and $\boldsymbol{L}$ = 21.6 ± 1 nm)

The length of 14.96 nm (indicated by the black dashed line) for the fully extended rotaxane at the coexistence force (8.51 pN) is quite compatible with the experimentally found shuttling distance (~15 nm). The free energy of stretching of the rotaxane ($\boldsymbol{\Delta G_{stretch}}$) can be calculated by integrating the area under the curve from 0 pN to the coexistence force, $\boldsymbol{f_{1/2}}$.

3.3 Results and discussion

3.3.1 Non-equilibrium experiments (pulling and relaxing individual rotaxane molecules)

To study the mechanical stability of the interactions of the tetraamide macrocycle with the fumaramide and succinic amide ester stations, individual rotaxane-dsDNA complexes were attached between the beads as described above (Figure 35B). These complexes were pulled and relaxed multiple times by moving the optical trap relatively to the glass micropipette at a constant rate of 200 nm/s. Due to the robustness of the system, it was possible to record up to one hundred force-extension curves for each DNA-rotaxane hybrid (see Figure 38)**.**

At low tensions (<10 pN, see below), the obtained force-extension curves resembled the elastic behavior of a polymer with a persistence length of 50 nm (found from the fit to the Worm-like chain model), characteristic of a single dsDNA molecule. When the applied force exceeded the strength of the four hydrogen bonds connecting the macrocycle with the fumaramide station, a sudden increase of extension was observed (see Figure 39A). Pulling-relaxing curves (450 cycles in total) were collected for six different rotaxane-dsDNA complexes and the average observed increment in extension, $\boldsymbol{\Delta L_c}$, was 15 ± 2 nm. This value corresponds to the contour length of the oligoethyleneglycol thread separating the two stations at the forces of the macrocycle transition. This results strongly suggest that this sudden increase in extension is due to the transition of the macrocycle from the fumaramide station to the more stable at high forces succinic amide ester station.

The average rupture force of the non-covalent interactions between the macrocycle and the fumaramide station was 8.8 ± 0.6 pN (Figure 39B). During the relaxing of the rotaxane-dsDNA molecule, an abrupt decrease of the molecular extension was observed and the original extension was recovered. This decrease is probably due to the macrocycle returning from the succinic amide ester station to the thermodynamically favorable at low forces fumaramide station. The average recovery force was 8.1 ± 0.5 pN (Figure 39B). The intersection of the rupture and recovery force distributions ($\boldsymbol{f_{1/2}}$ = 8.51 pN, Figure 39B) corresponds to the force at which the probability of the macrocycle residing over either of the two stations is equal, the so-called coexistence force.

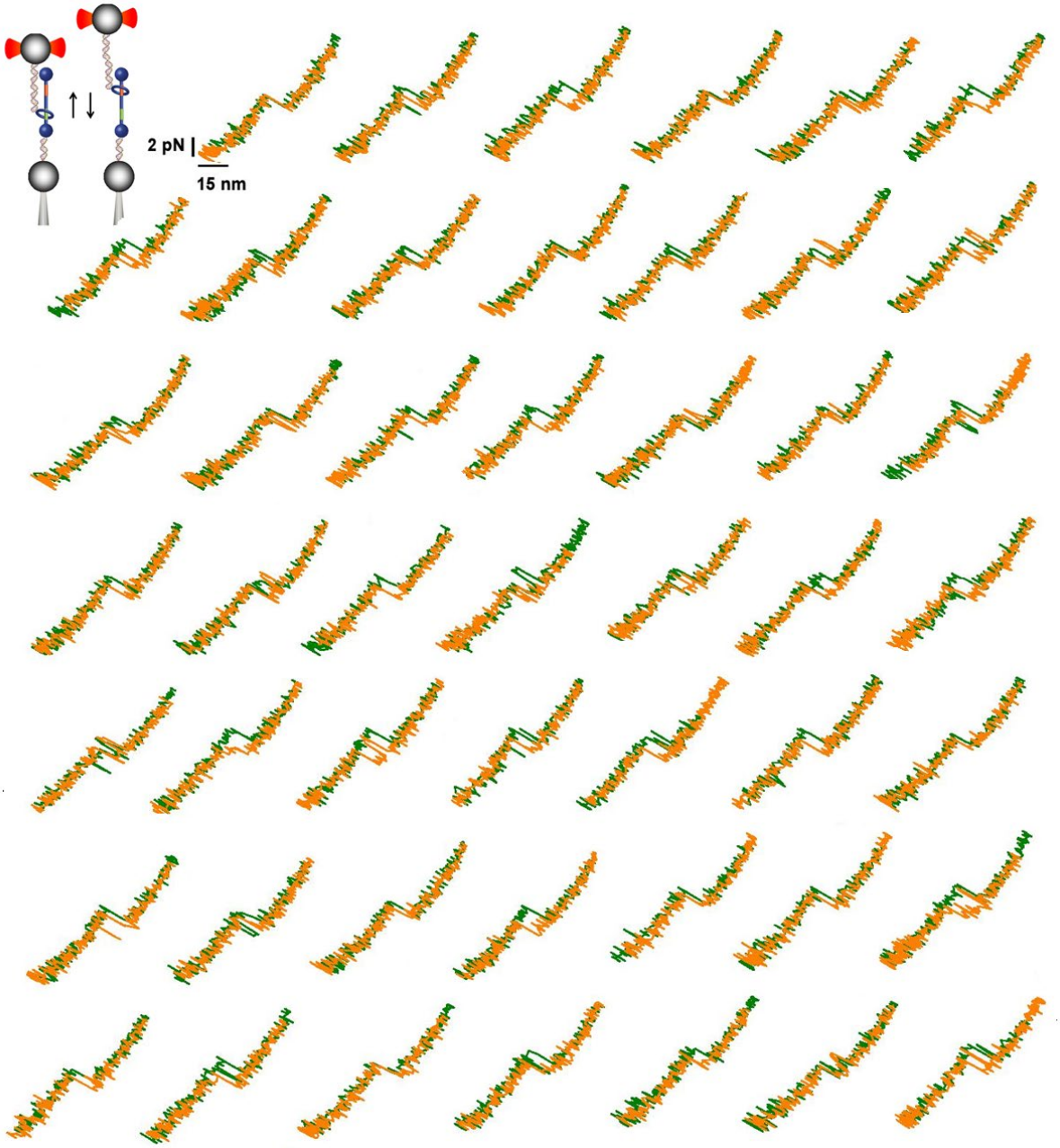

Figure 38. 48 consecutive pulling (green)-relaxing (orange) cycles of a representative rotaxane-DNA construct (pulling rate 200 nm s^{-1}). The bi-stability of the molecule can be seen clearly in several curves as rapid oscillations of distance at forces close to $f_{1/2}$.

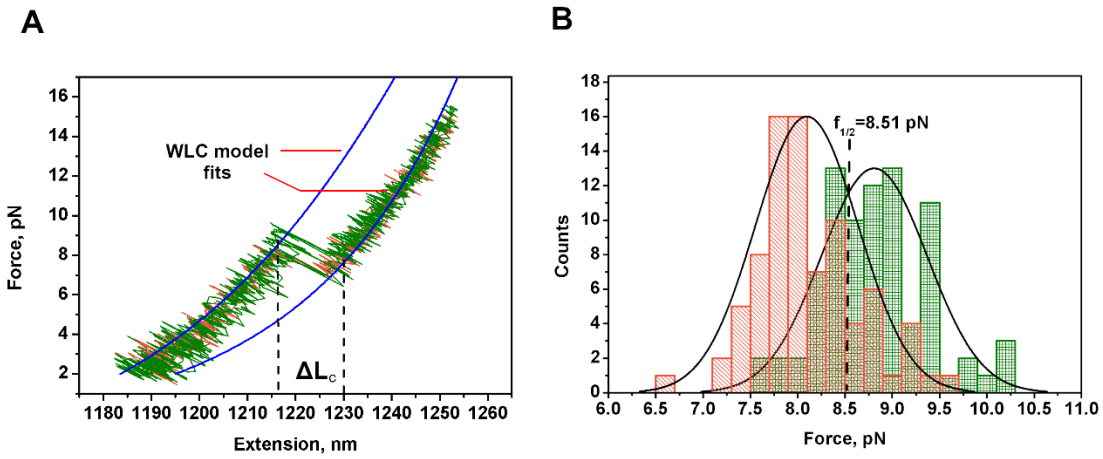

Figure 39. A Force-extension curves characterizing mechanical stretching (green) and relaxing (orange) of a single dsDNA-rotaxane complex at a pulling rate of 200 nm s^{-1}. Blue lines represent fits of the experimental curves with the WLC model (persistence length ~50 nm)). ΔL_c is an increment of the contour length of the dsDNA-rotaxane complex after a shuttling event (ΔL_c ~15 nm). **B** Distribution of breaking forces at each station. The intersection of the distributions of breaking forces at fumaramide (green Gaussian fit) and succinic amide ester (orange Gaussian fit) stations gives the coexistence force, $f_{1/2}$ = 8.51 pN (N = 450 curves).

Using Jarzynski equality ([212], [213]), the total free energy of the shuttling can be approximated as the product of the coexistence force, $\boldsymbol{f_{1/2}}$, and the shuttling distance between the two stations, $\boldsymbol{\Delta L_c}$. The obtained value of 31 ± 4 k_BT (18 ± 2 kcal/mol) corresponds to the sum of the energy of the shuttling from the fumaramide station to the succinic amide ester station at zero force, plus the free energy of the stretching of the rotaxane-dsDNA complex from $\boldsymbol{f}$ = 0 to $\boldsymbol{f} = \boldsymbol{f_{1/2}}$. This energy is composed of the free energy of stretching of dsDNA handles and the energy of stretching of a rotaxane molecule (see section 3.2.4.5), and it was calculated as 11.8 k_BT. Therefore, the free energy of the shuttling at zero fore is 19 ± 4 k_bT (11 ± 2 kcal/mol).

3.3.2 Near-equilibrium measurements. (Determination of force-dependent shuttling rates)

Next, we aimed to determine the real-time shuttling kinetics of the macrocycle between the two chemical stations. To do so, we maintained single rotaxane-dsDNA complexes (N=25) under constant tension close to the coexistence force found from the pulling-relaxing data (Figure 40). For every single rotaxane-dsDNA complex held at a constant force, continuous shuttling events between the two stations were followed for several minutes by recording extension traces over time. The obtained traces present well-defined residence times at each station (Figure 40). The residence times, $\boldsymbol{\tau_{fum}}$ and $\boldsymbol{\tau_{fum}}$, for each

molecular shuttle were calculated as described in the section 3.2.3.2 and it was found that they were exponentially distributed, as expected for a two-state system in equilibrium (Figure 41).

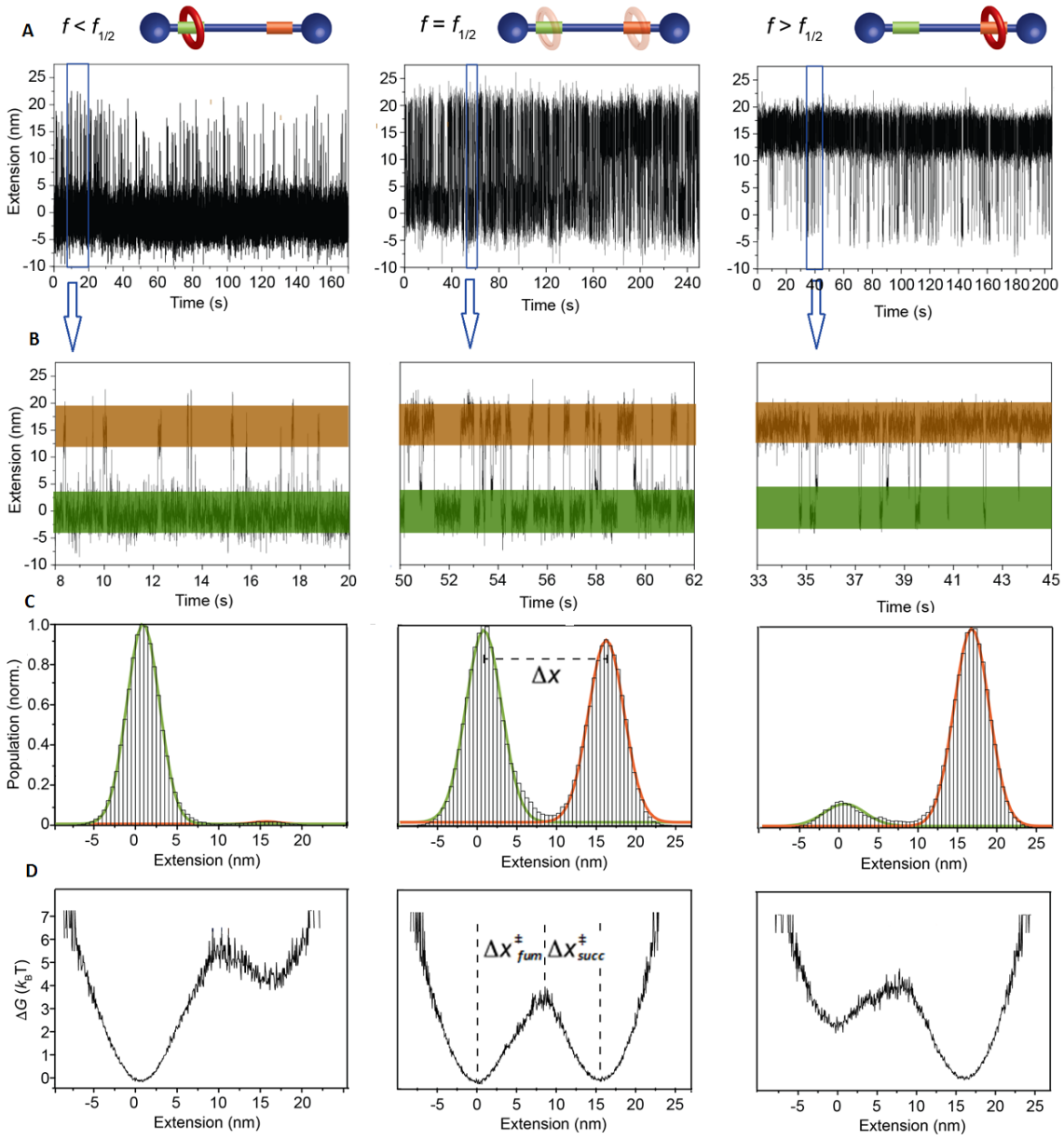

Figure 40. A Examples of recorded extension versus time data for three molecular shuttles studied at different constant forces (8.2, 8.7 and 10.0 pN). **B** Zoom-in on the extension traces data. **C** Extension histograms fitted with two Gaussian functions (the distance between the stations is defined by the distance between the peaks of the two Gaussians). **D** Potential energy profiles obtained from the extension distributions.

At tensions close to the coexistence force the macrocycle spent approximately equal amounts of time at each station. By applying tensions either slightly higher or lower than the coexistence force (+/- 0.5 pN), it was possible to favor the occupancy of either the succinic amide ester or the fumaramide stations (Figure 40): at forces higher than the coexistence force, the macrocycle preferentially resided at the succinic amide ester station, whereas at forces lower than the coexistence force, the occupancy of the fumaramide station was favored. The extension histograms obtained from the recorded traces show two peaks that fit well to two Gaussian distributions separated by $\boldsymbol{\Delta x}$ = 15.5 ± 2.5 nm, equal to the distance separating the two stations found in the pulling-relaxing experiments.

By using the inverse Boltzmann distribution, it was possible to obtain the overall energetic profiles of the shuttling reaction at different forces directly from the extension distributions (see section 3.2.4.4). The energetic profiles display a well-defined transition state between two minima, the relative height of which varies with force (Figure 40D).

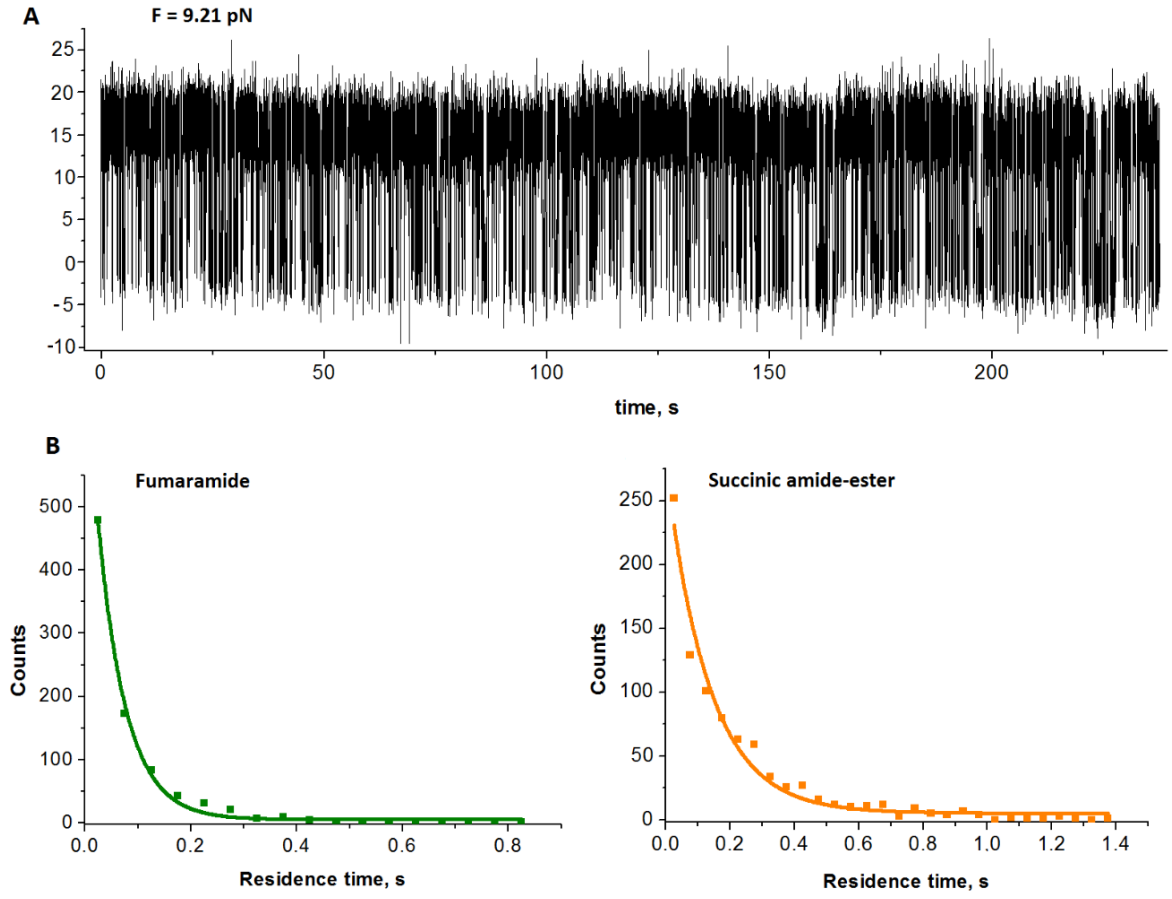

Figure 41. A Extension recorded over time at the constant force, $\boldsymbol{f}$ = 9.2 pN. **B** The residence time distributions at the fumaramide (green) station and succinic amide ester station (orange). The residence times are exponentially distributed, as expected for a two-state system in equilibrium

The kinetic rates of direct and reverse shuttling, $\boldsymbol{k_{fum}}$ and $\boldsymbol{k_{succ}}$, were calculated for each molecular shuttle as described in section 3.2.3.2. The obtained values of $\boldsymbol{k_{fum}}$ and $\boldsymbol{k_{succ}}$ present an exponential dependence on force and fit well to the Bell-Evans model along the entire range of forces measured (Figure 42). The Bell-Evans theory can be used to extract from the calculated residence time values some useful kinetic and energetic parameters of the shuttling process ([220], [221]), such as the coexistence force, the free energy of shuttling and the position of the transition state relative to the fumaramide and the succinic amide ester stations.

The coexistence force ($\boldsymbol{f_{1/2}}$), at which the kinetic rates of the direct and reverse shuttling are equal, can be found as an intersection of the linear fits to the natural logarithms of the kinetic rates during direct and reverse shuttling (Figure 42). The obtained value, $\boldsymbol{f_{1/2}} =$ 8.83 pN, is consistent with the value obtained from the intersection of the rupture forces distributions (8.51 pN, Figure 39B). In this case, the product of the coexistence force and the shuttling distance between the two stations obtained from the extension distributions (Figure 41C, $\boldsymbol{\Delta x}$) gives the free energy of the shuttling ($\boldsymbol{\Delta G} = \boldsymbol{f_{1/2}} \cdot \boldsymbol{\Delta x} = 33 \pm 5$ k_BT). The obtained value for the free energy of the shuttling is similar to the value found from the pulling-relaxing data.

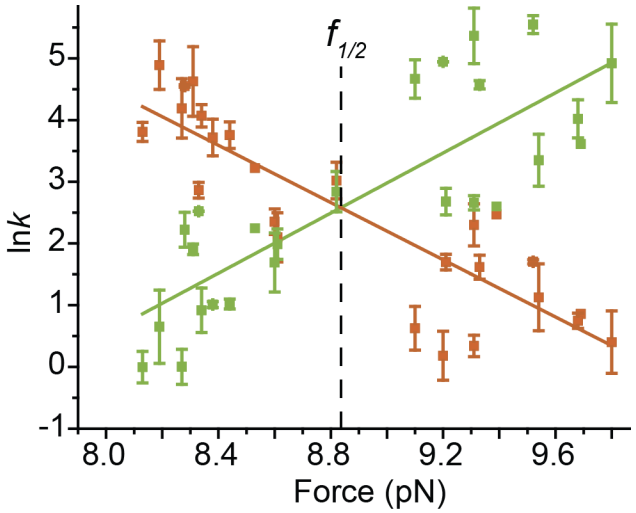

Figure 42. The shuttling rates from the fumaramide station to the succinic amide ester station, k_{fum} (green), and the backward rates, k_{succ} (orange), present exponential dependence on force. The values of *lnk* are represented as mean ± standard deviation. The intersection of the linear fits to the *lnk* for direct and reverse shuttling revealed the coexistence force, the free energy of shuttling and the position of the transition state.

The position of the transition state, relative to the fumaramide station ($\boldsymbol{x^{\ddagger}_{fum}}$) and the succinic amide ester station ($\boldsymbol{x^{\ddagger}_{succ}}$), is defined by the slopes of the linear fits to the $\boldsymbol{lnk}$

data (Figure 42). The values of $\boldsymbol{x}_{\boldsymbol{fum}}^{\ddagger}$ and $\boldsymbol{x}_{\boldsymbol{succ}}^{\ddagger}$ obtained from the data represented in Figure 42 are 10 ± 2 nm and 6 ± 2 nm correspondingly.

3.1 Conclusions

Synthetic switchable molecular shuttles have recently attracted interest from the research community due to their potential applications in biomedicine and nanotechnology ([195] -[197]). The idea of controlling the motion of these molecular devices has become one of the major research challenges. Although the kinetics and thermodynamics of these systems in bulk are well-understood [195], the information on the operational dynamics of these synthetic devices remains missing. In this thesis, it was described how to obtain this elusive information from individual rotaxane molecules using the single-molecule manipulation technique of optical tweezers, which presents exquisite force control and force resolution. It was shown that the unique biochemical and mechanical properties of dsDNA can be readily exploited to study and manipulate the operation of synthetic devices in real-time. By coupling rotaxane molecules with dsDNA, it is possible to solubilize them and study them under near-physiological conditions. In addition, dsDNA was used as a handle to manipulate the macrocycle, as a spacer to separate the device from the surface of the beads and as a single-molecule reporter. It is noteworthy, that in the experimental setup described in this thesis it is possible to change the conditions *in situ* to study the combined effect of force and other different additional factors on the operation of a rotaxane. For instance, changing the ionic strength of the solution (gradually increasing or decreasing the salt concentration), chemically modifying one of the two stations of the rotaxane (by adding different reagents or applying light) or changing the temperature of the reaction medium, would shed light into the inner thermo-mechanical and mechano-chemical processes that govern the operation these synthetic devices. The method described in this thesis could be applied to study the mechanical strength and the real-time operation of other artificial systems at the single-molecule level, which will represent a valuable contribution to the advancement of the fascinating field of single-molecule supramolecular chemistry.

References

[1] Stock D, Leslie AGW, Walker JE: Molecular Architecture of the Rotary Motor in ATP Synthase,» *Science,* vol. 286, nº 5445, pp. 1700-1705, 1999.

[2] Lewis JS: Chapter Two - The E. coli DNA Replication Fork,» de *The Enzymes Volume 39 DNA Replication Across Taxa*, M. O. Laurie S. Kaguni, Ed., Elsevier, 2016, pp. 31-88.

[3] Chung DK, Mekhail K: Repair by a molecular DNA ambulance,» *Oncotarget,* vol. 6, nº 23, pp. 19358–19359, 2015.

[4] Gelles J, Landick R: RNA Polymerase as a Molecular Motor. *Cell,* vol. 93, nº 1, pp. 13-16, 1998.

[5] Rao VB, Feiss M: The Bacteriophage DNA Packaging Motor. *Annual Review of Genetics,* vol. 42, pp. 647-681, 2008.

[6] G. M. Cooper: Actin, Myosin, and Cell Movement. de *The Cell, 2nd edition*, Sinauer Associates, 2000.

[7] Martin A, Baker TA, Sauer RT: Rebuilt AAA + motors reveal operating principles for ATP-fuelled machines. *Nature,* vol. 437, pp. 1115–1120, 2005.

[8] Kolomeisky AB: Motor proteins and molecular motors: how to operate machines at the nanoscale. *Journal of Physics: Condensed Matter,* vol. 25, nº 40, 2013.

[9] Verhey KJ, Kaul N, Soppina V: Kinesin Assembly and Movement in Cells. *Annual Review of Biophysics,* vol. 40, pp. 267-288, 2011.

[10] Senior AE, Nadanaciva S, Weber J: The molecular mechanism of ATP synthesis by F1F0-ATP synthase. *Biochimica et Biophysica Acta,* vol. 1553, pp. 188-211, 2001.

[11] Howard J, Hudspeth AJ, Vale RD: Movement of microtubules by single kinesin molecules. *Nature,* vol. 342, nº 6246, pp. 154-158, 1989.

[12] Block SM, Goldstein LS, Schnapp BJ: Bead movement by single kinesin molecules studied with optical tweezers. *Nature,* vol. 348, nº 6299, pp. 348-352, 1990.

[13] Svoboda K, Block SM: Force and velocity measured for single kinesin molecules. *Cell,* vol. 77, nº 5, pp. 773-784, 1994.

[14] Meyhöfer E, Howard J: The force generated by a single kinesin molecule against an elastic load. *PNAS,* vol. 92, pp. 574–578, 1995.

[15] Visscher K, Schnitzer MJ, Block SM: Single kinesin molecules studied with a molecular force clamp. *Nature,* vol. 400, nº 6740, pp. 184–189, 1999.

[16] Nishiyama M, Higuchi H, Yanagida T: Chemomechanical coupling of the forward and backward steps of single kinesin molecules. *Nature Cell Biology,* vol. 4, pp. 790-797, 2002.

[17] Vladimir V.Bulygin,Yakov M.Milgrom: A bi-site mechanism for Escherichia coli F1-ATPase accounts for the observed positive catalytic cooperativity. *Biochimica et Biophysica Acta (BBA) - Bioenergetics,* vol. 1787, nº 8, pp. 1016-1023, 2009.

[18] Nath S: The thermodynamic efficiency of ATP synthesis in oxidative phosphorylation. *Biophysical Chemistry,* vol. 219, pp. 69-74, 2016.

[19] Cajens, SR: The DNA-packaging nanomotor of tailed bacteriophages. *Nat Rev Microbiol,* vol. 9, nº 9, pp. 647-657, 2011.

[20] Hetherington CL, Moffitt JR, Jardine PJ, Bustamante C: Viral DNA Packaging Motors. de *Comprehensive Biophysics Vol.4*, E. O. Y.I. Goldman, Ed., Oxford, Elsevier Inc., 2012, pp. 420-446.

[21] Chemla YR, Aathavan K, Michaelis J, Grimes S, Jardine PJ, Anderson DL, Bustamante C: Mechanism of Force Generation of a Viral DNA Packaging Motor. *Cell,* vol. 122, nº 5, pp. 683-692, 2005.

[22] Smith DE, Tans SJ, Smith SB, Grimes S, Anderson DL, Bustamante C: The bacteriophage φ29 portal motor can package DNA against a large internal force. *Nature,* vol. 413, pp. 748–752, 2001.

[23] Shibasaki M, Stoddart JF, Vögtle F, Stimulating Concepts in Chemistry, Weinheim: Wiley, 2000.

[24] Balzani V, Credi A, Raymo FM, Stoddart JF: Artificial Molecular Machines. *Angewandte Chemie,* vol. 39, nº 19, pp. 3348-3391, 2000.

[25] Pease AR, Jeppesen JO, Stoddart JF, Luo Y, Collier CP, Heath JR: Switching Devices Based on Interlocked Molecules. *Acc. Chem. Res,* vol. 34, nº 6, pp. 433-444, 2001.

[26] Gil-Ramírez G , Leigh DA, Stephens AJ: Catenanes: Fifty Years of Molecular Links. *Angewandte Chemie,* vol. 54, nº 21, pp. 6110-6150, 2015.

[27] Koumura N, Zijlstra RWJ, van Delden RA, Harada N, Feringa BL: Light-driven monodirectional molecular rotor. *Nature,* vol. 401, pp. 152-155, 1999.

[28] Leigh DA, Wong JKY, Dehez F, Zerbetto F: Unidirectional rotation in a mechanically interlocked molecular rotor. *Nature,* vol. 424, pp. 174–179, 2003.

[29] Hernández HV, Kay ER, Leigh DA: A Reversible Synthetic Rotary Molecular Motor. *Science,* vol. 306, nº 5701, pp. 1532-1537, 2004.

[30] Berná J, Leigh DA, Lubomska M, Mendoza SM, Pérez EM, Rudolf P, Teobaldi G, Zerbetto F: Macroscopic transport by synthetic molecular machines. *Nature materials,* vol. 4, pp. 704–710, 2005.

[31] Liu Y, Flood AH, Bonvallet PA, Vignon SA, Northrop BH, Tseng HR, Jeppesen JO, Huang TJ, Brough B, Baller M, Magonov S, Solares SD, Goddard WA, Ho CM, Stoddart JF: Linear Artificial Molecular Muscles. *JACS,* vol. 127, nº 7, pp. 9745-9759, 2005.

[32] Eelkema R, Pollard MM, Vicario J, Katsonis N, Serrano Ramon B, Bastiaansen CWM, Broer DJ, Feringa BL: Nanomotor rotates microscale objects. *Nature,* vol. 440, pp. 163, 2006.

[33] Li Q, Fuks G, Moulin E, Maaloum M, Rawiso M, Kulic I, Foy JT, Giuseppone N: Macroscopic contraction of a gel induced by the integrated motion of light-driven molecular motors. *Nature Nanotechnology,* vol. 10, pp. 161-165, 2015.

[34] Ponomarenko EA, Poverennaya EV, Ilgisonis EV, Pyatnitskiy MA, Kopylov AT, Zgoda VG, Lisitsa AV, Archakov AI: The size of the human proteome: the width and depth. *International Journal of Analytical Chemistry,* vol. 2016, 2016.

[35] Schwanhäusser B, Busse D, Li N, Dittmar G, Schuchhardt J, Wolf J, Chen W, Selbach M: Global quantification of mammalian gene expression control. *Nature,* vol. 473, pp. 337–342, 2011.

[36] Cooke R: The mechanism of muscle contraction. *CRC Crit Rev Biochem.,* vol. 21, nº 1, pp. 53-118, 1986.

[37] Astumian RD, Bier M: Fluctuation driven ratchets: Molecular motors. *Physical Review Letterts,* vol. 72, nº 11, pp. 1766-1769, 1994.

[38] Binnig G, Quate CF, Gerber C: Atomic Force Microscope. *Physical Review Letterts,* vol. 56, nº 9, pp. 930-934, 1986.

[39] Strick TR, Allemand JF, Bensimon D, Bensimon A, Croquette V: The Elasticity of a Single Supercoiled DNA Molecule. *Science,* vol. 271, nº 5257, pp. 1835-1837, 1996.

[40] Ashkin A, Dziedzic JM, Bjorkholm JE, Chu S: Observation of a single-beam gradient force optical trap for dielectric particles. *Optics letters,* vol. 11, nº 5, pp. 288-290, 1986.

[41] Bustamante C, Macosko JC, Wuite GJL: Grabbing the cat by the tail: manipulating molecules one by one. *Nature Reviews Molecular Cell Biology,* vol. 1, pp. 130-136, 2000.

[42] Neuman KC, Nagy A: Single-molecule force spectroscopy: optical tweezers, magnetic tweezers and atomic force microscopy. *Nature Methods,* vol. 5, pp. 491-505, 2008.

[43] Ashkin A: Atomic-Beam Deflection by Resonance-Radiation Pressure. *Physical Review Letters,* vol. 25, nº 19, pp. 1321, 1970.

[44] Ashkin A, Dziedzic JM: Optical trapping and manipulation of viruses and bacteria. *Science,* vol. 235, nº 4795, pp. 1517-1520, 1987.

[45] Ashkin A, Dziedzic JM, Yamane T: Optical Trapping and Manipulation of Single Cells Using Infrared Laser Beams. *Nature,* vol. 330, pp. 769–771, 1987.

[46] Svoboda K, Schmidt CF, Schnapp BJ, Block SM: Direct observation of kinesin stepping by optical trapping interferometryz. *Nature,* vol. 365, pp. 721–727, 1993.

[47] Finer JT, Simmons RM, Spudich JA: Single myosin molecule mechanics: piconewton forces and nanometre steps. *Nature,* vol. 368, pp. 113–119, 1994.

[48] Ishijima A, Kojima H, Funatsu T, Tokunaga M, Higuchi H, Tanaka H, Yanagida T: Simultaneous Observation of Individual ATPase and Mechanical Events by a Single Myosin Molecule during Interaction with Actin. *Cell,* vol. 92, pp. 161-171, 1998.

[49] Bustamante C, Smith SB, Liphardt J, Smith D: Single-molecule studies of DNA mechanics. *Current Opinion in Structural Biology,* vol. 10, nº 3, pp. 279-285, 2000.

[50] Harcourt EM, Ehrenschwender T, Batista PJ, Chang HY, Kool ET: Identification of a Selective Polymerase Enables Detection of N6-Methyladenosine in RNA. *JACS,* vol. 135, nº 51, pp. 19079-19082, 2013.

[51] Dame RT, Noom MC, Wuite GJ: Bacterial chromatin organization by H-NS protein unravelled using dual DNA manipulation.. *Nature,* vol. 444, pp. 387-390, 2006.

[52] Heller I, Hoekstra TP, King GA, Peterman, EJG, Wuite GJL: Optical Tweezers Analysis of DNA–Protein Complexes. *Journal of proteome research,* vol. 14, nº 6, pp. 3087-3119, 2014.

[53] Morin JA, Cerrón F, Jarillo J, Beltran-Heredia E, Ciesielski GL, J. Arias-Gonzalez R, Kaguni LS, Cao FJ, Ibarra B: DNA synthesis determines the binding mode of the human mitochondrial single-stranded DNA-binding protein. *Nucleic acids research,* vol. 12, nº 7, pp. 7237–7248, 2017.

[54] Cecconi C, Shank EA, Bustamante C, Marqusee S: Direct Observation of the Three-State Folding of a Single Protein Molecule. *Science,* vol. 309, nº 5743, pp. 2057-2060, 2005.

[55] Bercy M, Bockelmann U: Hairpins under tension: RNA versus DNA. *NAR,* vol. 43, nº 20, pp. 9928–9936, 2015.

[56] Alemany A, Ritort F: Force-Dependent Folding and Unfolding Kinetics in DNA Hairpins Reveals Transition-State Displacements along a Single Pathway. *The Journal of Physical Chemistry Letters,* vol. 8, nº 5, pp. 895-900, 2017.

[57] Nishizaka T, Miyata H, Yoshikawa H, Ishiwata, Kinosita K Jr: Unbinding force of a single motor molecule of muscle measured using optical tweezers. *Natutre,* vol. 377, pp. 251–254, 1995.

[58] Liu N, Chistol, Cui Y, Bustamante C: Mechanochemical coupling and bi-phasic force-velocity dependence in the ultra-fast ring ATPase SpoIIIE.. *eLife,* vol. 7, 2018.

[59] Maillard RA, Chistol G, Sen M, Righini M, Tan J, Kaiser CM, Hodges C, Martin A, Bustamante C.: ClpX(P) Generates Mechanical Force to Unfold and Translocate Its Protein Substrates. *Cell,* vol. 145, nº 3, pp. 459-469, 2011.

[60] Cheng W, Arunajadai SG, Moffitt JR, Tinoco I Jr, Bustamante C: Single–Base Pair Unwinding and Asynchronous RNA Release by the Hepatitis C Virus NS3 Helicase. *Science,* vol. 333, nº 6050, pp. 1746-1749, 2011.

[61] Chistol G, Liu S, Hetherington CL, Moffitt JR, Grimes S, Jardine PJ, Bustamante C.: High degree of coordination and division of labor among subunits in a homomeric ring ATPase. *Cell,* vol. 151, nº 5, pp. 1017-1028, 2012.

[62] Smith SB, Cui Y, Bustamante C: Optical-trap force transducer that operates by direct measurement of light momentum. *Methods Enzymol.,* vol. 361, pp. 134-162, 2003.

[63] Neuman KC, Nagy A: Single-molecule force spectroscopy: optical tweezers, magnetic tweezers and atomic force microscopy. *Nature Methods,* vol. 5, pp. 491-505, 2008.

[64] Hormeño S, Arias-Gonzalez JR: Exploring mechanochemical processes in the cell with optical tweezers. *Biology of the Cell,* vol. 98, nº 12, pp. 679-695, 2012.

[65] de Lorenzo, S: Single Molecule Studies in a temperature-jump optical trap. Doctoral thesis. 2015.

[66] Vermeulen KC, Wuite GJL, Stienen GJM, Schmidt CF: Optical trap stiffness in the presence and absence of spherical aberrations. *Applied Optics,* vol. 45, nº 8, pp. 1812-1819, 2006.

[67] Smith SB, Cui Y, Bustamante C: Optical-trap force transducer that operates by direct measurement of light momentum. de *Methods in Enzymology Vol. Biophotonics, Part B*, G. M. a. I. Parker, Ed., Elsevier Inc., 2003, pp. 134-162.

[68] Tedeschi H, Harris DL: The osmotic behavior and permeability to non-electrolytes of mitochondria. *Archives of Biochemistry and Biophysics,* vol. 58, nº 1, pp. 52-67, 1995.

[69] Jouaville LS, Pinton P, Bastianutto C, Rutter GA, Rizzuto R: Regulation of mitochondrial ATP synthesis by calcium: Evidence for a long-term metabolic priming. *PNAS,* vol. 96, nº 24, pp. 13807-13812, 1998.

[70] Kluck RM, Bossy-Wetzel E, Green DR, Newmeyer DD: The Release of Cytochrome c from Mitochondria: A Primary Site for Bcl-2 Regulation of Apoptosis. *Science,* vol. 275, nº 5303, pp. 1132-1136, 1997.

[71] Yang J, Liu X, Bhalla K, Kim CN, Ibrado AM, Cai J, Peng TI, Jones DP, Wang X: Prevention of Apoptosis by Bcl-2: Release of Cytochrome c from Mitochondria Blocked. *Science,* vol. 275, nº 5303, pp. 1129-1132, 1997.

[72] An I. Jonckheere, Jan A. M. Smeitink, and Richard J. T. Rodenburg: Mitochondrial ATP synthase: architecture, function and pathology. *J Inherit Metab Dis,* vol. 35, nº 2, pp. 211–225, 2012.

[73] Baughman JM, Perocchi F, Girgis HS, Plovanich M, Belcher-Timme CA, Sancak Y, Bao XR, Strittmatter L, Goldberger O, Bogorad RL, Koteliansky V, Mootha VK: Integrative genomics identifies MCU as an essential component of the mitochondrial calcium uniporter. *Nature,* vol. 476, pp. 341-345, 2011.

[74] De Stefani D, Raffaello A, Teardo E, Szabò I, Rizzuto R: A forty-kilodalton protein of the inner membrane is the mitochondrial calcium uniporter. *Nature,* vol. 276, pp. 336–340, 2011.

[75] Marchi S, Pinton P: The mitochondrial calcium uniporter complex: molecular components, structure and physiopathological implications. *The Journal of Physiology,* vol. 592(Pt.5), pp. 829–839, 2014.

[76] Carafoli E, Tiozzo R, Lugli G, Crovetti F, Kratzing C: The release of calcium from heart mitochondria by sodium. *Journal of Molecular and Cellular Cardiology,* vol. 6, pp. 361, 1974.

[77] Crompton M, Moser R, Ludi H, Carafoli E: The interrelations between the transport of sodium and calcium in mitochondria of various mammalian tissues. *European Journal of Biochemistry,* vol. 82, pp. 25, 1978.

[78] Denton RM, McCormak JG: The role of calcium in the regulation of mitochondrial metabolism. *Biochemical Society Transactions,* vol. 8, pp. 266-268, 1980.

[79] Stout AK, Raphael HM, Kanterewicz BI, Klann E, Reynolds IJ: Glutamate-induced neuron death requires mitochondrial calcium uptake. *Nature Neuroscience,* vol. 1, pp. pages366–373, 1998.

[80] Kroemer G, Galluzzi L, Brenner C: Mitochondrial Membrane Permeabilization in Cell Death. *Physiological Reviews,* vol. 87, pp. 99-163, 2007.

[81] Anderson S, Bankier AT, Barrell BG, de Bruijn MHL, Coulson AR, Drouin J, Eperon IC, Nierlich DP, Roe BA, Sanger F, Schreier PH, Smith AJH, Staden R, Young IG: Sequence and organization of the human mitochondrial genome. *Nature,* vol. 290, pp. 457–465, 1981.

[82] Chinnery PF, Johnson MA, Wardell TM, Singh-Kler R, Hayes C, Brown DT, Taylor RW, Bindoff LA, Turnbull DM : The epidemiology of pathogenic mitochondrial DNA mutations. *Annals of Neurology,* vol. 48, nº 2, pp. 188-193, 2000.

[83] Trifunovic A, Wredenberg A, Falkenberg M, Spelbrink JN, Rovio AT, Bruder CE, Bohlooly-Y M, Gidlöf S, Oldfors A, Wibom R, Törnell J, Jacobs HT, Larsson NG: Premature ageing in mice expressing defective mitochondrial DNA polymerase. *Nature,* vol. 429, pp. 417–423, 2004.

[84] Hockenbery DM: A mitochondrial Achilles' heel in cancer?. *Cancer Cell,* vol. 2, nº 1, pp. 1-2, 2002.

[85] Radpour R, Cheng Fan AX, Kohler C, Holzgreve W, Zhong XY: Current Understanding of Mitochondrial DNA in Breast Cancer. *The Breast Journal,* vol. 15, nº 5, pp. 505-509, 2002.

[86] Korhonen JA, Pham XH, Pellegrini M, Falkenberg M: Reconstitution of a minimal mtDNA replisome in vitro. *EMBO J,* vol. 23, nº 12, pp. 2423-2429, 2004.

[87] Lestienne P: Evidence for a direct role of the DNA polymerase gamma in the replication of the human mitochondrial DNA in vitro. *Biochemical and Biophysical Research Communications,* vol. 146, nº 3, pp. 1146-1153, 1987.

[88] Johnson AA, Johnson KA: Exonuclease proofreading by human mitochondrial DNA polymerase.. *Journal of Biological Chemistry,* vol. 276, nº 41, pp. 38097-107, 2001.

[89] Rothwell PJ, Waksman G: Structure and mechanism of DNA polymerases. *Advances in Protein Chemistry,* vol. 71, pp. 401-440, 2005.

[90] Golosov AA, Warren JJ, Beese LS, Karplus M: The Mechanism of the Translocation Step in DNA Replication by DNA Polymerase I: A Computer Simulation Analysis. *Structure,* vol. 18, nº 1, pp. 83-93, 2010.

[91] Miller BR III, Beese LS, Parish CA, Wu EY: The Closing Mechanism of DNA Polymerase I at Atomic Resolution. *Structure,* vol. 23, nº 9, pp. 1609-1620, 2015.

[92] Joyce CM, Benkovic SJ: DNA polymerase fidelity: kinetics, structure, and checkpoints. *Biochemistry,* vol. 43, nº 45, pp. 14317-14324, 2004.

[93] Morin JA, Cao FJ, Lázaro JM, Arias-Gonzalez JR, Valpuesta JM, Carrascosa JL, Salas M, Ibarra B: Mechano-chemical kinetics of DNA replication: identification of the translocation step of a replicative DNA polymerase. *Nucleic acids research,* vol. 43, nº 7, pp. 3643–3652, 2015.

[94] Falkenberg M, Larsson NG, Gustafsson CM: DNA Replication and Transcription in Mammalian Mitochondria. *Annual Review of Biochemistry,* vol. 76, pp. 679-699, 2007.

[95] Donlin MJ, Patel SS, Johnson KA: Kinetic partitioning between the exonuclease and polymerase sites in DNA error correction. *Biochemistry,* vol. 30, nº 2, pp. 538-546, 1991.

[96] Lee YS, W. Kennedy D, Yin YW: Structural Insight into Processive Human Mitochondrial DNA Synthesis and Disease-Related Polymerase Mutations. *Cell,* vol. 139, nº 2, pp. 312-324, 2009.

[97] Kunkel TA, Mosbaugh DW: Exonucleolytic proofreading by a mammalian DNA polymerase. *Biochemistry,* vol. 7, nº 98, pp. 988-995, 1989.

[98] Kunkel TA, Soni A: Exonucleolytic proofreading enhances the fidelity of DNA synthesis by chick embryo DNA polymerase-gamma. *Journal of Biological Chemistry,* vol. 263, pp. 4450-4459, 1988.

[99] Sherman LA, Gefter ML: Studies on the mechanism of enzymatic DNA elongation by Escherichia coli DNA polymerase II. *Journal of Molecular Biology,* vol. 103, nº 1, pp. 61-76, 1976.

[100] LaDuca RJ, Fay PJ, Chuang C, McHenry CS, Bambara RA: Site-specific pausing of deoxyribonucleic acid synthesis catalyzed by four forms of Escherichia coli DNA polymerase III. *Biochemistry,* vol. 22, nº 22, pp. 5177–5188, 1983.

[101] Weaver DT, DePamphilis ML: The role of palindromic and non-palindromic sequences in arresting DNA synthesis in vitro and in vivo. *Journal of Molecular Biology,* vol. 180, nº 4, pp. 961-986, 1984.

[102] Hacker KJ, Alberts BM: The rapid dissociation of the T4 DNA polymerase holoenzyme when stopped by a DNA hairpin helix. A model for polymerase release following the termination of each Okazaki fragment. *Journal of Biological Chemistry,* vol. 269, nº 39, pp. 24221–24228, 1994.

[103] Macao B, Uhler JP, Siibak T, Zhu X, Shi Y, Sheng W, Olsson M, Stewart JB, Gustafsson CM, Falkenberg M: The exonuclease activity of DNA polymerase γ is required for ligation during mitochondrial DNA replication. *Nature Communications,* vol. 6, nº 7303, 2015.

[104] Uhler JP, Falkenberg M: Primer removal during mammalian mitochondrial DNA replication. *DNA repair,* vol. 34, pp. 28-38, 2015.

[105] Canceill D, Viguera E, Ehrlich SD: Replication Slippage of Different DNA Polymerases Is Inversely Related to Their Strand Displacement Efficiency. *Journal of Biological Chemistry,* vol. 274, pp. 27481-27490, 1999.

[106] Engler MJ, Lechner RL, Richardson CC: Two forms of the DNA polymerase of bacteriophage T7. *Journal of Biological Chemistry,* vol. 258, nº 18, pp. 11165-1117, 1983.

[107] Esteban JA, Soengas MS, Salas M, Blanco L: 3'-->5' exonuclease active site of phi 29 DNA polymerase. Evidence favoring a metal ion-assisted reaction mechanism. *Journal of Biological Chemistry,* vol. 269, nº 50, pp. 31946-31954, 1994.

[108] Reha-Krantz LJ, Stocki S, Nonay RL, Dimayuga E, Goodrich LD, Konigsberg WH, Spicer EK: DNA polymerization in the absence of exonucleolytic proofreading: in vivo and in vitro studies. *PNAS,* vol. 88, nº 6, pp. 2417-2421, 1991.

[109] Farge G, Pham XH, Holmlund T, Khorostov I, Falkenberg M: The accessory subunit B of DNA polymerase γ is required for mitochondrial replisome function. *Nucleic acids research,* vol. 35, nº 3, pp. 902–911, 2007.

[110] Bratic A, Kauppila TES, Macao B, Grönke S, Siibak T, Stewart JB, Baggio F, Dols J, Partridge L, Falkenberg M, Wredenberg A, Larsson NG: Complementation between polymerase- and exonuclease-deficient mitochondrial DNA polymerase mutants in genomically engineered flies. *Nature Communications,* vol. 6, nº 8808, 2015.

[111] Sen D, Nandakumar D, Tang GQ, Patel SS: Human Mitochondrial DNA Helicase TWINKLE Is Both an Unwinding and Annealing Helicase. *Journal of Biological Chemistry,* vol. 287, nº 18, pp. 14545–14556, 2012.

[112] Fernández-Millán P, Lázaro M, Cansız-Arda S, Gerhold JM, Rajala N, Schmitz CA, Silva-Espiña C, Gil D, Bernadó P, Valle M, Spelbrink JN, Solà M: The hexameric structure of the human mitochondrial replicative helicase Twinkle. *Nucleic acids research,* vol. 43, nº 8, pp. 4284–4295, 2015.

[113] Korhonen JA, Gaspari M, Falkenberg M: TWINKLE Has 5′ → 3′ DNA Helicase Activity and Is Specifically Stimulated by Mitochondrial Single-stranded DNA-binding Protein. *Journal of Biological Chemistry,* vol. 278, nº , pp. 48627-48632, 2003.

[114] Kaur P, Longley MJ, Pan H, Wang W, Countryman P, Wang H, Copeland WC: Single-molecule level structural dynamics of DNA unwinding by human mitochondrial Twinkle helicase. *Journal of Biological Chemistry,* vol. 295, nº 17, pp. 5564-5576, 2020.

[115] Patel SS, Picha KM: Structure and function of hexameric helicases. *Annual Review of Biochemistry,* vol. 69, pp. 651-97, 2000.

[116] Matson SW, Tabor S, Richardson CC: The gene 4 protein of bacteriophage T7. Characterization of helicase activity. *Biological Chemistry,* vol. 258, nº 22, pp. 14017-14024, 1983.

[117] Jemt E, Farge G, Bäckström S, Holmlund T, Gustafsson CM, Falkenberg M: The mitochondrial DNA helicase TWINKLE can assemble on a closed circular template and support initiation of DNA synthesis. *Nucleic acids research,* vol. 39, nº 21, pp. 9238-9249, 2011.

[118] Sen D, Patel G, Patel SS: Homologous DNA strand exchange activity of the human mitochondrial DNA helicase TWINKLE. *Nucleic acids research,* vol. 44, nº 9, pp. 4200-4210, 2016.

[119] Picha KM, Ahnert P, Patel SS: DNA binding in the central channel of bacteriophage T7 helicase-primase. *Biochemistry,* vol. 39, pp. 6401–6409, 2000.

[120] Ahnert P, Patel SS: Asymmetric interactions of hexameric bacteriophage T7 DNA helicase with the 5'- and. *Journal of Biological Chemistry,* vol. 272, pp. 32267–32273, 1997.

[121] Oliveira MT, Kaguni LS: Functional Roles of the N- and C-Terminal Regions of the Human Mitochondrial Single-Stranded DNA-Binding Protein. *PLoS ONE,* vol. 5, nº 10, 2010.

[122] Yakubovskaya E, Lukin M, Chen Z, Berriman J, Wall JS, Kobayashi R, Kisker C, Bogenhagen DF: The EM structure of human DNA polymerase gamma reveals a localized contact between the catalytic and accessory subunits. *EMBO J,* vol. 26, nº 19, pp. 4283-4891, 2007.

[123] Suksombat S, Khafizov R, Kozlov AG, Lohman TM, Chemla YR: Structural dynamics of E. coli single-stranded DNA binding protein reveal DNA wrapping and unwrapping pathways. *eLife,* pp. 1-23, 2015.

[124] Sen D, Nandakumar D, Tang GQ, Patel SS: Human Mitochondrial DNA Helicase TWINKLE Is Both an Unwinding and Annealing Helicase. *Journal of Biological Chemistry,* vol. 287, pp. 14545-14556, 2012.

[125] Yang C, Curth U, Urbanke C, Kang C: Crystal structure of human mitochondrial single-stranded DNA binding protein at 2.4 A resolution.. *Nature Structural & Molecular Biology,* vol. 4, nº 2, pp. 153-7, 1997.

[126] Raghunathan S, Ricard CS, Lohman TM, Waksman G: Crystal structure of the homo-tetrameric DNA binding domain of Escherichia coli single-stranded DNA-binding protein determined by multiwavelength X-ray diffraction on the selenomethionyl protein at 2.9-angstrom resolution.. *PNAS,* vol. 94, nº 13, pp. 6652–6657, 1997.

[127] Lohman TM, Ferrari ME: ESCHERICHIA COLI SINGLE-STRANDED DNA-BINDING PROTEIN: Multiple DNA-Binding Modes and Cooperativities. *Annual Review of Biochemistry,* vol. 63, pp. 527-570, 1994.

[128] Ruhanen H, Borrie S, Szabadkai G, Tyynismaa H, Jones AW, Kang D, Taanman JW, Yasukawa T.: Mitochondrial single-stranded DNA binding protein is required for maintenance of mitochondrial DNA and 7S DNA but is not required for mitochondrial nucleoid organisation.. *Biochim Biophys Acta,* vol. 1803, nº 8, pp. 931-9, 2010.

[129] Steen KW, Doseth B, Westbye MP, Akbari M, Kang D, Falkenberg M, Slupphaug G: mtSSB may sequester UNG1 at mitochondrial ssDNA and delay uracil processing until the dsDNA conformation is restored.. *DNA Repair,* vol. 11, pp. 82-91, 2012.

[130] Griffith JD, Harris LD, Register J III: Visualization of SSB-ssDNA Complexes Active in the Assembly of Stable RecA-DNA Filaments. *Cold Spring Harbor Symposia on Quantitative Biology,* vol. 49, pp. 553-559, 1984.

[131] Lohman TM, Overman LB: Two binding modes in Escherichia coli single strand binding protein-single stranded DNA complexes. Modulation by NaCl concentration. *Journal of Biological Chemistry,* vol. 260, pp. 3594-3603, 1985.

[132] Spenkelink LM, Lewis JS, Jergic S, Xu ZQ, Robinson A, Dixon NE, van Oijen AM: Recycling of single-stranded DNA-binding protein by the bacterial replisome. *Nucleic acids research,* vol. 47, nº 8, pp. 4111–4123, 2019.

[133] Ciesielski GL, Bermek O, Rosado-Ruiz FA, Hovde SL, Neitzke OJ, Griffith JD, Kaguni LS: Mitochondrial Single-stranded DNA-binding Proteins Stimulate the Activity of DNA Polymerase γ by Organization of the Template DNA*. *Journal of Biological Chemistry,* vol. 290, pp. 28697-28707, 2015.

[134] Cerrón F, de Lorenzo S, Lemishko KM, Ciesielsk GL, Kaguni LS, Cao FJ, Ibarra B: Replicative DNA polymerases promote active displacement of SSB proteins during lagging strand synthesis. *Nucleic acids research,* vol. 47, nº 11, pp. 5723–5734, 2019.

[135] Farr CL, Wang Y, Kaguni LS: Functional interactions of mitochondrial DNA polymerase and single-stranded DNA-binding protein. template-primer dna binding and initiation and elongation of dna strand synthesis. *Journal of Biological Chemistry,* vol. 274, nº 21, pp. 14779-14785, 1999.

[136] Graziewicz MA, Longley MJ, Bienstock RJ, Zeviani M, Copeland WC: Structure-function defects of human mitochondrial DNA polymerase in autosomal dominant progressive external ophthalmoplegia. *Nature Structural & Molecular Biology,* vol. 11, nº 8, pp. 770-6, 2004.

[137] Copeland WC: Inherited mitochondrial diseases of DNA replication.. *Annual Review of Medicine,* vol. 59, pp. 131-46, 2008.

[138] Hudson G, Chinnery PF: Mitochondrial DNA polymerase-gamma and human disease. *Human Molecular Genetics,* vol. 15, nº suppl_2, pp. R244–R252, 2006.

[139] Longley MJ, Clark S, Yu Wai Man C, Hudson G, Durham SE, Taylor RW, Nightingale S, Turnbull DM, Copeland WC, Chinnery PF: Mutant POLG2 disrupts DNA polymerase gamma subunits and causes progressive external ophthalmoplegia.. *American Journal of Human Genetics,* vol. 78, nº 6, pp. 1026-34, 2006.

[140] Spelbrink JN, Li FY, Tiranti V, Nikali K, Yuan QP, Tariq M, Wanrooij S, Garrido N, Comi G, Morandi L, Santoro L, Toscano A, Fabrizi GM, Somer H, Croxen R, Beeson D, Poulton J, Suomalainen A, Jacobs HT, Zeviani M, Larsson C: Human mitochondrial DNA deletions associated with mutations in the gene encoding Twinkle, a phage T7 gene 4-like protein localized in mitochondria.. *Nature Genetics,* vol. 28, nº 3, pp. 223-31, 2001.

[141] Suomalainen A, Majander A, Wallin M, Setälä K, Kontula K, Leinonen H, Salmi T, Paetau A, Haltia M, Valanne L, Lonnqvist J, Peltonen L, Somer H: Autosomal dominant progressive external ophthalmoplegia with multiple deletions of mtDNA: clinical, biochemical, and molecular genetic features of the 10q-linked disease.. *Neurology,* vol. 48, nº 5, pp. 1244-53, 1997.

[142] Mikhailov VS, Bogenhagen DF: Termination within Oligo(dT) Tracts in Template DNA by DNA Polymerase γ Occurs with Formation of a DNA Triplex Structure and Is Relieved by Mitochondrial Single-stranded DNA-binding Protein. *Journal of Biological Chemistry,* vol. 271, pp. 30774-30780, 1996.

[143] Jiang HL, Sun HF, Gao SP, Li LD, Huang S, Hu X, Liu S, Wu J, Shao ZM, Jin W: SSBP1 Suppresses TGFβ-Driven Epithelial-to-Mesenchymal Transition and Metastasis in Triple-Negative Breast Cancer by Regulating Mitochondrial Retrograde Signaling. *Cancer Research,* vol. 76, nº 4, pp. 952-964, 2015.

[144] Robberson DL, Kasamatsu H, Vinograd J: Replication of Mitochondrial DNA. Circular Replicative Intermediates in Mouse L Cells. *PNAS,* vol. 69, nº 3, pp. 737–74, 1972.

[145] Bogenhagen DF, Clayton DA: The mitochondrial DNA replication bubble has not burst.. *Trends in Biochemical Sciences,* vol. 28, nº 7, pp. 357-60, 2003.

[146] Martens PA, Claytin DA: Mechanism of mitochondrial DNA replication in mouse L-cells: localization and sequence of the light-strand origin of replication.. *Journal of Molecular Biology,* vol. 135, pp. 327-351, 1979.

[147] Fusté JM, Wanrooij S, Jemt E, Granycome CE, Cluett TJ, Shi Y, Atanassova N, Holt IJ, Gustafsson CM, Falkenberg M.: Mitochondrial RNA polymerase is

needed for activation of the origin of light-strand DNA replication.. *Molecular Cell,* vol. 37, nº 1, pp. 67-78, 2010.

[148] Fusté JM ,Shi Y, Wanrooij S, Zhu X, Jemt E, Persson O, Sabouri N, Gustafsson CM, Falkenberg M: In Vivo Occupancy of Mitochondrial Single-Stranded DNA Binding Protein Supports the Strand Displacement Mode of DNA Replication. *PLOS genetics,* vol. 12, nº 10, 2014.

[149] McKinney EA, Oliveira MT: Replicating animal mitochondrial DNA. *Genetics and Molecular Biology,* vol. 36, nº 3, pp. 308-315, 2013.

[150] Yang MY, Bowmaker M, Reyes A, Vergani L, Angeli P, Gringeri E, Jacobs HT, Holt IJ: Biased incorporation of ribonucleotides on the mitochondrial L-strand accounts for apparent strand-asymmetric DNA replication.. *Cell,* vol. 111, nº 4, pp. 495-505, 2002.

[151] Holt IJ, Lorimer HE, Jacobs HT: Coupled leading- and lagging-strand synthesis of mammalian mitochondrial DNA. *Cell,* vol. 100, nº 5, pp. 515-24, 2000.

[152] Bowmaker M, Yang MY, Yasukawa T, Reyes A, Jacobs HT, Huberman JA, Holt IJ: Mammalian mitochondrial DNA replicates bidirectionally from an initiation zone.. *Journal of Biological Chemistry,* vol. 278, nº 51, pp. 50961-9, 2003.

[153] Oliveira MT, Kaguni LS: Comparative Purification Strategies for Drosophila and Human Mitochondrial DNA Replication Proteins: DNA Polymerase γ and Mitochondrial Single-Stranded DNA-Binding Protein. de *Mitochondrial DNA. Methods and protocols*, 2 ed., J. A. Stuart, Ed., Totowa, NJ Humana Press, 2009, pp. 37-58.

[154] Rosado-Ruiz FA, So M, Kaguni LS: Purification and Comparative Assay of the Human Mitochondrial Replicative DNA Helicase. de *Methods in Molecular Biology. Mitochondrial DNA Volume 1351*, M. McKenzie, Ed., New York, Humana Press, 2016, pp. 185-198.

[155] Kratky O, Porod G: Röntgenuntersuchung gelöster Fadenmoleküle. *Recueil des Travaux Chimiques des Pays-Bas,* vol. 68, nº 12, pp. 1106-1122, 1949.

[156] Marko JF, Siggia ED: Statistical mechanics of supercoiled DNA. *PHYSICAL REVIEW E,* vol. 52, nº 3, pp. 2912, 1995.

[157] Odijk T: Stiff Chains and Filaments under Tension. *Macromolecules,* vol. 28, nº 20, pp. 7016-7018, 1995.

[158] Smith SB, Cui Y, Bustamante C: Overstretching B-DNA: the elastic response of individual double-stranded and single-stranded DNA molecules.. *Science,* vol. 271, nº 5250, pp. 795-799, 1996.

[159] Watson JD, Crick FHC: Molecular Structure of Nucleic Acids: A Structure for Deoxyribose Nucleic Acid. *Nature,* vol. 171, pp. 737–738, 1953.

[160] Betterton MD, Jülicher F: Opening of nucleic-acid double strands by helicases: Active versus passive opening. *PHYSICAL REVIEW E,* vol. 71, nº 1, 2005.

[161] Johnson DS, Bai L, Smith BY, Patel SS, Wang MD: Single-molecule studies reveal dynamics of DNA unwinding by the ring-shaped T7 helicase. *Cell,* vol. 129, nº 7, pp. 1299-3109, 2007.

[162] Markham NR, Zuker M: DINAMelt web server for nucleic acid melting prediction. *NAR,* vol. 33, nº suppl_2, pp. W577–W581, 2005.

[163] Morin JA, Cao FJ, Lázaro JM, Arias-Gonzalez JR, Valpuesta JM, Carrascosa JL, Salas M, Ibarra B: Active DNA unwinding dynamics during processive DNA replication. *PNAS,* vol. 109, nº 21, pp. 8115-8120, 2012.

[164] Longley MJ, Ropp PA, Lim SE, Copeland WC: Characterization of the Native and Recombinant Catalytic Subunit of Human DNA Polymerase γ: Identification of Residues Critical for Exonuclease Activity and Dideoxynucleotide Sensitivity. *Biochemistry,* vol. 37, nº 29, pp. 10529-10539, 1998.

[165] Ibarra B, Chemla YR, Plyasunov S, Smith SB, Lázaro JM, Salas M, Bustamante C.: Proofreading dynamics of a processive DNA polymerase. *The EMBO Journal,* vol. 28, nº 18, pp. 2794-802, 2009.

[166] Kim S, Schroeder CM, Xie XS: Single-Molecule study of DNA polymerization activity of HIV-1 reverse transcriptase on DNA templates. *Journal of Molecular Biology,* vol. 395, pp. 996-1006, 2010.

[167] Maier B, Bensimon D, Croquette V: Replication by a single DNA polymerase of a stretched single-stranded DNA. *PNAS,* vol. 97, nº 22, pp. 12002–12007, 2000.

[168] Manosas M, Spiering MM, Ding F, Bensimon D, Allemand JF., Benkovic SJ, Croquette V: Mechanism of strand displacement synthesis by DNA replicative polymerases. *Nucleic acids research,* vol. 40, nº 13, pp. 6174–6186, 2012.

[169] Naufer MN, Murison DA, Rouzina I, Beuning PJ, Williams MC: Single-molecule mechanochemical characterization of E. coli pol III core catalytic activity. *Protein Science,* vol. 26, nº 7, pp. 1413–1426, 2017.

[170] Wuite GJL, Smith SB, Young M, Keller D: Single-molecule studies of the effect of template tension on T7 DNA polymerase activity. *Nature,* vol. 404, pp. 103-106, 2000.

[171] Manosas M, Spiering MM, Ding F, Croquette V, Benkovic SJ: Collaborative coupling between polymerase and helicase for leading-strand synthesis. *Nucleic acids research,* vol. 40, nº 13, pp. 6187–6198, 2012.

[172] He Q, Shumate CK, White MA, Molineux IJ, Yin YW: Exonuclease of human DNA polymerase gamma disengages its strand displacement function. *Mitochondrion,* vol. 13, nº 6, pp. 592-601, 2013.

[173] Berman AJ, Kamtekar S, Goodman JL, Lázaro JM, de Vega M, Blanco L, Salas M, Steitz TA: Structures of phi29 DNA polymerase complexed with substrate: The mechanism of translocation in B-family polymerases. *EMBO J,* vol. 26, nº 14, pp. 3494–3505, 2007.

[174] Johnson DS, Bai L, Patel SS, Wang MD: Single-Molecule Studies Reveal Dynamics of DNA Unwinding by the Ring-Shaped T7 Helicase. *Cell,* vol. 129, nº 7, pp. 1299-1309, 2007.

[175] Lionnet T, Spiering MM, Benkovic SJ, Bensimon D, Croquette V: Real-time observation of bacteriophage T4 gp41 helicase reveals an unwinding mechanism. *PNAS,* vol. 104, nº 50, pp. 19790-19795, 2007.

[176] Ribeck N, Kaplan DL, Bruck I, Saleh OA: DnaB Helicase Activity Is Modulated by DNA Geometry and Force. *Biophysical Journal,* vol. 99, nº 7, pp. 2170-2179, 2010.

[177] Koc KN, Stodola JL, Burgers PM, Galletto R: Regulation of yeast DNA polymerase δ-mediated strand displacement synthesis by 5′-flaps. *Nucleic acids research,* vol. 43, nº 8, pp. 4179–4190, 2015.

[178] Antony E, Lohman TM: Dynamics of E. coli single stranded DNA binding (SSB) protein-DNA complexes. *Seminars in Cell & Developmental Biology,* vol. 86, pp. 102-111, 2019.

[179] Hernandez AJ, Richardson CC: Gp2.5, the multifunctional bacteriophage T7 single-stranded DNA binding protein. Semin. Cell Dev. Biol. *Seminars in Cell & Developmental Biology,* vol. 86, pp. 92-101, 2019.

[180] Thömmes P, Farr CL, Marton RF, Kaguni LS, Cotterill S: Mitochondrial single-stranded DNA-binding protein from Drosophila embryos. Physical and biochemical characterization.. *Journal of Biological Chemistry,* vol. 270, pp. 21137-21143, 1995.

[181] Rigler MN, Romano LJ: Differences in the Mechanism of Stimulation of T7 DNA Polymerase by Two Binding Modes of Escherichia coli Single-stranded DNA-binding Protein. *Journal of Biological Chemistry,* vol. 270, pp. 8910-8919, 1995.

[182] Ali JA, Lohman TM: Kinetic Measurement of the Step Size of DNA Unwinding by Escherichia coli UvrD Helicase. *Science,* vol. 275, nº 5298, pp. 377-380, 1997.

[183] Manosas M, Xi XG, Bensimon D, Croquette V: Active and passive mechanisms of helicases. *Nucleic acids research,* vol. 38, nº 16, pp. 5518–5526, 2010.

[184] Pincus DL, Chakrabarti S, Thirumalai D: Helicase Processivity and Not the Unwinding Velocity Exhibits Universal. *Biophysical Journal,* vol. 109, nº 2, pp. 120-130, 2015.

[185] Dumont S, Cheng W, Serebrov V, Beran RK, Tinoco I Jr, Pyle AM, Bustamante C: RNA Translocation and Unwinding Mechanism of HCV NS3 Helicase and Its Coordination by ATP. *Nature,* vol. 439, nº 7072, pp. 105-108, 2006.

[186] Rajagopal V, Patel SS: Single Strand Binding Proteins Increase the Processivity of DNA Unwinding by the Hepatitis C Virus Helicase. *Journal of Molecular Biology,* vol. 376, nº 1, pp. 69-79, 2008.

[187] Bagchi D, Manosas M, Zhang W, Manthei KA, Hodeib S, Ducos B, Keck JL, Croquette V: Single molecule kinetics uncover roles for E. coli RecQ DNA helicase domains and interaction with SSB. *Nucleic acids research,* vol. 46, nº 16, pp. 8500–8515, 2018.

[188] Stano NM, Jeong YJ, Donmez I, Tummalapalli P, Levin MK, Patel SS: DNA synthesis provides the driving force to accelerate DNA unwinding by a helicase. *Nature,* vol. 435, pp. 370-373, 2005.

[189] Nandakumar D, Pandey M, Patel SS: Cooperative base pair melting by helicase and polymerase positioned one nucleotide from each other. *eLife,* 2015 4: e06562.

[190] Kim S, Dallmann HG, McHenry CS, KJ Marians : Coupling of a replicative polymerase and helicase: a tau-DnaB interaction mediates rapid replication fork movement. *Cell,* vol. 94, nº 4, pp. 643-650, 1996.

[191] Zhang H, Lee SJ, Zhu B, Tran NQ, Tabor S, Richardson CC: Helicase-DNA polymerase interaction is critical to initiate leading-strand DNA synthesis. *PNAS,* vol. 108, nº 23, pp. 9372-9377, 2011.

[192] Hamdan SM, Marintcheva B, Cook T, Lee S-J, Tabor S, Richardson CC: A unique loop in T7 DNA polymerase mediates the binding of helicase-primase, DNA binding protein, and processivity factor. *PNAS,* vol. 102, nº 14, pp. 5096-5101, 2005.

[193] Gao Y, Cui Y, Fox T, Lin S, Wang H, de Val N, Zhou ZH, Yang W: Structures and operating principles of the replisome. *Science,* vol. 363, nº 6429, pp. eaav7003, 2019.

[194] Farge G, Pham XH, Holmlund T, Khorostov I, Falkenberg M: The accessory subunit B of DNA polymerase γ is required for mitochondrial replisome function. *Nucleic acids research,* vol. 35, nº 3, pp. 902–911, 2007.

[195] van Dongen SFM, Cantekin S, Elemans J, Rowan AE, Nolte RJM: Functional interlocked systems. *Chemical Society Reviews,* vol. 43, pp. 99, 2014.

[196] Dvornikovs V, House BE, Kaetzel M, Dedman JR, Smithrud DB: Host-[2]rotaxanes as cellular transport agents.. *JACS,* vol. 125, pp. 8290, 2003.

[197] Nishimura D, Takashima Y, Aoki H, Takahashi T, Yamaguchi H, Ito S, Harada A: Single-molecule imaging of rotaxanes immobilized on glass substrates: observation of rotary movement. *Angew. Chem., Int. Ed.,* vol. 47, pp. 6077, 2008.

[198] Anelli PL, Spencer N, Stoddart JF: A molecular shuttle. *Journal of the American Chemical Society,* vol. 113, pp. 5131-5133, 1991.

[199] Stoddart JF: Mechanically Interlocked Molecules (MIMs)—Molecular Shuttles, Switches, and Machines (Nobel Lecture). *Angewandte Chemie,* vol. 56, nº 37, pp. 11094-11125, 2017.

[200] Bissell RA, Córdova E, Kaifer AE, Stoddart JF: A chemically and electrochemically switchable molecular shuttle. *Nature,* vol. 369, pp. 133-137, 1994.

[201] Biedermann F, Schneider HJ: Experimental Binding Energies in Supramolecular Complexes. *Chemical Reviews,* vol. 116, nº 9, pp. 5216-5300, 2016.

[202] Wang MD, Schnitzer MJ, Yin H, Landick R, Gelles J, Block SM: Force and Velocity Measured for Single Molecules of RNA polymerase. *Science,* vol. 282, nº 5390, pp. 902-907, 1998.

[203] Meyhöfer E, Howard J: The force generated by a single kinesin molecule against an elastic load. *PNAS,* vol. 92, nº 2, pp. 574-578, 1995.

[204] Edwards DT, Faulk JK, LeBlanc MA , Perkins TT: Force Spectroscopy with 9-μs Resolution and Sub-pN Stability by Tailoring AFM Cantilever Geometry. *Biophysical Journal,* vol. 113, nº 12, pp. 2595-2600, 2017.

[205] Walder R, Van Patten WJ, Adhikari A, Perkins TT: Going Vertical To Improve the Accuracy of Atomic Force Microscopy Based Single-Molecule Force Spectroscopy.. *ACS Nano,* vol. 12, nº 1, pp. 198-207, 2018.

[206] Li PT, Collin D, Smith SB, Bustamante C, Tinoco I Jr: Probing the mechanical folding kinetics of TAR RNA by hopping, force-jump, and force-ramp methods. *Biophysical Journal,* vol. 90, nº 1, pp. 250-260, 2006.

[207] Wen JD, Manosas M, Li PTX, Smith SB, Bustamante C, Ritort F, Tinoco I Jr.: Force unfolding kinetics of RNA using optical tweezers. I. Effects of experimental variables on measured results.. *Biophysical Journal,* vol. 92, nº 9, pp. 2996-3009, 2007.

[208] Alemany A, Ritort F: Force-Dependent Folding and Unfolding Kinetics in DNA Hairpins Reveals Transition-State Displacements along a Single Pathway. *Journal of Physical Chemistry Letters,* vol. 8, nº 5, pp. 895-900, 2017.

[209] Jiao J, Rebane AA, Ma L, Zhang Y: Single-Molecule Protein Folding Experiments Using High-Precision Optical Tweezers. de *Optical tweezers. Methods and protocols*, vol. 1486, A. Gennerich, Ed., Springer, 2017, pp. 357-390.

[210] Naranjo T, Lemishko KM, de Lorenzo S, Somoza A, Ritort F, Pérez EM, Ibarra B: Dynamics of individual molecular shuttles under mechanical force. *Nature Communications,* vol. 9, 2018.

[211] Crooks GE: The Entropy Production Fluctuation Theorem and the Nonequilibrium Work Relation for Free Energy Differences. *Physical Review E,* vol. 60, nº 3, pp. 2721, 1999.

[212] Collin D, Ritort F, Jarzynski C, Smith SB, Tinoco I Jr, Bustamante C: Verification of the Crooks fluctuation theorem and recovery of RNA folding free energies. *Nature,* vol. 437, pp. 231–234, 2005.

[213] Liphardt J, Dumont S, Smith SB, Tinoco I Jr., Bustamante C: Equilibrium Information from Nonequilibrium Measurements in an Experimental Test of Jarzynski's Equality. *Science,* vol. 296, nº 5574, pp. 1832-1835, 2002.

[214] Bell GI: Models for the specific adhesion of cells to cells. *Science,* vol. 200, nº 4342, pp. 618-627, 1978.

[215] Evans E, Ritchie K: Dynamic strength of molecular adhesion bonds. *Biophysical Journal,* vol. 72, pp. 1541-1555, 1997.

[216] Merkel R, Nassoy P, Leung A, Ritchie K, Evans E: Energy landscapes of receptor–ligand bonds explored with dynamic force spectroscopy. *Nature,* vol. 397, pp. 50-53, 1999.

[217] Evans E: Probing the Relation Between Force—Lifetime—and Chemistry in Single Molecular Bonds. *Annu Rev Biophys Biomol Struct,* vol. 30, pp. 105-128, 2001.

[218] Smith S, Finzi L, Bustamante C: Direct mechanical measurements of the elasticity of single DNA molecules by using magnetic beads.. *Science,* vol. 258, pp. 1122-1126, 1992.

[219] Mark JE, Flory PJ: The configuration of the polyoxyethylene chain.. *JACS,* vol. 87, pp. 1415-1423, 1965.

[220] Bell G: Models for the specific adhesion of cells to cells. *Science,* vol. 200, nº 513, pp. 25, 1978.

[221] Evans E, Leung A, Hammer D, Simon S: Chemically distinct transition states govern rapid dissociation of single L-selectin bonds under force.. *PNAS,* vol. 98, nº 7, pp. 3784, 2001.

[222] H. F. DeLuca, G. W. Engstrom: Calcium uptake by rat kidney mitochondria. *PNAS,* vol. 47, nº 11, pp. 1744-1750, 1961.

[223] Yufeng Qian and Kenneth A. Johnson: The human mitochondrial single-stranded DNA-binding protein displays distinct kinetics and thermodynamics of DNA binding and exchange. *The Journal of Biological Chemistry,* vol. 292, pp. 13068-13084, 2017.

[224] Narendra Tuteja Renu Tuteja: Prokaryotic and eukaryotic DNA helicases. Essential molecular motor proteins for cellular machinery. *European Journal of Biochemistry,* vol. 271, nº 10, pp. 1835-1848, 2004.

[225] Jonckheere AI, Smeitink JA, Rodenburg RJ: Mitochondrial ATP synthase: architecture, function and pathology. *The Journal of Inherited Metabolic Disease,* vol. 35, nº 2, pp. 211-225, 2012.

[226] Peter Eaton and Paul West, Atomic Force Microscopy, 1 ed., Oxford University Press, 2010.

[227] Michelle D. Wang, Mark J. Schnitzer, Hong Yin, Robert Landick, Jeff Gelles, Steven M. Block: Force and Velocity Measured for Single Molecules of RNA Polymerase. *Science,* vol. 282, nº 5390, pp. 902-907, 1998.

[228] E Meyhöfer and J Howard: The force generated by a single kinesin molecule against an elastic load. *PNAS,* vol. 92, nº 2, pp. 574-578, 1995.

[229] J. R. Arias-González and M. Nieto-Vesperinas: Optical forces on small particles: attractive and repulsive nature and plasmon-resonance conditions. *ournal of the Optical Society of America A,* vol. 20, nº 7, pp. 1201-1209, 2003.

[230] Malik I, Qiu C, Snavely T, Kaplan CD: Wide-ranging and unexpected consequences of altered Pol II catalytic activity in vivo. *NAR,* vol. 48, nº 5, pp. 4431-4451, 2017.

[231] Maria Manosas, Michelle M. Spiering, Fangyuan Ding, David Bensimon, Jean-François Allemand, Stephen J. Benkovic, Vincent Croquette: Mechanism of strand displacement synthesis by DNA replicative polymerases. *NAR,* vol. 40, nº 3, pp. 6174–6186, 2012.

[232] J. C. Maxwell: Illustrations of the dynamical theory of gases. Part I. On the motions and collisions of perfectly elastic spheres.. *The London, Edinburgh, and Dublin Philosophical Magazine and Journal of Science, 4th Series,* vol. 19, pp. 19-32, 1860.

[233] L. Boltzmann: Weitere studien über das Wärmegleichgewicht unter Gasmolekülen.. *Sitzungsberichte der Kaiserlichen Akademie der Wissenschaften in Wien, mathematisch-naturwissenschaftliche Classe,* vol. 66, pp. 275-370, 1872.

[234] Sarah Rice, Abel W. Lin, Daniel Safer, Cynthia L. Hart, Nariman Naber, Bridget O. Carragher, Shane M. Cain, Elena Pechatnikova, Elizabeth M. Wilson-Kubalek, Michael Whittaker, Edward Pate,Roger Cooke, Edwin W. Taylor,Ronald A. Milligan and Ronald D. Vale : A structural change in the kinesin motor protein that drives motility. *Nature,* vol. 402, pp. 778–784, 1999.

[235] Mikhailenko SV, Oguchi Y, Ishiwata S: Insights into the mechanisms of myosin and kinesin molecular motors from the single-molecule unbinding force measurements. *J R Soc Interface,* vol. 7, nº Suppl_3, pp. 295-306, 2010.

[236] Dong-Eun Kim, Murli Narayan, Smita S Patel: T7 DNA Helicase: A Molecular Motor that Processively and Unidirectionally Translocates Along Single-stranded DNA. *Journal of Molecular Biology,* vol. 321, nº 5, pp. 807-819, 2002.

[237] Matson SW, Kaiser-Rogers KA: DNA helicases. *Annu Rev Biochem,* vol. 59, pp. 289–329, 1990.

[238] Natalie M. Stano, Yong-Joo Jeong, Ilker Donmez, Padmaja Tummalapalli, Mikhail K. Levin and Smita S. Patel : DNA synthesis provides the driving force to accelerate DNA unwinding by a helicase. *Nature,* vol. 435, pp. 70–373, 2005.

[239] Vaishnavi Rajagopal, Smita S. Patel: Single Strand Binding Proteins Increase the Processivity of DNA Unwinding by the Hepatitis C Virus Helicase. *Journal of Molecular Biology,* vol. 376, nº 1, pp. 69-79, 2008.

[240] Derek N. Fuller, Dorian M. Raymer, Vishal I. Kottadiel, Venigalla B. Rao, and Douglas E. Smith: Single phage T4 DNA packaging motors exhibit large force generation, high velocity, and dynamic variability. *PNAS,* vol. 104, nº 43, pp. 16868-16873, 2007.

[241] Derek N. Fuller, Dorian M. Raymer, John Peter Rickgauer, Rae M. Robertson, Carlos E. Catalano, Dwight L. Anderson, Shelley Grimes, Douglas E. Smith: Measurements of Single DNA Molecule Packaging Dynamics in Bacteriophage λ Reveal High Forces, High Motor Processivity, and Capsid Transformations. *Journal of Molecular Biology,* vol. 373, nº 5, pp. 1113-1122, 2007.

[242] Branden Brough, Brian H. Northrop, Jacob J. Schmidt, Hsian-Rong Tseng, Kendall N. Houk, J. Fraser Stoddart, and Chih-Ming Ho: Evaluation of synthetic linear motor-molecule actuation energetics. *PNAS,* vol. 103, nº 23, pp. 8583-8588, 2006.

[243] Lussis P, Svaldo-Lanero T, Bertocco A, Fustin CA, Leigh DA, Duwez AS: A single synthetic small molecule that generates force against a load. *Nature Nanotechnology,* vol. 6, nº 9, pp. 553-557, 2011.

[244] Van Quaethem, A., Lussis, pp., Leigh, D. A., Duwez, A.-S. and Fustin, C.-A.: Probing the mobility of catenane rings in single molecules. *Chem. Sci,* vol. 5, nº 4, pp. 1449–1452, 2014.

[245] Hanozin E, Mignolet B, Morsa D, Sluysmans D, Duwez AS, Stoddart JF, Remacle F, De Pauw E.: Where Ion Mobility and Molecular Dynamics Meet To Unravel the (Un)Folding Mechanisms of an Oligorotaxane Molecular Switch. *ACS Nano,* vol. 11, nº 10, pp. 10253-10263, 2017.

[246] Sluysmans, D., Devaux, F., Bruns, C. J., Stoddart, J. F. and Duwez, A.-S.: Dynamic force spectroscopy of synthetic oligorotaxane foldamers. *PNAS,* vol. 115, nº 38, pp. 9362-9366, 2018.

[247] Sluysmans D, Hubert S, Bruns CJ2, Zhu Z, Stoddart JF, Duwez AS.: Synthetic oligorotaxanes exert high forces when folding under mechanical load. *Nature Nanotechnology,* vol. 13, nº 3, pp. 209-213, 2018.

[248] Jonathon Howard: Motor Proteins as Nanomachines: The Roles of Thermal Fluctuations in Generating Force and Motion. de *Biological Physics*, V. Rivasseau, Ed., Basel, Springer, 2009, pp. 47-59.

[249] E.C. Slater and K.W. Cleland: The effect of calcium on the respiratory and phosphorylative activities of heart-muscle sarcosomes. *Biochem. J,* vol. 55, pp. 566, 1953.

[250] Yong Hwan Jin, Rao Ayyagari, Michael A. Resnick, Dmitry A. Gordenin and Peter M. J. Burgers: Okazaki fragment maturation in yeast. II. Cooperation between the polymerase and 3'-5'-exonuclease activities of Pol delta in the creation of a ligatable nick. *The Journal of Biological Chemistry,* vol. 278, pp. 1626-1633, 2003.

[251] Yali Zhu, Kelly S. Trego, Liping Song, Deborah S. Parris: 3′ to 5′ Exonuclease Activity of Herpes Simplex Virus Type 1 DNA Polymerase Modulates Its Strand Displacement Activity. *Journal of Virology,* vol. 77, nº 18, pp. 10147-10153, 2003.

[252] W. C. E. J. L.-S. G. T. J. Thomas D. Pollard, Ed.: Motor Proteins. de *Cell Biology*, Elsevier Inc., 2017, pp. 623-638.

[253] Jenny A. Korhonen, Martina Gaspari and Maria Falkenberg: TWINKLE Has 5′ → 3′ DNA Helicase Activity and Is Specifically Stimulated by Mitochondrial Single-stranded DNA-binding Protein. *Journal of Biological Chemistry,* vol. 278, pp. 48627-48632, 2003.

[254] Bulygin VV, Milgrom YM: A bi-site mechanism for Escherichia coli F1-ATPase accounts for the observed positive catalytic cooperativity. *Biochimica et Biophysica Acta (BBA) - Bioenergetics,* vol. 1787, nº 8, pp. 1016-1023, 2009.

[255] Nath S: The thermodynamic efficiency of ATP synthesis in oxidative phosphorylation. *Biophysical Chemistry,* vol. 219, pp. 69-74, 2016.

[256] Jonckheere AI, Smeitink JAM, Rodenburg RJT: Mitochondrial ATP synthase: architecture, function and pathology. *Journal of Inherited Metabolic Disease,* vol. 35, nº 2, pp. 211–225, 2012.

[257] Korhonen JA, Gaspari M, Falkenberg M: TWINKLE Has 5′ → 3′ DNA Helicase Activity and Is Specifically Stimulated by Mitochondrial Single-stranded DNA-binding Protein. *Journal of Biological Chemistry,* vol. 278, pp. 48627-48632, 2003.

[258] Tabor S, Richardson CC: DNA sequence analysis with a modified bacteriophage T7 DNA polymerase. *PNAS,* vol. 84, nº 14, pp. 4767-4771, 1987.

[259] Kohler C, Radpour R, Barekati Z, Asadollahi R, Bitzer J, Wight E, Bürki N, Diesch C, Holzgreve W, Yan Zhong X: Levels of plasma circulating cell free nuclear and mitochondrial DNA as potential biomarkers for breast tumors. *Molecular Cancer,* vol. 8, nº 105, 2009.